

## Review

# Chemically engineered persistent luminescence nanoprobes for bioimaging

Thomas Lécuyer,<sup>1,2</sup> Elliott Teston,<sup>1,2</sup> Gonzalo Ramirez-Garcia,<sup>1,2</sup> Thomas Maldiney,<sup>1,2</sup> Bruno Viana,<sup>2,3</sup> Johanne Seguin,<sup>1,2</sup> Nathalie Mignet,<sup>1,2</sup> Daniel Scherman,<sup>1,2</sup> Cyrille Richard<sup>1,2</sup>✉

1. Unité de Technologies Chimiques et Biologiques pour la Santé (UTCBS), UMR 8258 CNRS, U 1022 Inserm, Université Paris Descartes, Sorbonne Paris Cité, Faculté des Sciences Pharmaceutiques et Biologiques, 75006 Paris, France.
2. Chimie-ParisTech, PSL, 75005 Paris, France.
3. Institut de Recherche de Chimie-Paris, CNRS UMR 8247, Chimie-ParisTech, 75005 Paris, France.

✉ Corresponding author: cyrille.richard@parisdescartes.fr.

© Ivyspring International Publisher. Reproduction is permitted for personal, noncommercial use, provided that the article is in whole, unmodified, and properly cited. See <http://ivyspring.com/terms> for terms and conditions.

Received: 2016.06.24; Accepted: 2016.09.18; Published: 2016.11.02

## Abstract

Imaging nanoprobes are a group of nanosized agents developed for providing improved contrast for bioimaging. Among various imaging probes, optical sensors capable of following biological events or progresses at the cellular and molecular levels are actually actively developed for early detection, accurate diagnosis, and monitoring of the treatment of diseases. The optical activities of nanoprobes can be tuned on demand by chemists by engineering their composition, size and surface nature. This review will focus on researches devoted to the conception of nanoprobes with particular optical properties, called persistent luminescence, and their use as new powerful bioimaging agents in preclinical assays.

Key words: Nanoparticles, chemistry, surface coating, persistent luminescence and in vivo imaging.

## Introduction

Current applications of materials as biomedical nanosystems play an important role in nanomedicine, not only due to their unique properties, but also to their versatile functionality [1,2]. In particular, small animal imaging is rapidly developing to study basic biological and pathological mechanisms in animal models, to provide important information regarding the pathogenesis, progression and treatment of diseases. Several imaging techniques have been developed to observe the structures and functions of biological systems, such as computed tomography (CT), ultrasound imaging (US), magnetic resonance imaging (MRI), single-photon emission computed tomography (SPECT), and positron emission tomography (PET) [3,4]. Recently, optical imaging (bioluminescence and fluorescence imaging) has received increasing attention due to its ease of use and ability to provide anatomical and physiological details of living systems [5]. However, existing optical nanoprobes still possess major drawbacks for

practical applications. For example, near-infrared quantum dots (QDs) suffer from potential cytotoxicity [6] and up-conversion luminescent nanoparticles (UCNPs) display rather low up-conversion efficiency and require the use of high energy lasers [7]. To meet the growing demand for optical nanoprobes, efforts have been put into looking for new optical materials. Among them, Scherman and co-workers have introduced in 2007 the use of persistent luminescence nanoparticles (PLNPs) for real-time optical imaging in living animals [8].

Persistent luminescence materials have been discovered almost 20 years ago [9, 10] and there are now 1189 papers in the literature on this topic (June 2016, Web of Science). Persistent luminescence materials can be compared to optical batteries. First, the material can be charged with light for a few minutes. Then, when the excitation is stopped, the emission of light can be observed [11]. Emergency signage used in case of electricity failures is one of the

main application of persistent luminescence phosphors but others applications were also proposed such as watch dials, decorative objects and toys [12] and more recently for energy [13] and outdoor applications [14]. Up to now, there are persistent phosphors for each of the primary colours, with the representative ones including  $\text{CaAl}_2\text{O}_4:\text{Eu}^{2+}$ ,  $\text{Nd}^{3+}$  (blue, emission for more than 10 hours) [15],  $\text{SrAl}_2\text{O}_4:\text{Eu}^{2+}$ ,  $\text{Dy}^{3+}$  (green, > 30 hours) [16] and  $\text{Y}_2\text{O}_2\text{S}:\text{Eu}^{3+}$ ,  $\text{Mg}^{2+}$ ,  $\text{Ti}^{4+}$  (red, > 5 hours) [17]. Among them,  $\text{CaAl}_2\text{O}_4:\text{Eu}^{2+}$ ,  $\text{Nd}^{3+}$  and  $\text{SrAl}_2\text{O}_4:\text{Eu}^{2+}$ ,  $\text{Dy}^{3+}$  are already commercialized and are being widely used as night vision materials in various important fields, for example in security signs, emergency route signs, traffic signage, dials and displays because of their sufficiently strong and long lasting persistent luminescence (> 10 hours) and their ability to be excited by sunlight and room light.

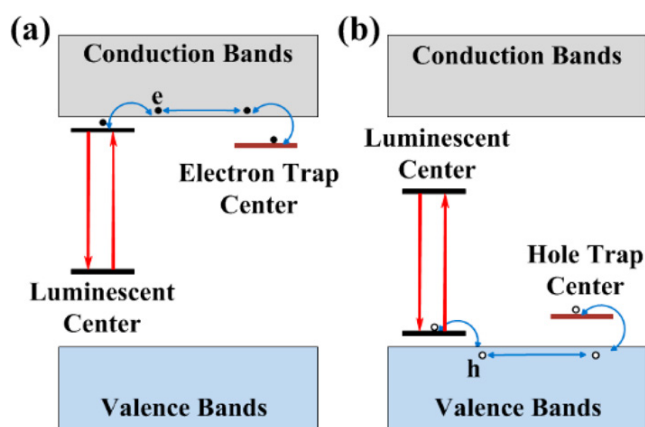


**Figure 1.** Illustration of possible mechanisms due to electron, e (a) and hole, h (b) traps that can directly contribute to the persistent luminescence. Reproduced with permission from reference [29].

The physics behind the persistent luminescence phenomenon is not that simple and intensive researches have been carried out during the last years [18]. In persistent phosphors, two kinds of active centers are involved: the trap centers and the emitter centers (see Figure 1). Traps can be due to lattice defects, impurities [19, 20], or various co-dopants introduced during the synthesis within the material energy bandgap, mainly just below the conduction band in the case of electron traps or just above the valence band in the case of hole traps [21,22]. Under light, excited levels are generated and instead of being radiatively relaxed they can be non-radiatively captured into traps. Traps usually do not emit radiation, but store the excitation energy for some time. This is the reason why this phenomenon can be related to an optical battery where, filling the traps

corresponds to the charging process. Then, in a second step corresponding to the discharge, the energy can be release by thermal or optical activation [23, 24] or by other physical stimulations such as mechano-stimulation for instance [25], resulting in stimulated emissions from the active centers [26, 27, 28 29, 30].

Persistent luminescence materials made with particular centers emitting in the red and near infrared range have recently emerged as new powerful nanoprobe for bioimaging [31, 32, 33, 34]. The main requirements that the materials must fulfill for this particular application are the following:

- have size ranging from 50 to 200 nm. Recent studies have shown that nanomaterials (NMs) with small sizes exhibited enhanced performance *in vivo*, such as greater tissue penetration, particularly those with size around or smaller than 50 nm. As such, there has been a major push recently in the field of NMs to miniaturize nanoparticle size using novel chemistry and engineering design [35,36],
- the NMs must be water resistant to prevent rapid dissolution in biological fluids and allow imaging for hours or days,
- the NMs should emit light in the tissue transparency window, between 650 and 1350 nm, to be able to pass through the animal body and be detected by a photon-counting system [37],
- since one of the physiologic functions of the liver is to efficiently capture and eliminate NMs, to delay subsequent blood clearance, nanoparticles may require modification to prevent both a rapid aggregation or lessen opsonization after intravenous administration. For this purpose, molecular surface modification is a widely used mechanism to decrease first-pass extraction and increase NPs serum half-life [38],
- in order to follow the biodistribution of the probe in real time, the NMs should have the longest light emission time [39].

Persistent luminescent nanoparticles could become a viable alternative to traditional tracer molecules, for instance in studying vascularization and targeting of tumors. Within this category of luminescent particles, red or NIR-emitting persistent luminescent particles hold several advantages over the use of other types of fluorescent materials, such as quantum dots or organic fluorophores. Indeed, fluorescence imaging suffers from a suboptimal signal-to-noise ratio (SNR) and a shallow detection depth (< 1 cm). These drawbacks are mainly associated with tissue autofluorescence, which is caused by the fluorescence from tissues under

constant external irradiation. Thus, ideally, an optical probe that can illuminate without external excitation would be free of autofluorescence and hence, enable significantly improved imaging sensitivity and depth. Despite some progress, quantum dots show high emission intensity upon excitation, but the excitation light inevitably induces a large autofluorescence background, lowering the SNR, unless time-resolved detection is used. Since the pioneer work by Scherman and co-workers [8], many studies have been conducted to develop improved persistent luminescence nanoparticles for optical imaging, as highlighted by the many articles and some reviews cited in the references. The removal of *in situ* excitation in the signal analysis process provides a unique solution to circumvent the interference from tissue autofluorescence. This manuscript gathers, for the first time, all the work that has been done since a decade in the field of persistent luminescence nanoparticles as new efficient probes for bioimaging: the different matrixes that have been synthesized (silicates, gallium oxides, gallogermanates, aluminates, titanates, phosphates, stannates), their physicochemical characterizations and surface coatings developed to obtain usable colloids and finally relevant examples of both *in vitro* and *in vivo* imaging applications are reported.

## The first generation of PLNPs for bioimaging: matrix silicate

### The historic nanoprobe: $\text{Ca}_{0.2}\text{Zn}_{0.9}\text{Mg}_{0.9}\text{Si}_2\text{O}_6$ doped with $\text{Eu}^{2+}$ , $\text{Dy}^{3+}$ and $\text{Mn}^{2+}$

In 2003, Wang et al reported the persistent luminescence properties of different materials (aluminate, silicates) doped with luminescent ions [40]. Among them a silicate doped with  $\text{Eu}^{2+}$ ,  $\text{Dy}^{3+}$  and  $\text{Mn}^{2+}$  had interesting optical properties for

bioimaging in term of emission wavelength but couldn't directly be used in its original form since it was prepared by solid state reaction giving micrometric particles. The pioneered work using persistent luminescence nanoparticles (PLNPs) for optical bioimaging was reported four years later by Scherman and co-workers [8]. In their work,  $\text{Ca}_{0.2}\text{Zn}_{0.9}\text{Mg}_{0.9}\text{Si}_2\text{O}_6$  doped with  $\text{Eu}^{2+}$ ,  $\text{Dy}^{3+}$  and  $\text{Mn}^{2+}$  was prepared by a sol/gel process starting from raw materials. Briefly, magnesium nitrate [ $\text{Mg}(\text{NO}_3)_2 \cdot 6\text{H}_2\text{O}$ ], zinc chloride ( $\text{ZnCl}_2$ ), calcium chloride ( $\text{CaCl}_2 \cdot 2\text{H}_2\text{O}$ ), europium chloride ( $\text{EuCl}_3 \cdot 6\text{H}_2\text{O}$ ), dysprosium nitrate [ $\text{Dy}(\text{NO}_3)_3 \cdot 5\text{H}_2\text{O}$ ], manganese chloride ( $\text{MnCl}_2 \cdot 4\text{H}_2\text{O}$ ) were dissolved in acidified water and tetraethoxysilane (TEOS) was then rapidly added and the solution stirred vigorously at room temperature until the solution became limpid. The solution was then heated at  $70^\circ\text{C}$  until the sol-to-gel transition occurred. The wet gel was then dried in an oven at  $110^\circ\text{C}$  and finally fired in a zirconium crucible in a reductive atmosphere (10%  $\text{H}_2$ , 90% Ar) at  $1050^\circ\text{C}$  for 10 hours. In this material, trapped centers were created through the introduction of small amounts of  $\text{Dy}^{3+}$ , and  $\text{Mn}^{2+}$  was the emitting center receiving energy from electron-hole pair recombination. Figure 2 reports the main optical characteristics of this material: excitation in the UV, emission at about 700 nm with a long-lasting luminescence for more than 1 hour.

This material was however too polydisperse and couldn't be directly used for animal injection. The team had then shown that hydroxy-nanoparticles of different sizes (hydrodynamic diameter of 80 to 180 nm) could be obtained after hydroxylation in NaOH, followed by centrifugation at different speeds (4500 to 13500 rpm) and time (5 to 10 minutes) (Figure 3).

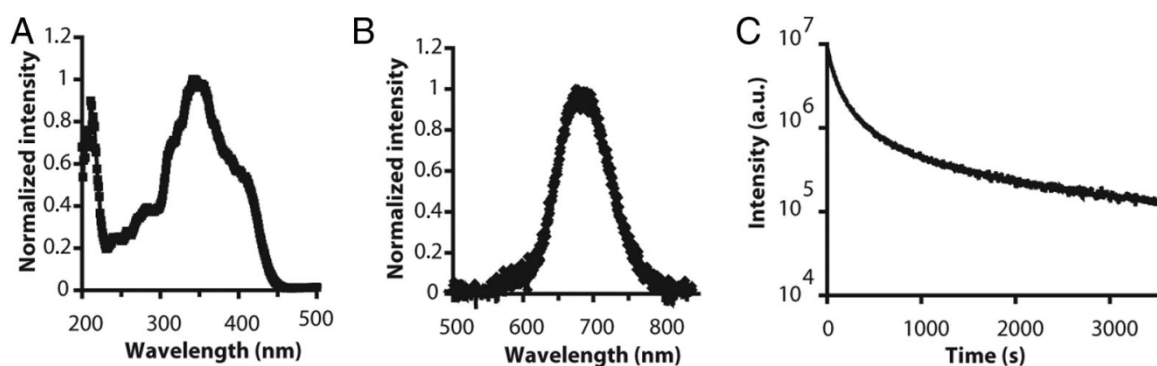


**Figure 2.** Optical characteristics of  $\text{Ca}_{0.2}\text{Zn}_{0.9}\text{Mg}_{0.9}\text{Si}_2\text{O}_6$ : Eu, Dy, Mn prepared by sol/gel reaction and calcination at  $1050^\circ\text{C}$ . A) Excitation spectrum. B) Long afterglow emission spectrum. C) Time dependence of the luminescence intensity of PLNPs measured after exposure to a 6-W UV lamp for 5 min and recorded for 1 hour. The luminous intensity was quantified straightforward by using an intensified charge-coupled device (ICCD) camera (PhotonImager; Biospace). Reproduced with permission from reference [8].

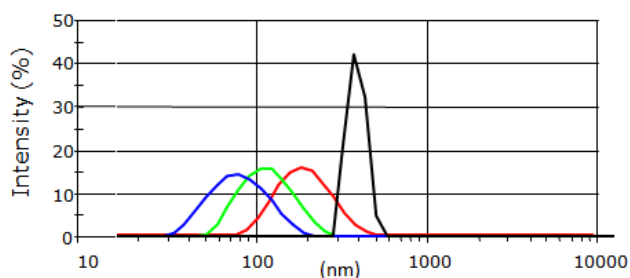


**Figure 3.** Different hydrodynamic diameters of the  $\text{Ca}_{0.2}\text{Zn}_{0.9}\text{Mg}_{0.9}\text{Si}_2\text{O}_6$ : Eu, Dy, Mn nanoparticles obtained after the centrifugation steps and measured by DLS.

### Functionalization for *in vivo* use

In order to study the influence of probe's surface on its distribution *in vivo*, modifications of the surface of the nanoparticles were then realized. First, the free hydroxyl groups present on the PLNPs and characterized by a negative surface electric charge (-34.3 mV), called zeta potential, at neutral pH can react with 3-aminopropyltriethoxysilane (APTES) in dimethylformamide (DMF). This reaction provides positively charged NPs (referred to as amino-PLNPs) resulting from the presence of free amino groups at the surface. The success of the grafting procedure can be assessed by zeta potential measurement (+35mV) and by a positive test with trinitrobenzene sulfonate (TNBS). The APTES in excess is removed by several sedimentation washing procedures. The surface charge of the amino-PLNPs can be reversed by reaction with diglycolic anhydride, which reacts with amines to give free carboxyl groups. The zeta

potential of these particles (carboxyl-PLNPs) at neutral pH is negative (-37mV). Finally a peptide coupling of amines with MeO-PEG<sub>5000</sub>-NHS leads to neutral particles (+5mV), Figure 4 [41].

The biodistribution of such PLNPs was studied as a function of surface coating and nanoparticle diameter (80, 120 and 180 nm). Biodistribution in healthy mice was achieved after systemic injection to validate the use of this probe for *in vivo* applications [42, 43, 44]. For that purpose, BALB/c mice were injected with a 100  $\mu\text{L}$  colloidal suspension of 1 mg of PLNPs suspended in 1 mL of sterile 150 mM NaCl. The excitation of the different PLNPs suspensions before injection was accomplished by direct exposure to a 6W UV lamp for 5 min at a distance of 2 cm (Figure 5A). After injection, the signal acquisition was done in real-time using a photon-counting system based on a cooled GaAs intensified charge-coupled device (ICCD) camera (Photon-Imager, Biospace, Paris, France) without external excitation source (Figure 5B).

This example was the first work reporting the possibility of using suitable PLNPs for *in vivo* bioimaging in small animal. However, due to the intrinsic luminescence decay associated with the use of persistent luminescence, the optical signal from these PLNPs couldn't be detected beyond 1 hour *in vivo*, impeding any long-time monitoring of the nanoparticles after intravenous injection, which could be a limit for some applications. Optimisation of the matrix or dopants was necessary.

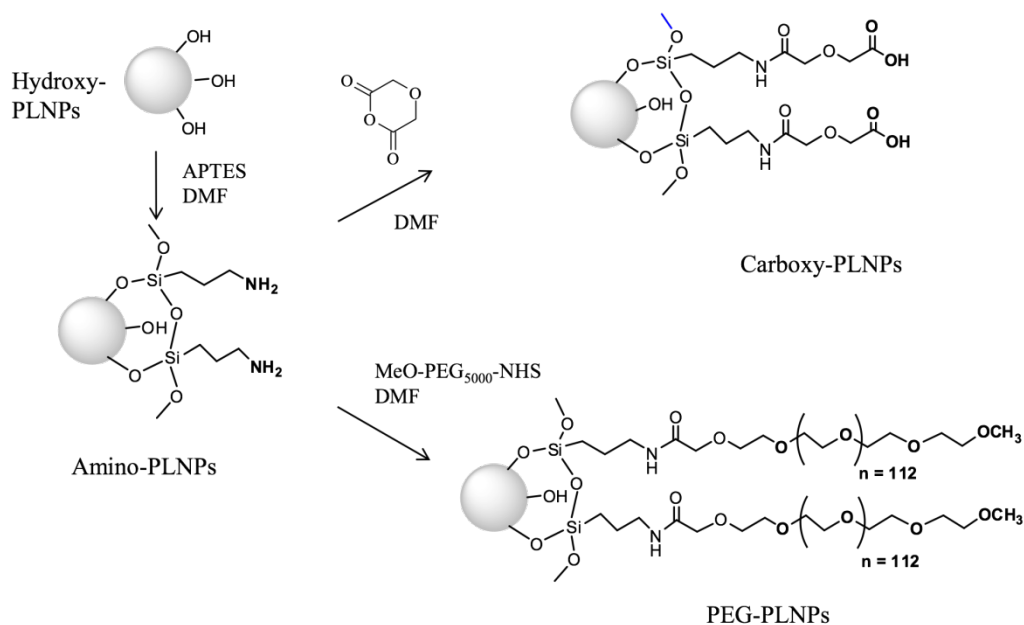


**Figure 4.** Chemical reactions on  $\text{Ca}_{0.2}\text{Zn}_{0.9}\text{Mg}_{0.9}\text{Si}_2\text{O}_6$ : Eu, Dy, Mn nanoparticles to introduce amino, carboxy or PEG groups on the surface.

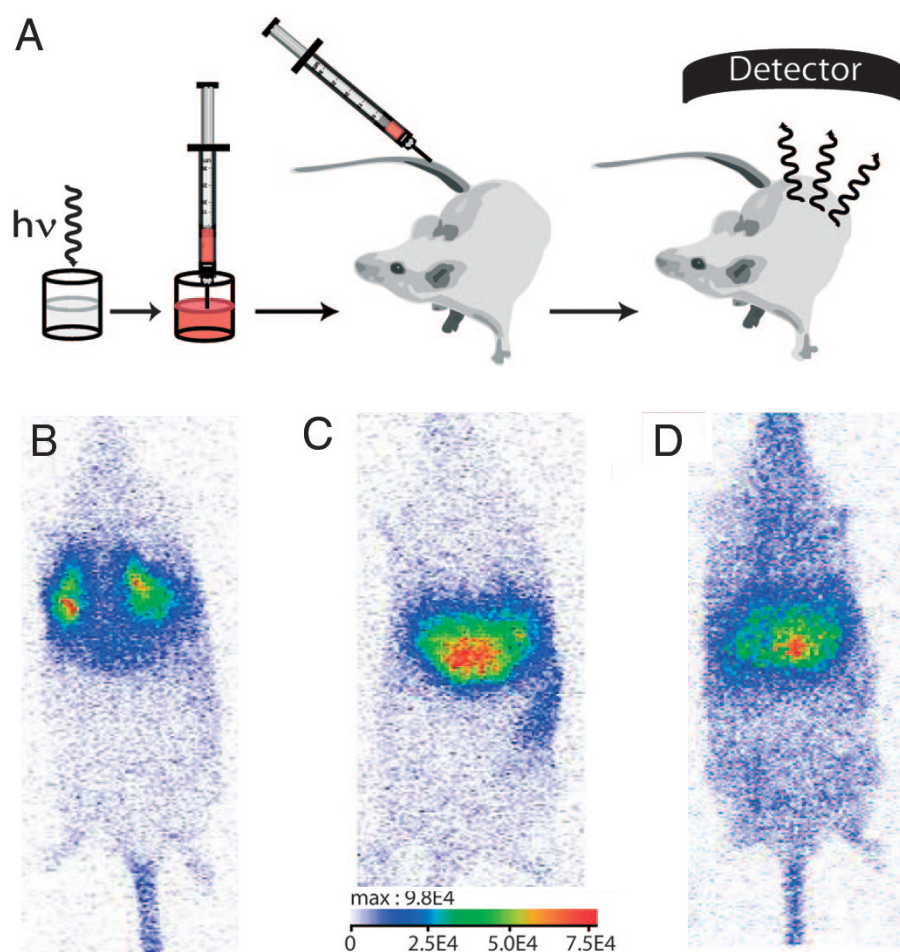


**Figure 5.** (A) Principle of *in vivo* imaging using PLNPs. A suspension containing a proper amount of NPs is first excited *ex vivo* with a UV lamp for few minutes and then directly injected into an anesthetized mouse. The signal is then acquired with an intensified charge-coupled device (CCD) camera in order to follow the influence of the coating (B: amino, C: carboxy or D: PEG). Reproduced with permission from reference [8].

## Optimization of nanoparticles composition

### Nitridosilicate

Since luminescence of the original nanophosphor was to be improved, a new host was tested. Smet and co-workers have shown that bulk nitridosilicate,  $\text{Ca}_2\text{Si}_5\text{N}_8:\text{Eu}^{2+}$ ,  $\text{Tm}^{3+}$  had outstanding long lasting luminescence at about 610 nm [45,46,47], a wavelength emission compatible for *in vivo* imaging applications.  $\text{Ca}_2\text{Si}_5\text{N}_8:\text{Eu}^{2+}$  (1%),  $\text{Tm}^{3+}$  (1%) was prepared by mixing appropriate amounts of  $\text{Ca}_3\text{N}_2$  and  $\alpha\text{-Si}_3\text{N}_4$  (precursors for the host material and  $\text{EuF}_3$  and  $\text{TmF}_3$  for the dopants), under a protective nitrogen atmosphere. The mixture was then sintered during 1 hour at  $1300^\circ\text{C}$  under reducing atmosphere (90%  $\text{N}_2$ , 10%  $\text{H}_2$ ) producing powder with grain sizes in the micrometer range, limiting a direct use in living animals. In order to obtain nanoparticles, two ways have been envisioned by the authors: first, a laser ablation treatment of bulk powder in solution, and a wet grinding of the same powder followed by

selective sedimentation in alkaline solution, as reported before [8]. Laser ablation combines many advantages compared to other extraction techniques, notably regarding size distributions of the resulting NPs [48,49]. Besides, various materials have already been obtained with this method such as metal NPs [50], semiconductors [51], dielectric compounds [52], but also nitride-based compounds such as  $\text{C}_3\text{N}_4$  [53]. For this reason, the authors focused on this technique in order to obtain nanoparticules. For these experiments, the third harmonic of a pulsed YAG: $\text{Nd}^{3+}$  laser (355 nm, 10 ns) was used. The preparation of the  $\text{Ca}_2\text{Si}_5\text{N}_8:\text{Eu}^{2+}$ ,  $\text{Tm}^{3+}$  persistent luminescence nanoparticles by pulsed laser ablation in solution gave PLNPs with diameters in the range of 3-5 nm but the low quantity in solution prevented further use for bioimaging. However, extraction of nanoparticles after wet grinding in NaOH, as used before [8], gave enough PLNPs to prove that such nitridosilicate can be used as optical probe for small animal *in vivo* imaging. This technique returned a narrow size distribution of negatively charged

hydroxyl-terminated nanoparticles (CSN-OH) with a mean diameter close to 200 nm and in 10% yield. Indeed, due to rapid surface oxidation at room temperature after exposure to oxygen containing atmosphere, air especially, silicon nitride-based compounds are known to display surface properties very close to silicon dioxide and silicate materials [54]. For this reason, it was possible to transpose the reaction for the functionalization of silicate-based persistent luminescence nanoparticles presented before (Figure 4) to the nitridosilicate surface. In order to investigate a possible application of nitridosilicate hosts for bioimaging in living animal, the biodistribution of two different surface coverages (hydroxy and PEG-terminated nitridosilicate) after systemic injection to BALB/c mice has been envisioned. For the experiment, mice were intravenously injected with either CSN-OH or CSN-PEG after 5 minutes excitation of both suspensions under UV light (6 W lamp, 254 nm). Figure 6 displays the characteristics of such PLNPs and optical images obtained 15 minutes after intravenous injection. Again, a few dozen of minutes after excitation and injection, no signal is detectable with the camera, preventing any long term following

of this nanoprobe [55].

#### CMSO:Eu, Pr, Mn

To better understand the origin of persistent luminescence phenomenon in the native CZMSO ( $\text{Ca}_{0.2}\text{Zn}_{0.9}\text{Mg}_{0.9}\text{Si}_2\text{O}_6$ :Eu, Dy, Mn) lattice, Lecointre et al have suggested a mechanism of persistent luminescence in the diopside host, with  $\text{Mn}^{2+}$  acting both as the hole trap and the recombination center [56,57]. Starting from the hypothesis that controlling electron traps depth could help to enhance the optical properties of PLNPs, Maldiney et al reported the synthesis of several  $\text{Mn}^{2+}$  diopside nanoparticles, co-doped with different trivalent lanthanide ions ( $\text{Ce}^{3+}$ ,  $\text{Pr}^{3+}$ ,  $\text{Nd}^{3+}$ , or  $\text{Dy}^{3+}$ ) and with  $\text{Eu}^{2+}$  to enable UV excitation [58]. These nanomaterials were compared to the historic hybrid  $\text{Ca}_{0.2}\text{Zn}_{0.9}\text{Mg}_{0.9}\text{Si}_2\text{O}_6$  doped with  $\text{Eu}^{2+}$ ,  $\text{Dy}^{3+}$  and  $\text{Mn}^{2+}$  and tested for *in vivo* imaging. Among the five prepared materials, the most promising result came from the comparison of the new CMSO:Eu, Pr, Mn nanoparticles to the first generation of CZMSO:Eu, Dy, Mn nanoparticles. Experimental results in Figure 7 show that the red luminescence from CMSO:Eu, Pr, Mn appears about 10 times more intense than the historical described

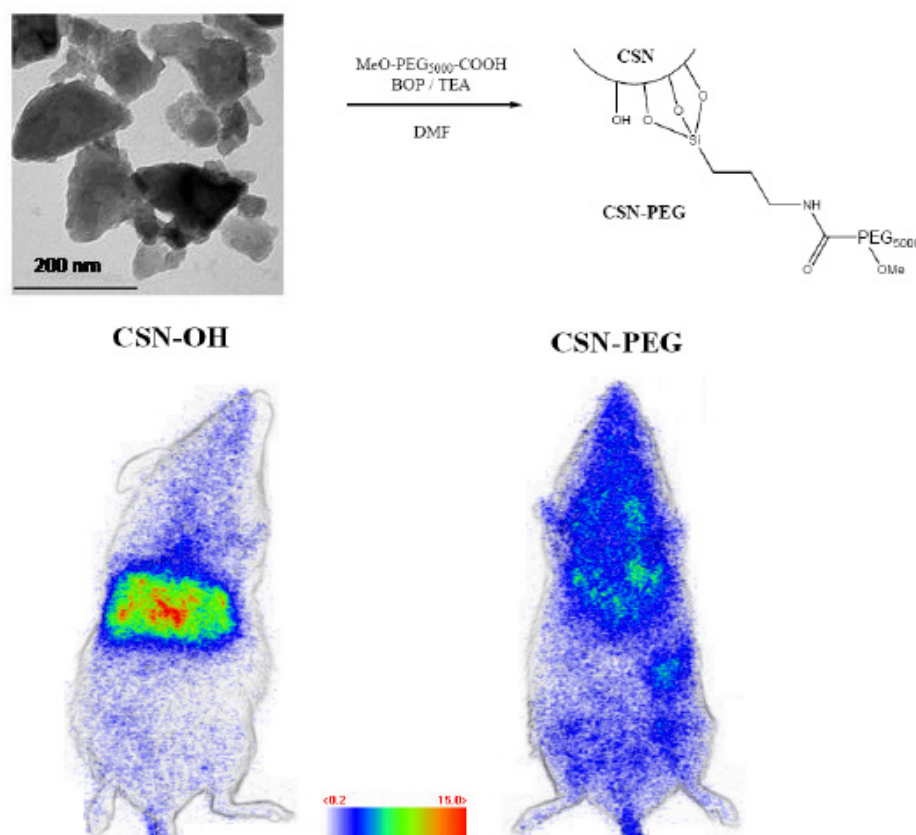


**Figure 6.** Characteristics of CSN nanoparticles, surface modification with PEG and proof of concept for *in vivo* imaging using both hydroxylated and PEGylated NPs. Reproduced with permission from reference [55].

$\text{Ca}_{0.2}\text{Zn}_{0.9}\text{Mg}_{0.9}\text{Si}_2\text{O}_6:\text{Eu}^{2+}, \text{Mn}^{2+}, \text{Dy}^{3+}$  PLNPs. The authors noticed that  $\text{Pr}^{3+}$  failed to increase the afterglow in hybrid CZMSO host, comprising both enstatite and diopside. Although  $\text{Pr}^{3+}$  seemed to be the optimal electron trap in diopside, this trend had no reason to be maintained in a different silicate host, enstatite in particular. In order to validate a potential use of this new efficient composition for *in vivo* imaging, the two candidates from polydisperse samples (CZMSO:EuDy, Mn and CMSO:Eu, Pr, Mn) were confronted with the exact same nano-sized distribution for mice bio-imaging (Figure 7).

As could be seen on Figure 7, by working on the chemical composition of the silicate, the authors were able to increase by a factor 5 the intensity of luminescence *in vivo*, allowing to perform imaging for longer time [58,59,60,61].

### Controllable size silicates synthesis

There are little reports about the synthesis of diopside nanoparticles with controllable size and morphology in a simple and efficient way and in large scale, which is very important to generalize their applications in biology. Template method is a facile and effective method in the synthesis of NMs with highly controllable sizes and morphologies [62,63]. For example, mesoporous silica nanospheres (MSNs) can be synthesized conveniently with tunable sizes or morphologies and have become one of the most important hard templates in the synthesis of various useful materials. Inspired by the wide application of MSNs as templates, Li et al have developed a convenient template method to synthesize PLNPs both with narrow size distributions and in large scale [64]. Briefly, mixed nitrate solution of  $\text{Ca}^{2+}$ ,  $\text{Mg}^{2+}$ ,  $\text{Eu}^{3+}$ ,  $\text{Pr}^{3+}$ ,  $\text{Mn}^{2+}$  was prepared by dissolving their corresponding nitrates with the final concentration 1.0

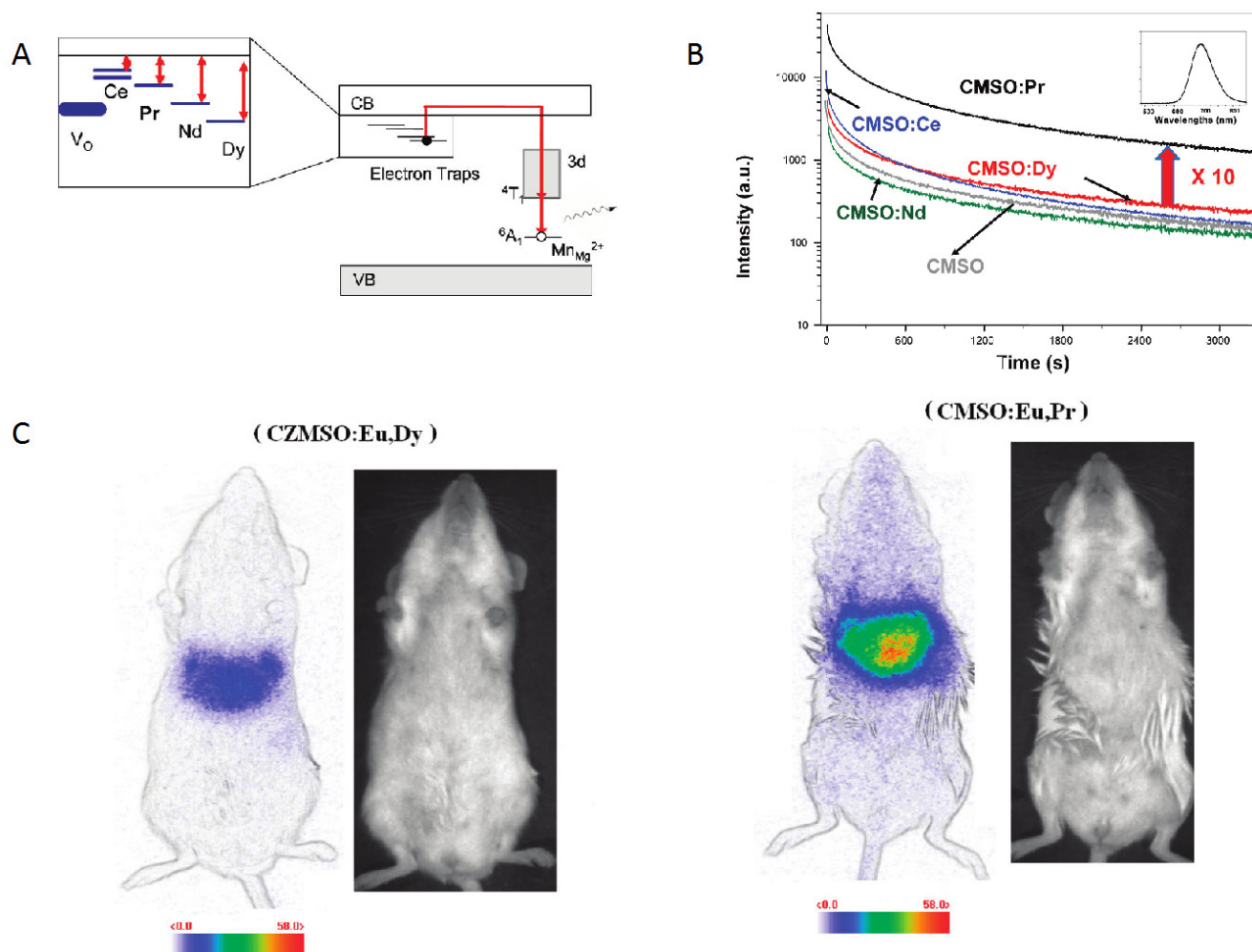


**Figure 7.** (A) Schematic energy level diagram of  $\text{Mn}^{2+}$  and  $\text{Ln}^{3+}$  (Ce, Pr, Nd or Dy) in CMSO. The main hole traps are  $\text{Mn}^{2+}$  ions in the  $\text{Mg}^{2+}$  site, while electrons are trapped by oxygen vacancies (VO) and  $\text{Ln}^{3+}$  ions. (B) Decay of the  $\text{Mn}^{2+}$  luminescence intensity at 685 nm of CMSO (grey curve) and rare-earth-codoped CMSO:Ln compounds, recorded after 10 min irradiation. (C) *In vivo* imaging of different CZMSO and CMSO diopside PLNPs under the photon-counting system; left (CZMSO:Eu,Dy) and right (CMSO:Eu,Pr). The signal was recorded for 15 min following systemic injection of 100  $\mu\text{g}$  of the probes excited 5 min under a 6W UV lamp. Reproduced with permission from reference [58].

M, 1.0 M, 0.010 M, 0.020 M, 0.10 M, respectively. 1.0 g of the as-synthesized MSNs was mixed with 20 mL of the as-prepared nitrate solution and was stirred for 24 hours. Then the ionic impregnated MSNs were centrifuged and dried at 80°C for 5 hours. The dried precursor was first annealed at 800 °C for 2 hours and then grinded using a mortar and pestle. NIR-PLNPs nanoparticles were finally formed after a second identical thermal treatment. The heating procedures were carried out under a weak reducing atmosphere (10%, H<sub>2</sub>/Ar). The key point of their method relies upon the use of MSNs both as silicon source to form CaMgSi<sub>2</sub>O<sub>6</sub> diopside phase and as some hard templates to control the morphologies of the resulting nanoparticles. The authors investigate the abilities of surface modified nanoparticles (EMP NPs) to be metabolized via the lymph circulation, which is as important as the blood circulation system, Figure 8.

The same group used a similar strategy to prepare SiO<sub>2</sub>/SrMgSi<sub>2</sub>O<sub>6</sub>:Eu, Dy nanoparticles [65]. In their experiments, metal ions (Sr<sup>2+</sup>, Mg<sup>2+</sup>, Eu<sup>3+</sup>, Dy<sup>3+</sup>) were impregnated into the pores of mesoporous silica nanospheres followed by high temperature calcination. The as-prepared silicate nanoparticles display spherical morphology with a narrow size distribution that can be tuned between 50 nm and 500 nm. Long afterglow properties, ranging from 400 nm

to 550 nm could be observed from the as prepared nanospheres. After the surface was modified with amino groups, grafted by PEG and irradiated with 365 nm UV light for 10 min, the afterglow signal could be observed in real time for more than 1 hour in a mouse after peritoneal injection (Figure 9).

### PLNPs for *in vitro* bioimaging

In parallel to the *in vivo* imaging applications using PLNPs, in 2011 Yan and co-workers reported for the first time the use of persistent luminescence to detect a biomarker *in vitro* based on a fluorescence resonance energy transfer (FRET) inhibition assay with  $\alpha$ -fetoprotein (AFP) excreted during cancer cell growth [66]. Serum levels of AFP often increase under conditions such as periods of rapid liver cancer cell growth, cirrhosis, and chronic active hepatitis as well as carbon tetrachloride intoxication. Therefore, detection of serum levels of AFP can lead to early diagnosis of hepatocellular carcinoma (HCC) [67]. The authors employed Eu<sup>2+</sup> and Dy<sup>3+</sup> doped Ca<sub>1.86</sub>Mg<sub>0.14</sub>ZnSi<sub>2</sub>O<sub>7</sub> nanoparticles since their photoluminescence emission spectra have maximum overlap with the absorption spectra of AFP-antibody-gold nanoparticle conjugates (Ab-AuNPs), resulting in maximum FRET efficiency (Figure 10).

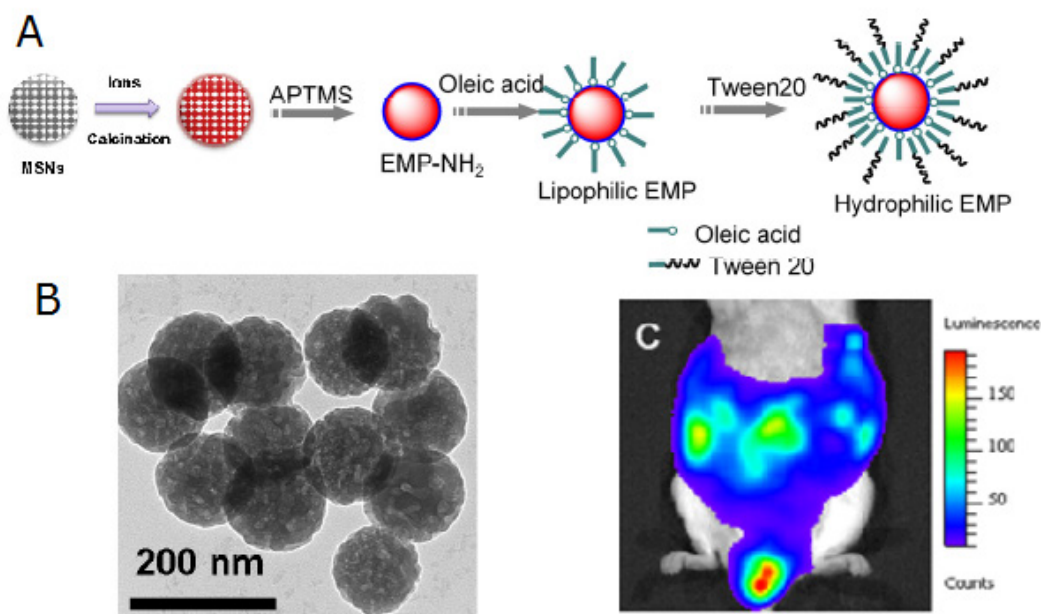


**Figure 8.** (A) Controllable size synthesis of CaMgSi<sub>2</sub>O<sub>6</sub>: Eu<sup>2+</sup>, Pr<sup>3+</sup>, Mn<sup>2+</sup> (EMP NPs). (B) TEM of the as-synthesized NPs. (C) Luminescence image of the distribution of the EMP NPs injected into the abdomen of a mouse 60 min after the injection. Reproduced with permission from reference [64].

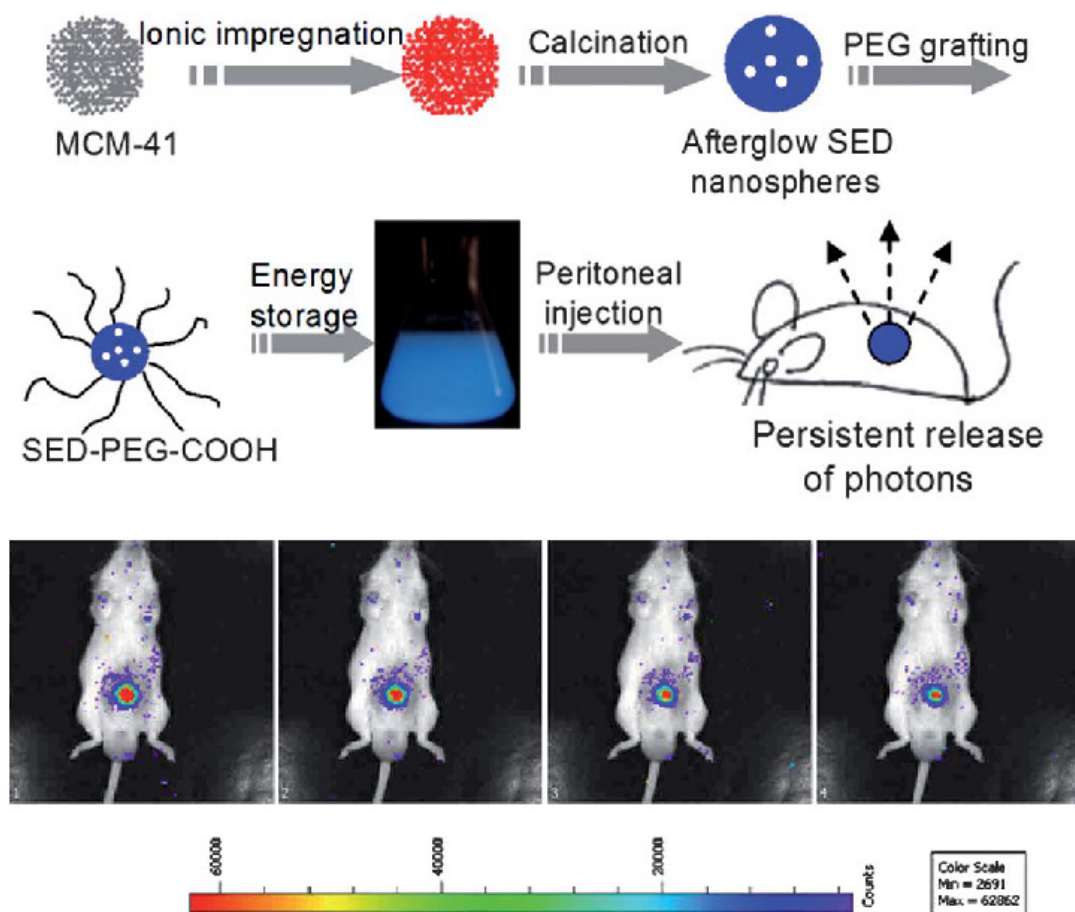


**Figure 9.** Controlled size synthesis of SiO<sub>2</sub>/SrMgSi<sub>2</sub>O<sub>6</sub>:Eu<sub>0.01</sub>, Dy<sub>0.02</sub> nanoparticles and *in vivo* imaging after intraperitoneal injection. Luminescence imaging *in vivo*, 60 s acquisition at intervals of every 5 min. Reproduced with permission from reference [65].

Thanks to the optical property of PLNPs, the same group developed another nanoprobe for highly selective and sensitive FRET immunoassay of PSA in human serum and cell extracts without the need for *in situ* excitation, [68]. Though enzyme linked immunosorbent assay (ELISA) and radioimmunoassay are widely used in the detection of PSA in human serum, several drawbacks are always unavoidable, such as tedious procedures, radioactive pollution and influence of environmental temperature or reaction time [69]. Therefore, the development of a simple, rapid and sensitive detection method calls urgent need for medical research [70]. To avoid the optical background from the autofluorescence of the biological matrix, mouse monoclonal PSA antibody (PS6) bioconjugated PLNPs were employed as the energy donor (PLNP-PS6) for an excitation-free type analysis. Rhodamine B (RhB) bonded to another mouse monoclonal PSA antibody (8A6) was chosen as the acceptor (RhB-8A6). PSA mediated FRET from the pre-excited PLNP-PS6 to RhB-8A6, and resulted in an

increase of the ratio of the luminescence intensity of RhB (at 585 nm) to the luminescence intensity of PLNP (at 524 nm) as the concentration of PSA increased, allowed sensitive and selective ratiometric photoluminescent detection of PSA in serum and cell extracts (Figure 11).

In 2014, Tang and co-workers [71] used a similar strategy to evaluate *in vitro* and *in vivo* the concentration of glutathione (GSH) which is one of the most prevalent small thiol molecule in living cells [72]. The role of GSH is to maintain a cellular reducing environment, cellular signal transduction, and gene regulation [73]. Moreover, GSH is an important antioxidant capable of trapping free radicals, thereby effectively protecting the cells from oxidative stress [74]. Changes in the level of GSH have been associated with a variety of human diseases, including liver damage, lung disease, Parkinson's disease, AIDS and cancer. For that purpose, the authors used the Eu<sup>2+</sup> and Dy<sup>3+</sup> doped Sr<sub>2</sub>MgSi<sub>2</sub>O<sub>7</sub> PLNPs as reported in Figure 12 for *in vitro* and *in vivo* assays.

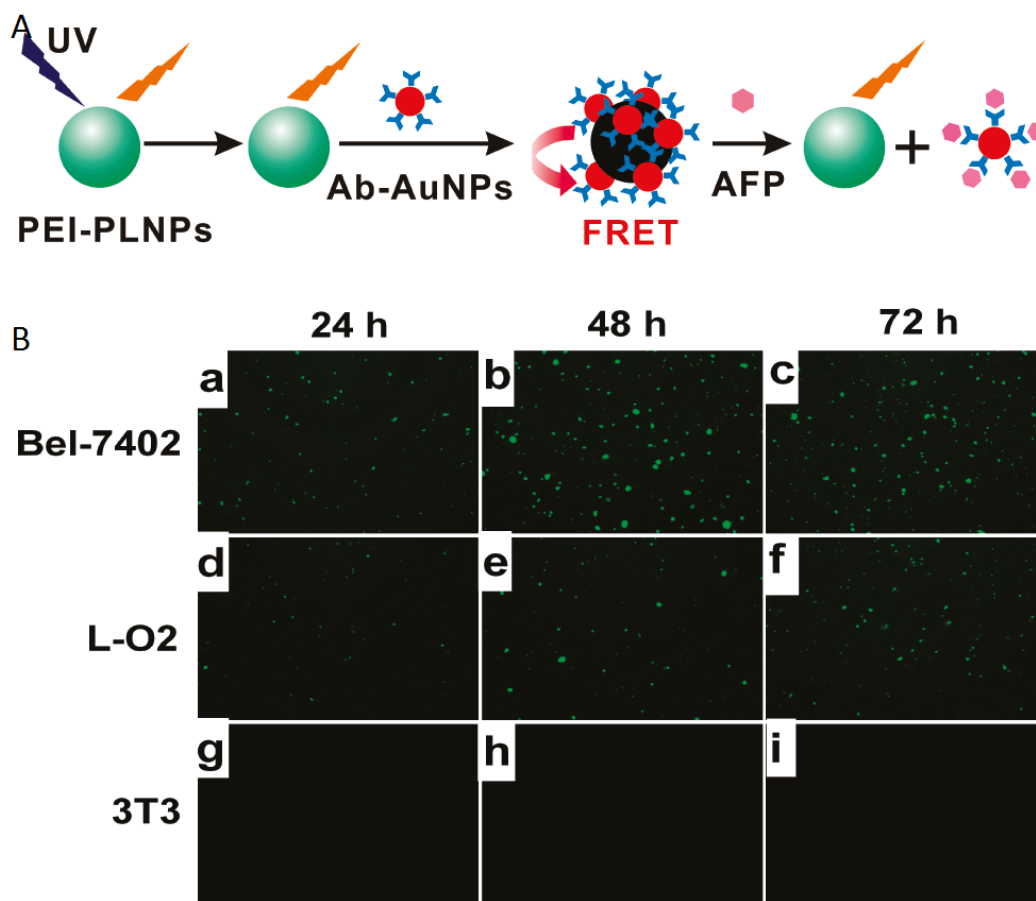
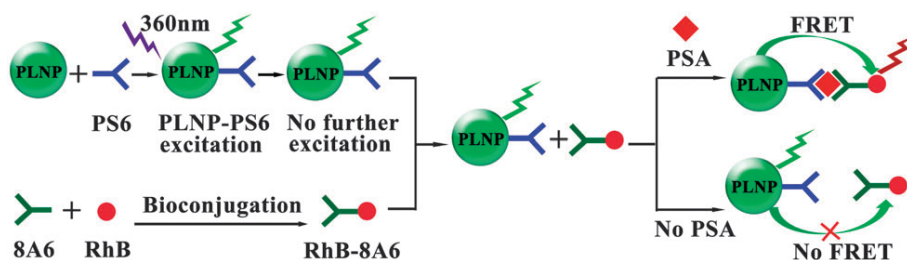


**Figure 10.** Principle of *in vitro* detection of AFP using modified PLNPs. (A) Schematic illustration of the FRET inhibition assay for AFP based on the PL quenching of PEI-PLNPs by Ab-AuNPs. (B) (a-i) Fluorescence images of Bel-7402, L-O2, and 3T3 cells stained with the FRET inhibition probe (PEI-PLNPs/Ab-AuNPs) after the cells had been cultured for 22, 46, and 70 h, respectively. Reproduced with permission from reference [66].



Samples	Concentration (mean ± s, n = 3)/μg L <sup>-1</sup>	
	ELISA	Our method
Serum 1	11.4 ± 0.6	11.1 ± 0.2
Serum 2	14.3 ± 2.8	13.7 ± 0.3
Serum 3	22.6 ± 1.9	21.3 ± 0.5
Serum 4	31.0 ± 4.1	29.3 ± 0.6
Serum 5	42.2 ± 10.2	39.4 ± 1.1
Serum 6	36.5 ± 7.9	37.6 ± 1.7
Serum 7	21.4 ± 4.2	19.8 ± 0.4
Serum 8	25.2 ± 6.2	25.6 ± 0.8
PC-3	10.7 ± 1.8	10.4 ± 0.3
RWPE-1	nd <sup>a</sup>	nd

<sup>a</sup> Not detected.

**Figure 11.** Schematic illustration of the PLNP based FRET immunoassay conception for PSA detection (up) and analytical results for the determination of PSA in real samples (down). Reproduced with permission from reference [68].

Using a similar strategy, the same group used the same PLNPs to detect ascorbic acid (AA). AA is an essential micronutrient required for numerous physiological and biochemical functions in the human body and is a potent water-soluble antioxidant capable of readily scavenging a number of reactive species and effectively protecting other biomolecules from oxidative damage [75]. For that purpose the authors functionalized the surface of their PLNPs with cobalt oxyhydroxide (CoOOH) [76]. When CoOOH was adsorbed on the surface of the PLNPs, the luminescence of the PLNPs was quenched. However, in the presence of AA, and only with AA, CoOOH was reduced to  $\text{Co}^{2+}$  and the luminescence of PLNPs was restored (see Figure 13).

The authors also assessed the ability of the nanoprobe to image AA in a mouse model. When an AA solution was added prior to CoOOH-modified PLNPs (excited by a 365 nm UV lamp for 10 min before injection), the luminescence of the nanoprobe could be collected without excitation as shown in Figure 13.

In 2015, Ju and co-workers reported the use of  $\text{Sr}_{1.6}\text{Mg}_{0.3}\text{Zn}_{1.1}\text{Si}_2\text{O}_7$  nanoparticles doped with  $\text{Eu}^{2+}$  and  $\text{Dy}^{3+}$  to design a time-resolved fluorescence resonance energy transfer (TR-FRET) platform for biosensing, lifetime imaging of cell apoptosis and *in situ* lifetime quantification of intracellular caspase-3 [77]. For that purpose, three kinds of PLNPs-based nanoprobes were covalently linked with dye-labelled peptides or DNA to carboxyl-functionalized PLNPs for the efficient detection of caspase-3, microRNA and platelet-derived growth factor (PDGF). The peptides-functionalized nanoprobe was also employed for fluorescence lifetime imaging to monitor cell apoptosis, which showed a dependence

of cellular fluorescence lifetime on caspase-3 activity and thus leads to an *in situ* quantification method. This work provided a proof-of-concept for PLNPs-based TR-FRET analysis and demonstrated its potential in exploring information of life process (Figure 14).

### Chromium-doped gallium oxide PLNPs

One limit of the first generation of PLNPs presented in the section II, made with silicate matrix and doped with different ions, was the relative short delay of luminescence after excitation, few hours, which could be a problem for some *in vivo* applications such as for passive tumour imaging which often requires to follow the probe for at least 5 hours and also to follow the probe over very long term (days, weeks). To do so, a strategy followed by several research groups was to change both the matrix and the luminescent ions.

### $\text{ZnGa}_2\text{O}_4:\text{Cr}$

The main limit of the first generation of PLNPs previously presented is that the nanoprobes (silicates) could only be excited *ex vivo* by ultraviolet light before the systemic administration, which prevents long term imaging in living animals. Thus, this type of PLNPs do not enable for example *in vivo* tumour homing strategies such as those relying on slow accumulation of stealth nanocarriers within malignant stroma by the enhanced permeability and retention effect [78,79]. Depending on the nanoparticle characteristics, such retention processes usually require from 2 to 24 hours [80,81]. This is far too long in relation to the emission from PLNPs, which hardly exceeds 1 to 3 hours *in vivo*.

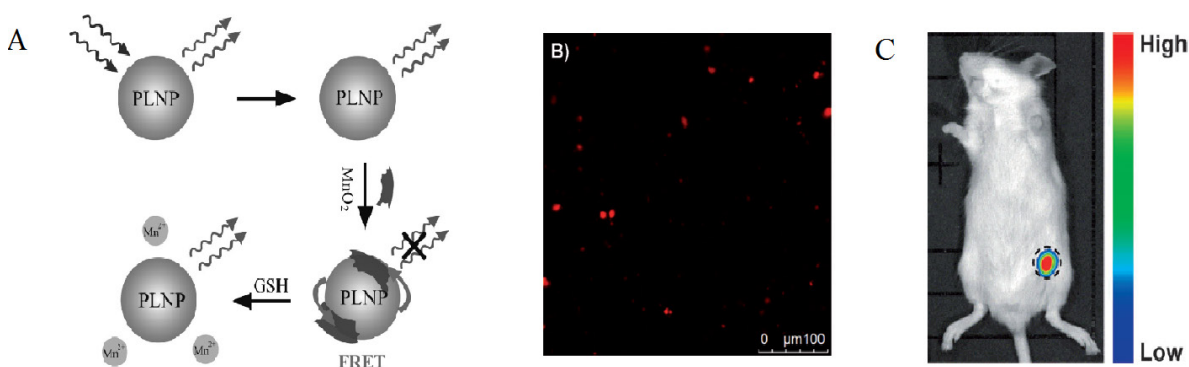


**Figure 12.** Detection of GSH *in vitro* and *in vivo* using PLNPs and FRET. (A) Schematic illustration of the design for GSH detection using  $\text{MnO}_2$  modified PLNPs. (B) *In vitro* PL image of GSH in RAW 264.7 macrophages. (C) *In vivo* PL image of the sample without excitation. The concentration of the nanoprobe was  $1 \text{ mg}\cdot\text{mL}^{-1}$ . The PL signals were collected at  $520 \pm 20 \text{ nm}$ . The centre of the black dashed circle is the injection site. Reproduced with permission from reference [71].

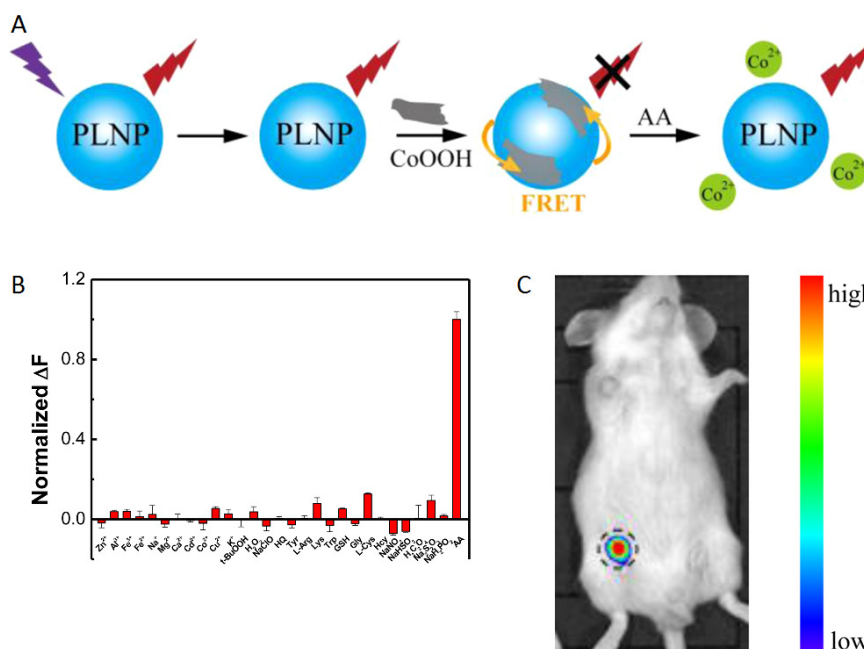


**Figure 13.** *In vitro* and *in vivo* detection of AA using modified PLNPs. (A) Schematic Illustration of the Design for AA Detection Using CoOOH-Modified PLNPs. (B) PL response of CoOOH-modified PLNPs solutions in the presence of different electrolytes and biomolecules. (C) Persistent luminescence image of the mouse injected with 0.1 mL of AA (0.1 mol/L) and the nanoprobe (right). Reproduced with permission from reference [75].

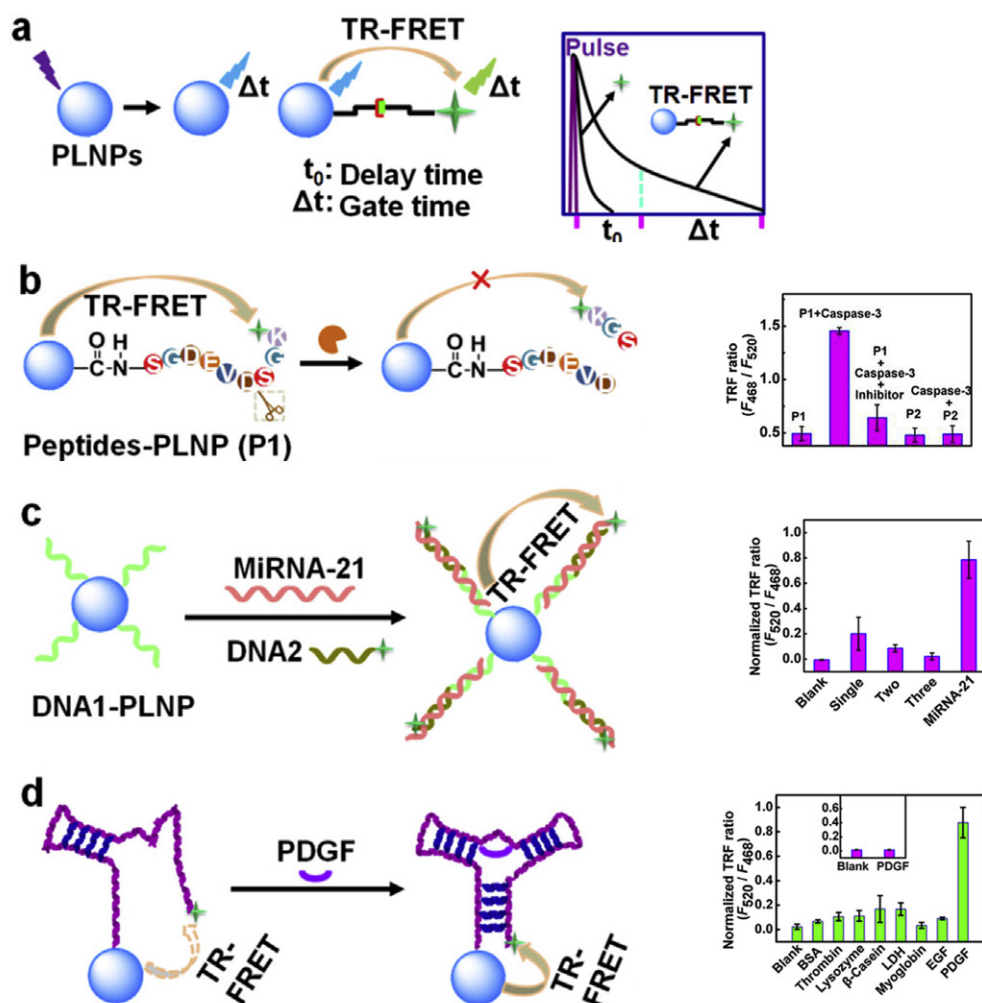


**Figure 14.** Schematic illustration for (a) PLNPs-based TR-FRET principle, (b–d) TR-FRET detection strategies of caspase-3 protease, miRNA-21 and PDGF protein by using caspase-specific peptide, DNA and aptamer-functionalized PLNPs probes. Reproduced with permission from reference [77].

To overcome this major restriction, efforts to unravel the mechanism of persistent luminescence have resulted in optimized compositions. In particular, bulk powder from trivalent chromium doped gallate ( $\text{ZnGa}_2\text{O}_4:\text{Cr}^{3+}$ ) has attracted serious attention, owing to its bright NIR persistent luminescence after ultraviolet excitation [82]. As can be seen on Figure 15A, this material has several excitation peaks, with one being at the limit of the tissue transparency window (rectangle with hatching). In 2014, Maldiney et al prepared nanosized  $\text{ZnGa}_2\text{O}_4:\text{Cr}$  (ZGO) and observed that the persistent luminescence also occurred *in vivo* after activation with visible orange/red light-emitting diodes (LEDs). In such conditions, there was no more time limit and the probe could be detected *in vivo* whenever wanted through a simple 2 minutes' excitation with the LEDs [83,84] (Figure 15C).

Such ZGO nanoparticles were synthesized by hydrothermal method and low-temperature sintering in air. First, gallium nitrate was formed by reacting gallium oxide with concentrated nitric acid under hydrothermal condition at  $150^\circ\text{C}$  overnight. Then, a mixture of chromium nitrate and zinc nitrate in water was added to the previous solution of gallium nitrate

under vigorous stirring. The resulting solution was adjusted to pH 7.5 with an ammonia solution and stirred for 3 hours at room temperature, and transferred into a 25 mL Teflon-lined stainless steel autoclave for 24h heat treatment at  $120^\circ\text{C}$ . The resulting compound was washed several times with water and ethanol before drying at  $60^\circ\text{C}$  for 2 hours. The dry white powder was finally sintered in air at  $750^\circ\text{C}$  for 5 hours. Hydroxylation was performed by basic wet grinding of the powder with a mortar and pestle in NaOH solution, and overnight vigorous stirring of the resulting suspension at room temperature. Finally, nanoparticles with a diameter of 60 nm were selected from the whole polydisperse colloidal suspension by centrifugation at 4500 rpm for 5 minutes.

The authors compared the optical performances of this nanoprobe to commercial quantum dots (QDs), emitting at the same wavelength and with the same coating, after a local injection (Fig 16a) of the same weight of probe in leg muscle or into the tail vein of healthy mice *in vivo* (Fig 16b). As could be seen on Figure 16, in both cases, signals with higher target to background ratio (TBR) have been obtained when using the ZGO PLNPs.

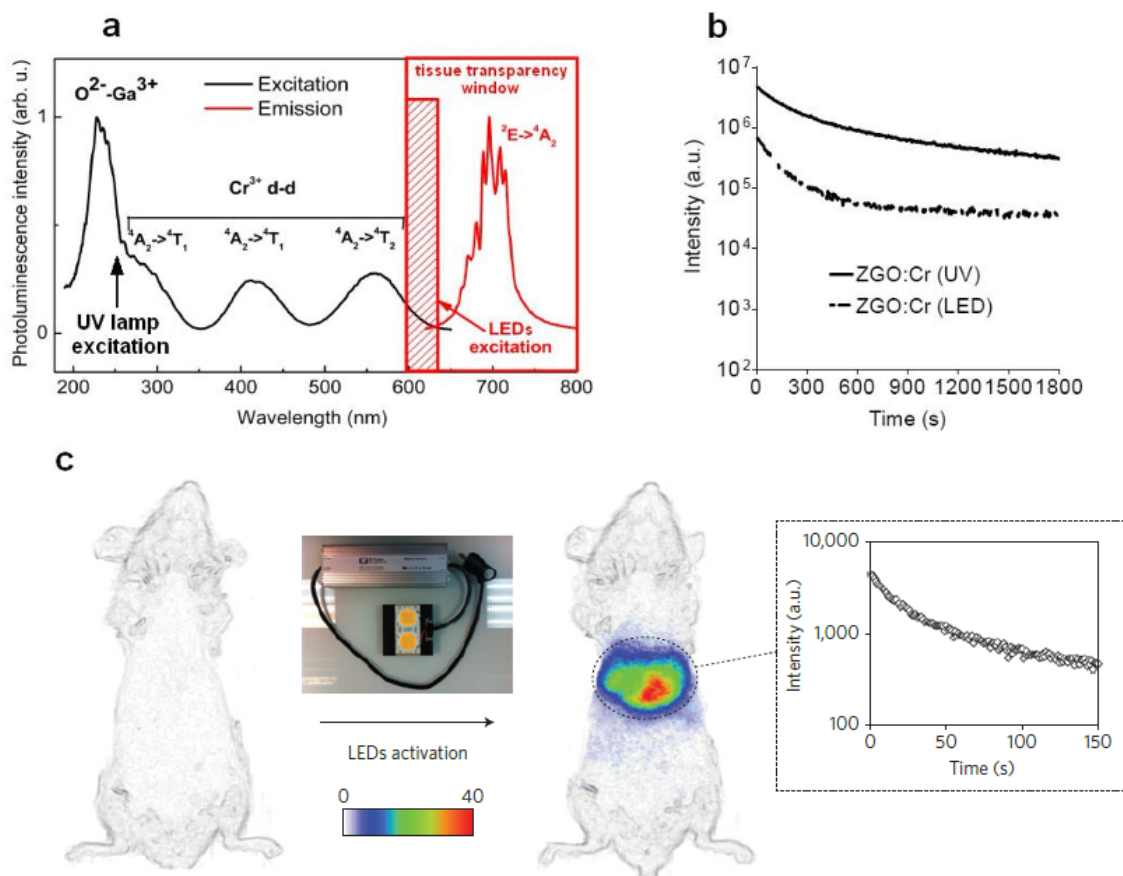


**Figure 15.** (A) PL excitation (black line) and emission (red line) spectra of  $\text{Cr}^{3+}$  doped ZGO. (B) Room-temperature persistent luminescence decay curves of ZGO obtained with two different excitations for 2 min under either UV light or a LEDs array source. (C) Persistent luminescence was activated through living tissues following a 2 min orange/red LEDs excitation, and immediately acquired for 3 min under the photon counting system. The inset shows a persistent luminescence decay curve corresponding to the signal from the liver. Reproduced with permission from reference [83].

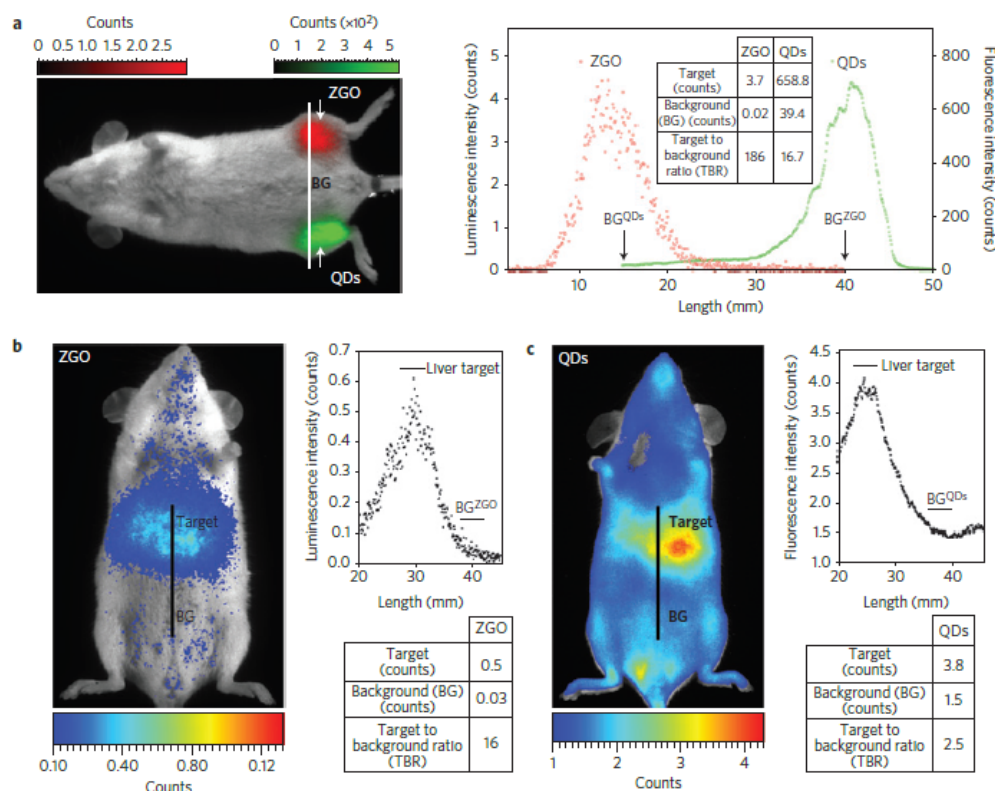


**Figure 16.** *In vivo* comparison of negatively charged QDs and PLNPs. (A) After intramuscular injection and (B-C) after intravenous injection in healthy mice. The experiments were conducted by injecting the same amount (50  $\mu\text{g}$  per mouse) of QDs (C) and PLNPs (B). Reproduced with permission from reference [83].

The same group then developed a process to get stealth ZGO able to stay for a long time into the blood. In particular, widespread preclinical studies *in vivo* unraveled the difficult task of controlling the biodistribution of nanoparticles, following intravenous injection in living animals, whose physiological path through systemic circulation generally leads to a rapid sequestration by macrophages from the mononuclear phagocyte system (MPS), also referred to as the reticuloendothelial system (RES) [85]. For that purpose a two steps process based on a first reaction with 3-aminopropyltriethoxysilane (APTES) either for three or six hours followed by a second reaction for 16 hours with PEG<sub>5000</sub> kDa-NHS was developed [86,87,88,89,90,91] (Figure 17A). As could be seen on Figure 17, the first reaction governs the ability of PEGylated ZGO to stay for a short or longer time in the blood (Figure 17, B-D). They authors have also shown that when such stealth ZGO were injected to tumour bearing mice, the tumours could be easily detected 6 hours after the injection of the probe and through an activation using the LEDs (Figure 17E).

The same group also showed that the luminescence of such nanoparticles after visible LEDs excitation could be used to monitor labelled cells (Figure 18A) after intravenous injection (Figure 18B),

or to follow the probe after oral administration, either in the form of a small pellet (Figure 18C) or as a suspension (Figure 18D) [83].

### LiGa<sub>5</sub>O<sub>8</sub>:Cr<sup>3+</sup>

Most PLNPs developed for bioimaging used thermoluminescence (the body temperature of the animal) to detrapp electrons responsible for light emission. In 2013, Pan and co-workers developed PLNPs which can be detrapped by photostimulation [92]. In conventional photostimulable storage phosphors, the optical signal stored either after X-ray or UV irradiation can be released as a visible photostimulated luminescence (PSL) signal under the stimulation of a low-energy light with appropriate wavelength. In their work, the authors reported a new optical read-out form, photostimulated persistent luminescence (PSPL) in the near-infrared (NIR), from a Cr<sup>3+</sup> doped LiGa<sub>5</sub>O<sub>8</sub> NIR persistent phosphor exhibiting a super-long NIR persistent luminescence of more than 1000 hours (when looking at discs made with such PLNPs). An intense PSPL signal peaking at 716 nm can be repeatedly obtained in a period of more than 1000 hours when an UV light pre-irradiated LiGa<sub>5</sub>O<sub>8</sub>:Cr<sup>3+</sup> phosphor is repeatedly stimulated with a visible light or a NIR light (Figure 19A). Such phosphor has promising applications in optical

information storage, night vision surveillance, but also for *in vivo* bioimaging. For that application,  $\text{LiGa}_5\text{O}_8:\text{Cr}^{3+}$  nanoparticles were synthesized by a sol-gel method followed by calcination in a muffle furnace at  $1100^\circ\text{C}$  for 3 to 5 hours.  $\text{LiGa}_5\text{O}_8:\text{Cr}^{3+}$  nanoparticles with diameters in the range of 50-150 nm were obtained following centrifugation and filtration. The authors used such probe for cell labelling and monitoring after small animal local injection. Before that, the nanoparticles that have been first coated with a cationic polymer (polyethylenimine, PEI, MW: ~25000). PEI, as a polycationic molecule, is known to aid cell uptake of

nanoparticles via endocytosis [93, 94].  $\text{LiGa}_5\text{O}_8:\text{Cr}^{3+}$  nanoparticles were dispersed in PEI and then stirred for two days. The raw PEI coated  $\text{LiGa}_5\text{O}_8:\text{Cr}^{3+}$  nanoparticles ( $\text{PEI}/\text{LiGa}_5\text{O}_8:\text{Cr}^{3+}$ ) were washed with water and collected by centrifugation. The purified  $\text{PEI}/\text{LiGa}_5\text{O}_8:\text{Cr}^{3+}$  nanoparticles were dispersed in PBS. A total of  $10^6$  murine breast cancer 4T1 cells were seeded and cultured in RPMI-1640 medium and  $100 \mu\text{g}/\text{ml}$   $\text{PEI}-\text{LiGa}_5\text{O}_8:\text{Cr}^{3+}$  at  $37^\circ\text{C}$  for two days. The labelled cells were then subcutaneously injected into athymic nude mice and monitored *in vivo* using a white LED flashlight for the PSPL phenomenon (Figure 19B).

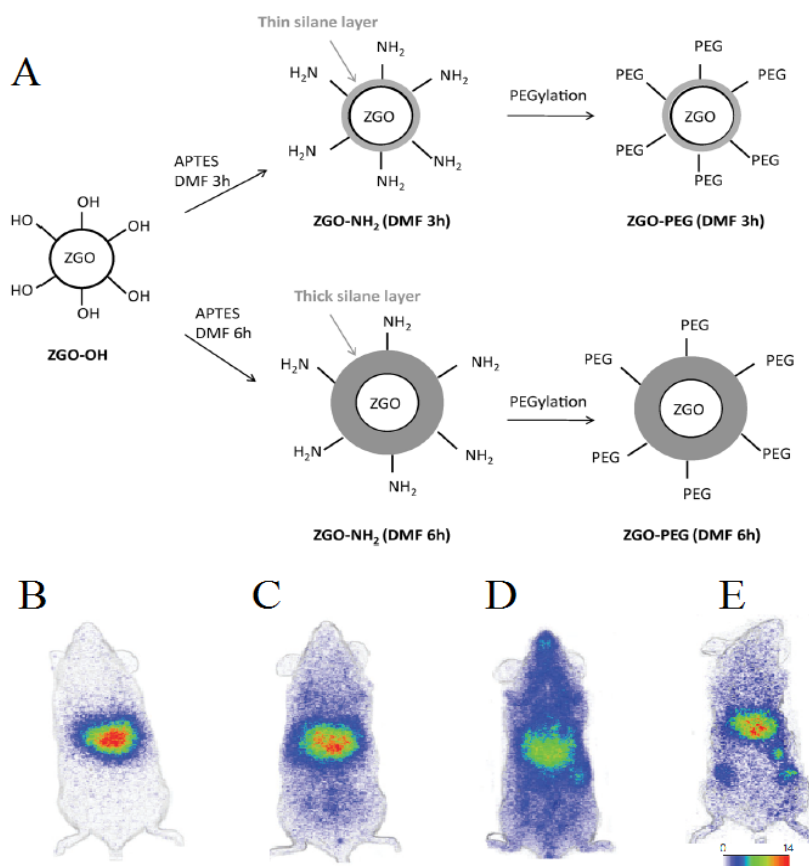


**Figure 17.** (A) Representation of ZGO functionalization routes with APTES and PEG<sub>5000kDa</sub>. (B) *In vivo* biodistribution in healthy mice of ZGO-OH, (C) ZGO-PEG<sub>3h</sub>, (D) ZGO-PEG<sub>6h</sub>, and of ZGO-PEG<sub>6h</sub> injected to tumor bearing mice (E). Reproduced with permission from reference [86].

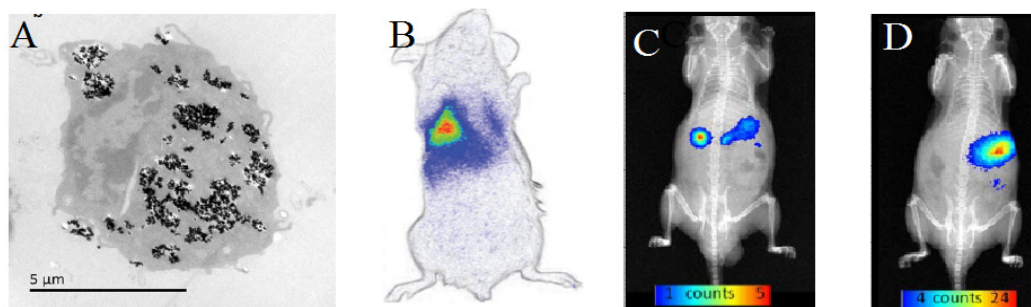


**Figure 18.** (A) ZGO-NH<sub>2</sub> PLNPs used for RAW cells labelling *in vitro* and cells tracking *in vivo* (B) or following oral administration (C-D). Reproduced with permission from reference [83].

In 2014, the same group also used  $\text{LiGa}_5\text{O}_8:\text{Cr}^{3+}$  (LGO:Cr) nanoparticles for cancer imaging. For this purpose, the nanoparticles were functionalized with polyvinylpyrrolidone (PVP) and human serum albumin (HSA), and then conjugated to c(RGDyK). c(RGDyK) is a small peptide with high affinity toward  $\alpha\text{v}\beta_3$  integrin, a tumor biomarker overexpressed on tumor vasculature and tumor cells of various types [95,96]. Figure 20 shows a tumor targeting study where c(RGDyK)-conjugated  $\text{LiGa}_5\text{O}_8:\text{Cr}^{3+}$  nanoparticles were intravenously injected into 4T1 tumor bearing mice. Good accumulation of the nanoparticles into the tumors could be observed after PSPL at 6 and 24 hours after injection (Figure 20) [97].

### Bimodal imaging

Multimodal imaging has drawn much attention in biomedical applications because it provides more accurate, complete, and reliable information on diagnosis [98]. Each imaging modality has its own advantages and disadvantages regarding sensitivity, spatial/temporal resolution, and penetration depth. The NIR optical imaging possesses the advantage of

high sensitivity but rather limited spatial resolution. In contrast, MRI provides excellent spatial resolution and unlimited depth penetration but remains at an inherently low sensitivity [99]. The combination of NIR emitting PLNPs and MRI contrast agent into one single nanopatform would offer attractive synergistic advantages in biomedical imaging with high sensitivity, good spatial resolution, high SNR, and no ionizing radiation.

In 2015, Maldiney et al reported a method to prepare PLNPs-based bimodal imaging agent. In their strategy, instead of using the surface of the PLNPs to link DTPA-Gd complexes, the authors incorporated various amount of  $\text{Gd}^{3+}$  ions at the beginning of the synthesis, by substituting  $\text{Ga}^{3+}$  ions. In such conditions, a negative contrast was obtained, with a  $r_2$  value close to  $60 \text{ mM}^{-1}\text{s}^{-1}$  (Figure 21A). Such nanomaterials have been intravenously injected to healthy mice, giving both optical imaging (Figure 21B) and negative MRI contrast into the liver (Figure 21C-E) [100].

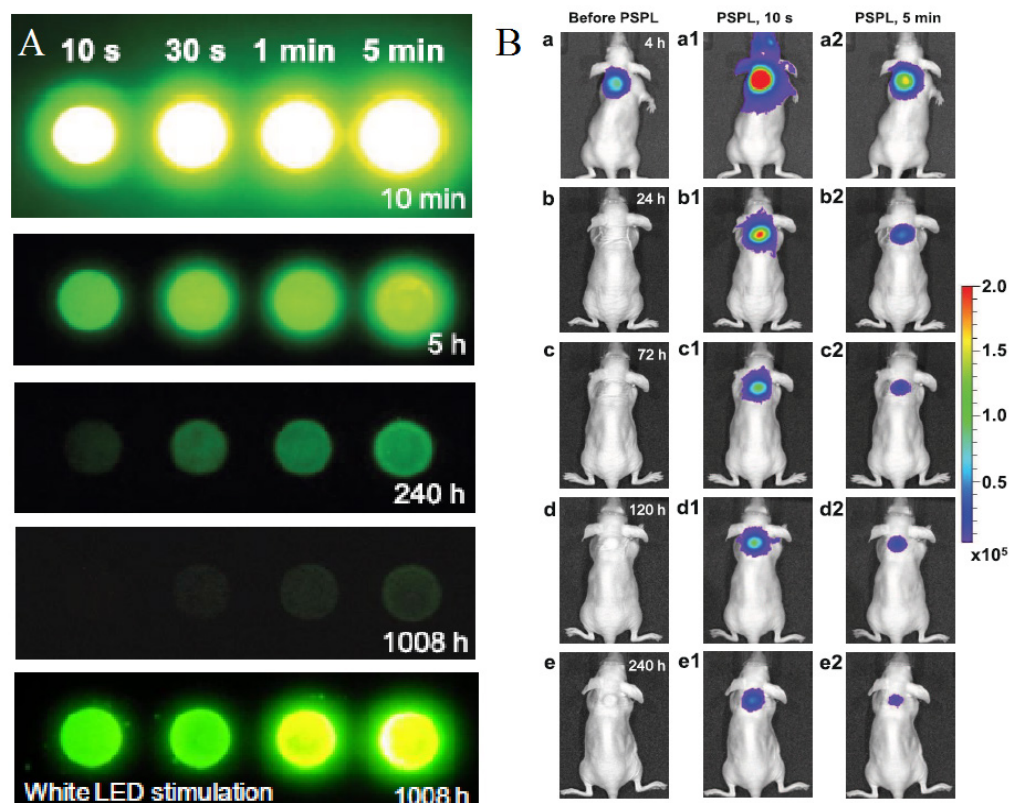


**Figure 19.**  $\text{LiGa}_5\text{O}_8:\text{Cr}^{3+}$  PLNPs used for *in vivo* PSPL experiments with labelled cells. (A) NIR images of four phosphor discs taken at different persistent luminescence times (10 min to 1,080 h) after irradiation by a 254 nm lamp for 10 s to 5 min. (B) The PEI- $\text{LiGa}_5\text{O}_8:\text{Cr}^{3+}$  nanoparticles labelled 4T1 cells ( $\sim 2.5 \times 10^7$  cells) were illuminated by a 4W 254 nm UV lamp for 15 min, and then subcutaneously injected into the back of a nude mouse. (a) Image taken at 4 h after cell injection. To get the PSPL signal, the mouse was exposed to a white LED for 15 s. (a1) and (a2), Images taken at 10 s and 5 min after the stimulation, respectively. The signals were attributed to PSPL. (b–e) The mouse was exposed daily to the LED flashlight for 15 s, and images were taken at 10 s and 5 min after the stimulation. All images were acquired in the bioluminescence mode with an exposure time of 2 min. Reproduced with permission from reference [92].

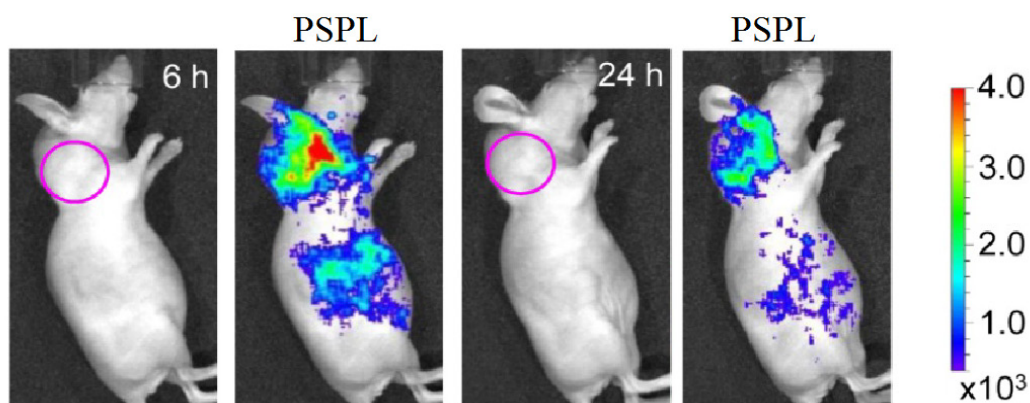


**Figure 20.** Active tumor targeting with c(RGDyK)-conjugated LGO:Cr nanoparticles in subcutaneous 4T1 tumor model. The c(RGDyK)-LGO:Cr nanoparticles were irradiated by a 254 nm UV lamp for 15 min before the intravenous injection. Luminescence images were acquired before (left) and after illuminating the mouse by a LED flashlight (for 15 s) at 6 h and 24 h after the cell injection. The tumor sites are indicated by pink circles. Reproduced with permission from reference [97].

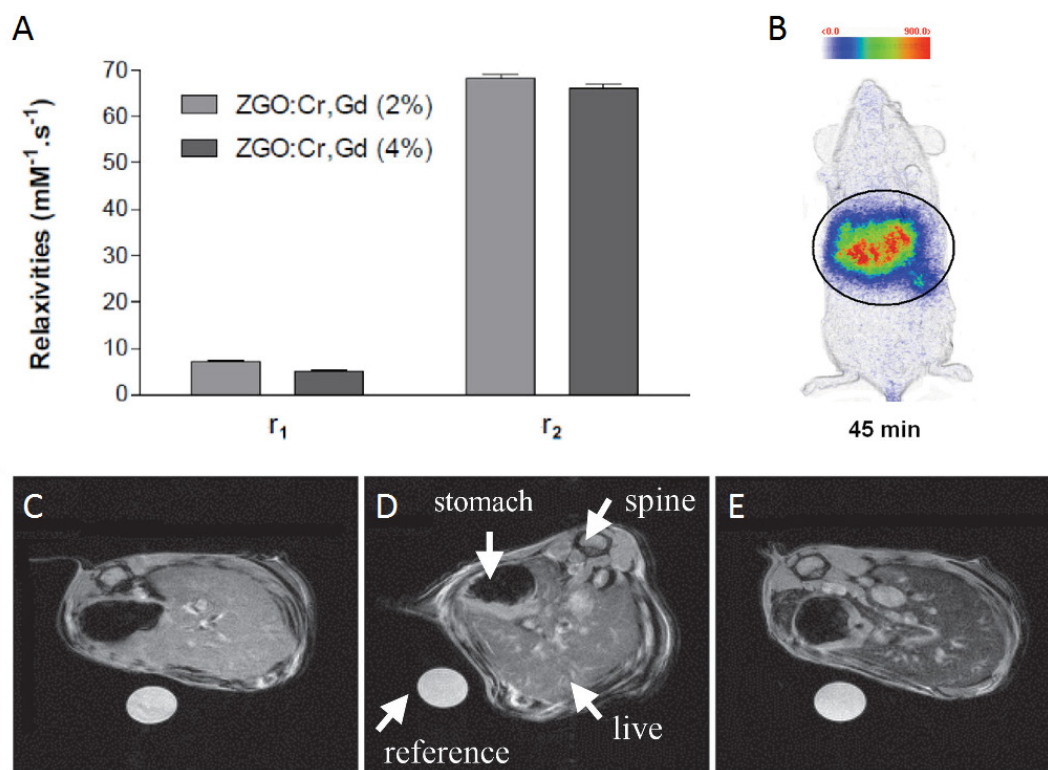


**Figure 21.** ZGO:Cr<sup>3+</sup>, Gd<sup>3+</sup> PLNPs as optical and negative MRI contrast agent. (A) Relaxivities  $r_1$  and  $r_2$  of ZGO nanoparticles suspended in NaOH at 7T. (B) Persistent luminescence images 45 minutes following the injection of UV-excited ZGO:Cr,Gd (4%) dispersed in 5% glucose solution. Black circle corresponds to a global region of interest comprising liver and spleen. (C-E) Magnetic resonance imaging of mice liver recorded at 7T. (C) Reference mouse before the injection of ZGO nanoparticles. (D) Reference mouse, 1 hour after the injection of ZGO:Cr,Gd (2%) nanoparticles. (E) Reference mouse, 1 hour after the injection of ZGO:Cr,Gd (4%) nanoparticles. Reproduced with permission from reference [100].

### Nanorods of Ga<sub>2</sub>O<sub>3</sub>:Cr<sup>3+</sup>

Most of nanoparticles have spherical shape. In 2015, Wang et al reported the synthesis @-Ga<sub>2</sub>O<sub>3</sub>: Cr<sup>3+</sup> nanorods. GaOOH: Cr<sup>3+</sup> was first synthesized through an improved hydrothermal process, in which both the reaction temperature and time decreased and wherein PEG<sub>400</sub> Da was employed as a template to orient the

attachment of GaOOH:Cr<sup>3+</sup>. After calcination of the obtained GaOOH: Cr<sup>3+</sup>, mesoporous @-Ga<sub>2</sub>O<sub>3</sub>:Cr<sup>3+</sup> nanorods were synthesized (Figure 22A). The authors have shown that the mesoporous nanoparticles could be loaded with doxorubicin, evaluated *in vitro* (Figure 22B-C) and followed *in vivo* (Figure 22D-E) [101].

## Multifunctional gallium oxides PLNPs incorporated into silica

### Size control

As seen before, NIR persistent phosphors crystal synthesis requires temperatures above 750 °C in traditional solid-state annealing reactions [102]. Moreover, to convert such bulk crystal into nanoparticles that are sufficiently dispersed for biological applications, certain tedious physical treatments such as grinding [38] or laser ablation [51] must be utilized. The afforded products are generally highly heterogeneous and suffer from severe agglomeration. In 2015, Han and co-workers proposed to use MSNs as a template to synthesize ZGC NIR persistent phosphors *in situ* with defined size and morphology (mZGC) [103]. Since temperatures beyond 750°C may lead to the collapse of the mesoporous silica nanostructures, the reaction temperature for the phosphor synthesis was explored systematically in their study. They found that at 600 °C, the as synthesized mZGC preserved defined size, morphology and mesoporous nanostructure of the MSNs as well as possessed optimal luminescence property. Moreover, the authors observed that mZGC were able to be repeatedly activated *in vivo* for persistent luminescence imaging in a mouse by using white LED as a light source (Figure 23).

### Drug delivery

Using mesoporous SiO<sub>2</sub> alone as a drug carrier it is impossible to monitor in real time or effectively locate a target site (i.e., tumor) due to the lack of detectable signals. In 2014, Maldiney et al introduce a multifunctional nanoplatform based on persistent luminescence nanoparticles for both *in vivo* optical imaging and drug delivery [104]. Taking advantage of the well-known biocompatibility of mesoporous silica and non-toxic ZGO, the authors modeled a novel core-shell structure on the basis of a hybrid chromium-doped zinc gallate/mesoporous silica architecture specifically designed to allow both highly sensitive optical detection through living tissues and concomitant drug delivery. Employing doxorubicin as a drug model for the purpose of this study, they demonstrate that these mesoporous persistent luminescence nanophosphors can be successfully loaded with an anticancer agent, and subsequently initiate its progressive release in a pH-sensitive manner. The use of such doxorubicin-loaded theranostic agent is finally shown to induce acute cytotoxicity toward U87MG cells *in vitro*, preserve persistent luminescence properties, and allow both sensitive and non-invasive localization of the carrier *in vivo* (Figure 24).

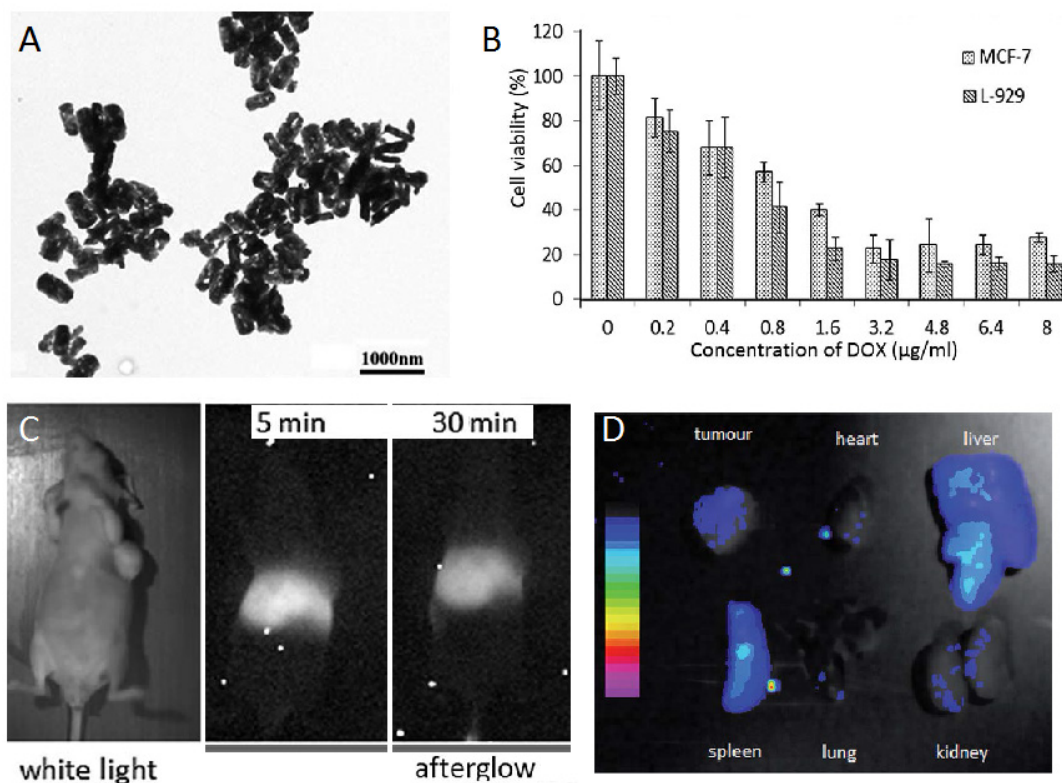


**Figure 22.** Nanorods of @-Ga<sub>2</sub>O<sub>3</sub>:Cr<sup>3+</sup> for drug loading and *in vivo* imaging. (A) TEM images of @-Ga<sub>2</sub>O<sub>3</sub>:Cr<sup>3+</sup> (B) Cells viabilities against DOX-loaded @-Ga<sub>2</sub>O<sub>3</sub>:Cr<sup>3+</sup> nanorod concentrations. (C) *In vivo* near infrared persistent luminescence images acquired after intravenous injection (D). Afterglow image of the isolated organs and tumour from a mouse bearing HeLa tumour 48 h post i.v. injection of @-Ga<sub>2</sub>O<sub>3</sub>:Cr<sup>3+</sup> re-excited by white light. Reproduced with permission from reference [101].

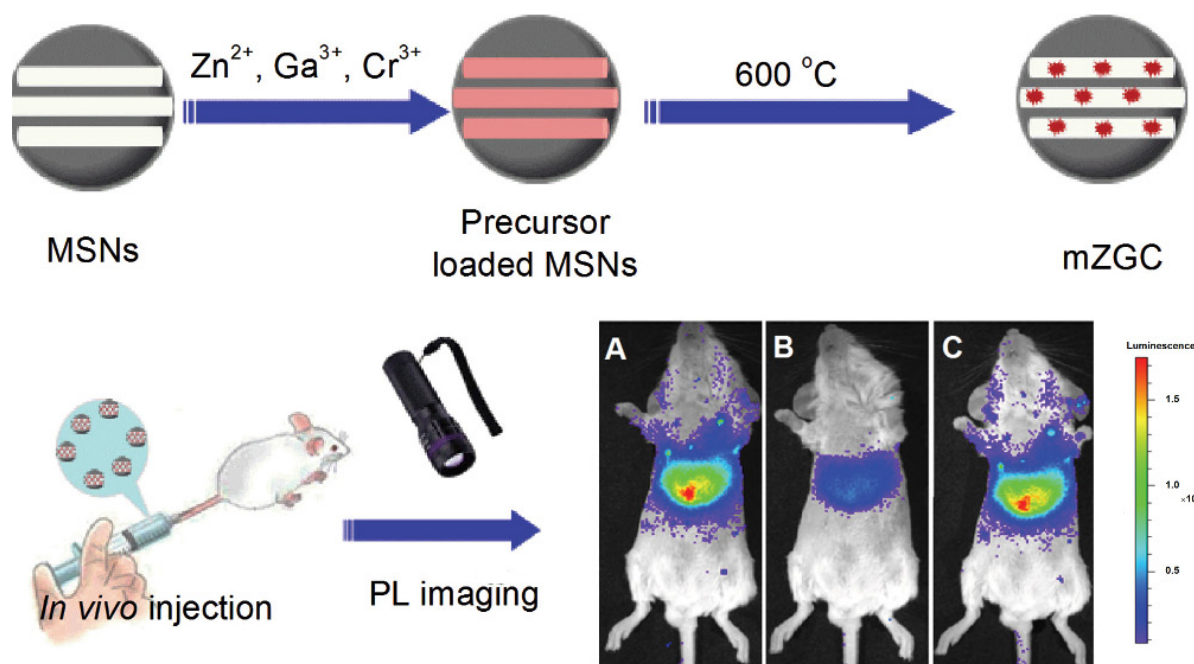


**Figure 23.** Illustration of the synthesis of controlled size mZGC using MSN template and their *in vivo* imaging application. *In vivo* recharging of mZGC for persistent luminescence imaging by using a white LED. (A) First charging, (B) 10 min after first charging, (C) second recharging. Reproduced with permission from reference [103].

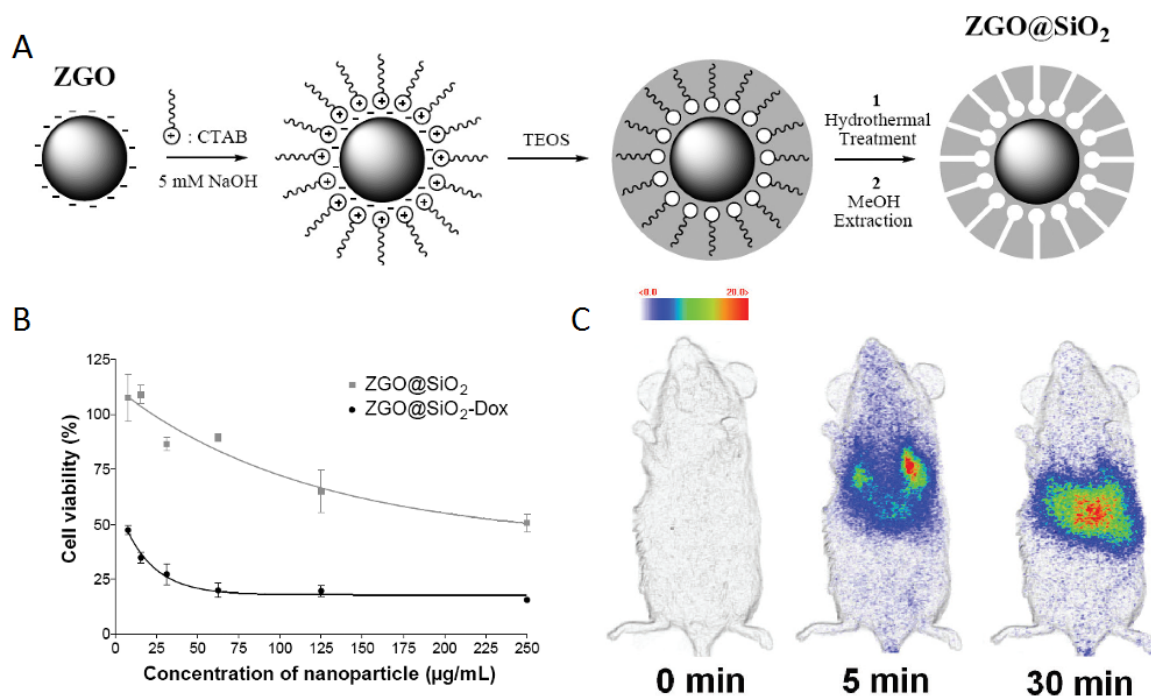


**Figure 24.** Mesoporous ZGO@SiO<sub>2</sub> for drug loading and *in vivo* imaging. (A) Schematic representation of ZGO@SiO<sub>2</sub> synthesis. (B) Relative cell viability of U87MG cells after a 24 hours incubation period with either ZGO@SiO<sub>2</sub> or ZGO@SiO<sub>2</sub>-Dox. (C) Persistent luminescence images up to 30 minutes after systemic injection to mouse. Reproduced with permission from reference [104].

As a single doped ion, Cr<sup>3+</sup> is an ideal candidate for obtaining red or NIR persistent luminescence since its 3d<sup>3</sup> electron configuration allows a narrow-band emission (695 nm) due to the spin forbidden <sup>2</sup>E → <sup>4</sup>A<sub>2</sub> transition or a broadband emission (ca. 650–1600 nm) ascribed to the spin-allowed <sup>4</sup>T<sub>2</sub> → <sup>4</sup>A<sub>2</sub> transition [79].

For further improving persistent luminescence properties, finding an appropriate co-dopant not only benefits optical properties but also contributes to revealing important information on the mechanism. In 2016, Zhang and co-workers reported the improvement of red PLNPs Zn<sub>0.97</sub>Ga<sub>2</sub>O<sub>3.97</sub>:Cr<sup>3+</sup>, Bi<sup>3+</sup>

(ZGOCB) by a biphasic synthesis route [105]. Meanwhile, mesoporous  $\text{SiO}_2$  was also employed as a drug carrier and as a morphology controlling template to design the core/shell structure nanoprobe  $\text{Gd}_2\text{O}_3@m\text{SiO}_2/\text{ZGOCB}$ . Due to the presence of  $\text{Gd}_2\text{O}_3$ ,  $\text{Gd}_2\text{O}_3@m\text{SiO}_2/\text{ZGOCB}$  also possesses magnetic properties, which indicates that it can also be used as an MRI agent (longitudinal contrast agent). Moreover, through appropriate surface functionalization with folic acid (FA) as a tumor targeting group,  $\text{Gd}_2\text{O}_3@m\text{SiO}_2/\text{ZGOCB}$  shows tumor targeting ability both *in vitro* and *in vivo* with a high SNR. Employing doxorubicin (Dox) as a drug model, the authors also demonstrate that this nanoprobe can be successfully loaded with an anticancer agent and can subsequently initiate its progressive release *in situ* to cure tumors (Figure 25).

### Magnetic targeting

*In vivo*, the spatial resolution of optical imaging remains low because of light scattering. As discussed above in the manuscript, a solution to this problem would be to prepare a multimodal nanoprobe associating optical imaging to magnetic resonance imaging (MRI) [97]. There are many reasons why MRI is preferred as a complementary modality to optical imaging in multimodal nanotools. First, while this technology shows a high spatial resolution, similar to the ones obtained with computed tomography X-rays or positron emission tomography (PET), MRI is harmless to the patient whereas the two other technologies are based on ionizing radiations. Furthermore, PET requires radiolabelled substances and is consequently costly and logistically complex. Additionally, many MRI active moieties have been recently introduced, leading to the development of multimodal nanoprobe combining optical imaging and a MRI contrast agent such as gadolinium

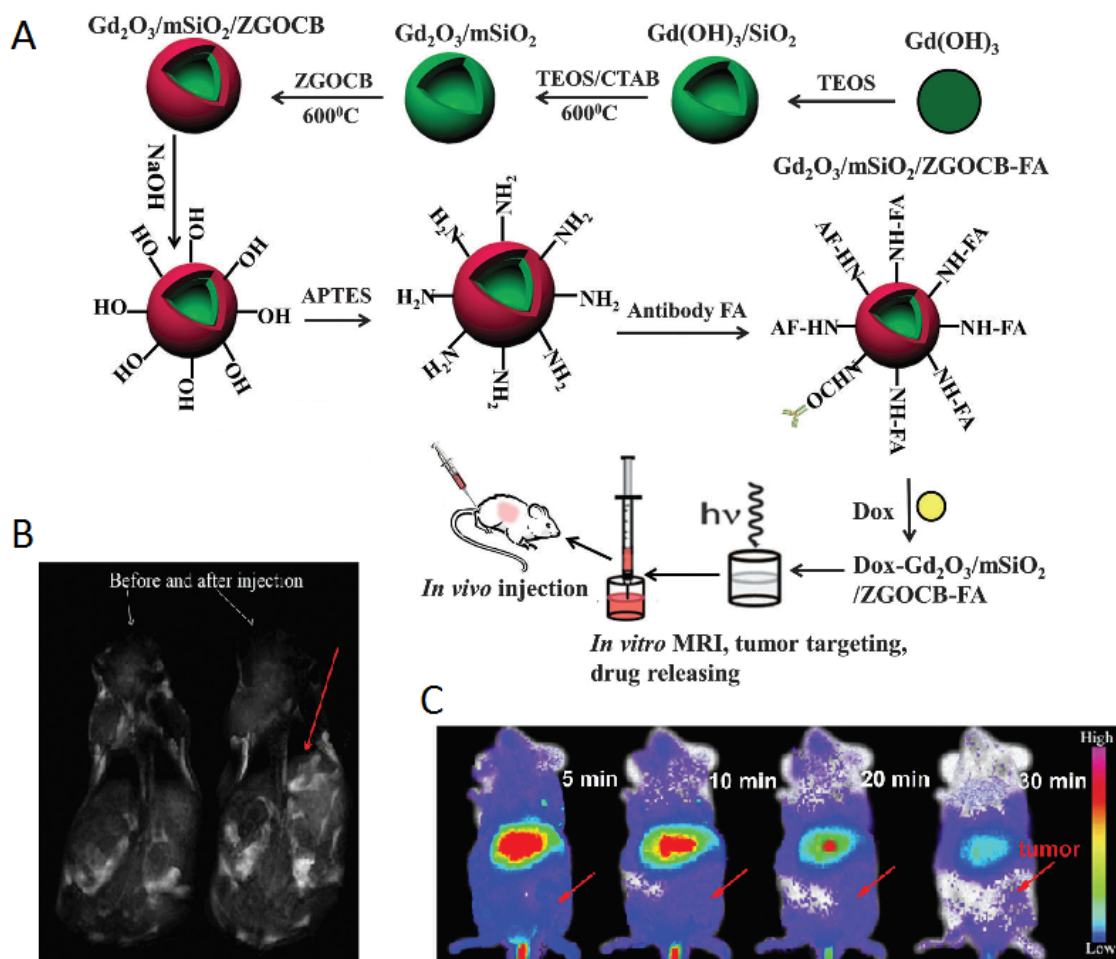


**Figure 25.** (A) Schematic illustration of the synthesis, surface functionalization and application of the core/shell structure nanoprobe  $\text{Gd}_2\text{O}_3@m\text{SiO}_2/\text{ZGOCB}$ . (B)  $T_1$ -weighted MR images of a mouse before (left) and after (right) intravenous injection of  $\text{Gd}_2\text{O}_3@m\text{SiO}_2/\text{ZGOCB}$ -NH<sub>2</sub> (0.15 mg), the red arrow shows the liver. (C) *In vivo* luminescence images of H22 tumor bearing mice (a) and normal mice (b) after intravenous injection of Dox-Gd<sub>2</sub>O<sub>3</sub>@mSiO<sub>2</sub>/ZGOCB-FA. (D) *Ex vivo* image of liver, spleen, kidneys, heart, lung and tumor corresponding biodistribution for each organ 6 h after systemic injection. Reproduced with permission from reference [105].

complexes or ultrasmall superparamagnetic iron oxides (USPIOs) [106]. In 2015, Teston et al reported the first synthesis of mesoporous nanohybrids (MPNHs) composed of a combination of PLNPs and USPIOs embedded in a mesoporous silica structure, their full optical and magnetic characteristics and *in vivo* detection (Figure 26) [107].

### Synthesis of small ZGO

The different synthesized PLNPs presented before are usually in the range of 40-150 nanometers with a polydispersed size distribution. The main reason for the polydispersity is due to non-control over the nanoparticle growth stage and agglomeration in commonly used hydrothermal or sol-gel synthetic procedures. Therefore, there was a need to develop new synthesis approaches for persistent luminescent NPs with size control. In 2015 Mao and co-workers reported the first successful synthesis of sub-ten nanometer persistent luminescent Cr doped ZnGa<sub>2</sub>O<sub>4</sub> NPs via a biphasic hydrothermal route [108]. In their work, the authors used a biphasic hydrothermal approach for the synthesis of Cr doped ZnGa<sub>2</sub>O<sub>4</sub> NPs with controlled size through the hydrolysis of corresponding inorganic salts in a

water-toluene system. The synthetic procedure is shown in Figure 29a. Typically, Zn(NO<sub>3</sub>)<sub>2</sub>, Ga(NO<sub>3</sub>)<sub>3</sub>, Cr(NO<sub>3</sub>)<sub>3</sub> (0.2 mol% with respect to Ga) were dissolved in water, followed by the addition of *tert*-butylamine to adjust the pH of the solution to the desired value, and then stirred for 30 minutes. After that, the solution was mixed with an organic solution of oleic acid and toluene. The resulting mixture was transferred to a 45 mL Teflon-lined stainless steel autoclave in ambient environment without stirring. The sealed autoclave was heated at 160°C for 24 hours (Figure 27a). The purified products were separated by centrifugation and can be easily re-dispersed in a variety of nonpolar solvents (e.g., toluene, hexane, and chloroform) and show transmission electron microscopy (TEM) images of the as-synthesized Cr:ZnGa<sub>2</sub>O<sub>4</sub> NPs (Figure 27b). These images clearly show that these NPs are nearly monodisperse with sub-10 nm size (6 nm). The crystal phase was further confirmed by XRD (Figure 27c). Such particles have the same optical characteristics as the previous larger ones in term of excitation/emission properties (Figure 27d) and display persistent luminescence decay (Figure 27e) [108].

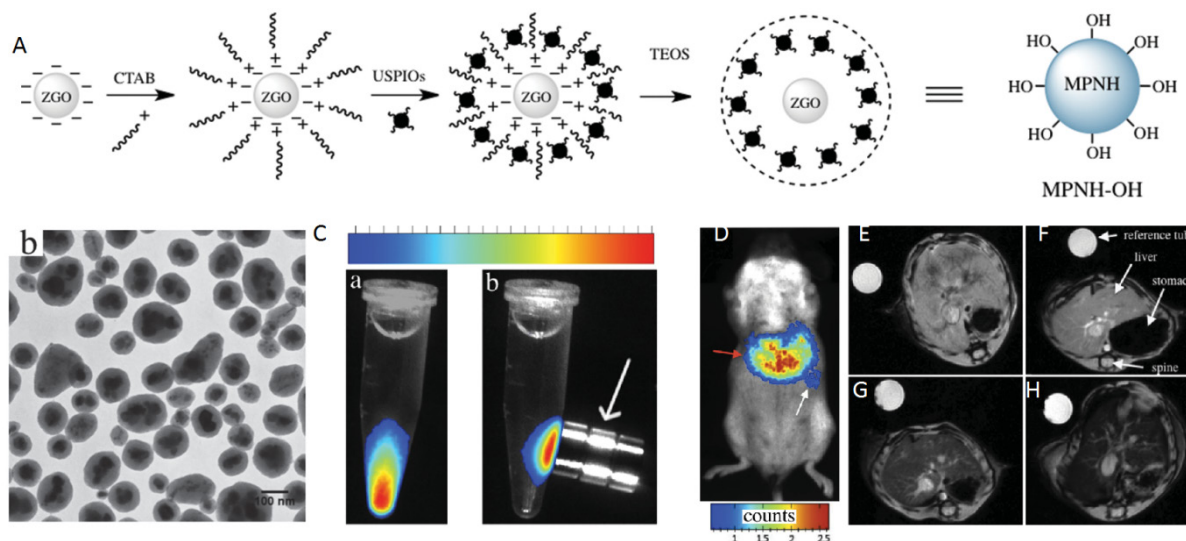


**Figure 26.** (A) Schematic representation of the synthetic route to prepare MPNHs-OH. (B) TEM characterization of non-functionalized MPNH-OH. (C) Luminescence detection of nanoparticles suspension before (a) and after (b) application of an external magnetic field. (D) MPNH-COOH biodistribution assessed by optical imaging 10 min after systemic injection. (E-H) T<sub>2</sub>\*-weighted MRI-based detection of MPNHs-COOH *in vivo*. (E) Abdominal cross-section of a mouse showing liver before MPNHs-COOH injection. (F-H) Respective abdominal cross-sections of mice after MPNH<sub>0</sub>, MPNH<sub>1</sub>, MPNH<sub>3</sub>-COOH injections showing liver contrast evolution. Reproduced with permission from reference [107].

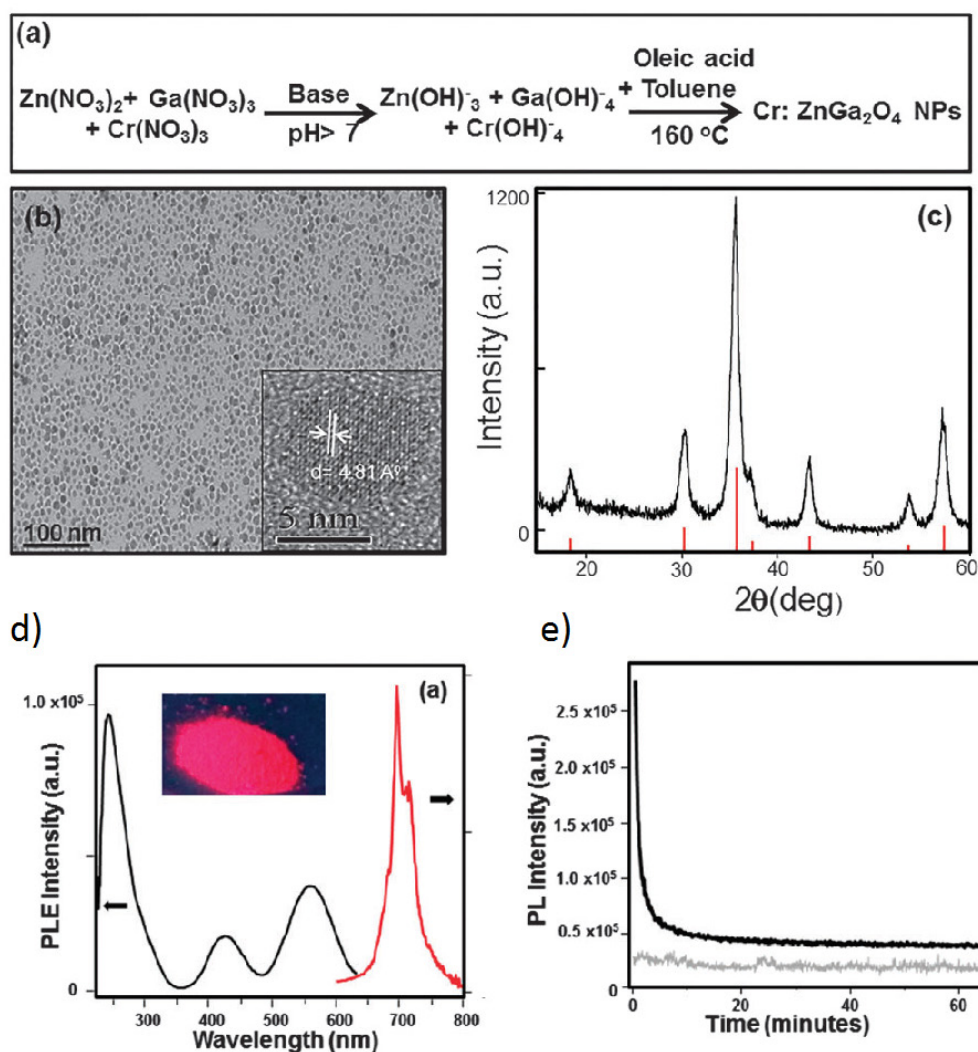


**Figure 27.** (a) Schematic of the synthetic procedure of sub-10 nm size Cr doped  $\text{ZnGa}_2\text{O}_4$  NPs. (b) Typical TEM image showing nearly monodispersed Cr doped  $\text{ZnGa}_2\text{O}_4$  NPs dispersed in hexane. The inset is a HRTEM image from a single nanoparticle. (c) XRD pattern of the as-synthesized Cr doped  $\text{ZnGa}_2\text{O}_4$  NPs (black curve) matching well with the diffraction pattern of corresponding spinel  $\text{ZnGa}_2\text{O}_4$  (red lines, JCPDS No. 38-1240). (d) Excitation (black curve, at the emission of 696 nm) and emission (red curve, excitation at 254 nm) spectra of the Cr:  $\text{ZnGa}_2\text{O}_4$  NPs dispersed in hexane. The inset is the Cr:  $\text{ZnGa}_2\text{O}_4$  NPs powder digital image under 254 nm hand-held lamp (6 W) excitation. (e) Afterglow decay of Cr:  $\text{ZnGa}_2\text{O}_4$  NPs powder after 5 min irradiation with a 254 nm UV lamp (black curve). The grey curve shows the background of the instrument without any sample under the same measurement conditions. Persistent luminescence intensity was monitored at 696 nm as a function of time. Reproduced with permission from reference [108].

However, no *in vivo* imaging was reported in this work. The same year, Teston et al described a facile one-pot synthesis of  $\text{ZnGa}_2\text{O}_4:\text{Cr}^{3+}$  as NIR USPLNPs also with an average diameter of 6 nm by using a non-aqueous sol-gel method assisted by microwave irradiation [109]. Indeed, this type of non-aqueous benzyl alcohol route has been established as a very powerful technique that takes place at moderate temperature and pressure to obtain very small metal oxide nanoparticles with high crystallinity, purity, and reproducibility [110]. Microwave heating offers a reduction of the reaction time (30 min) in comparison to traditional heating in an autoclave (24 hours) [111]. One special advantage of this technique is that the one pot process does not need further high-temperature treatment, which is conventionally used for the

synthesis of such materials and generally leads to coalescence and larger particles [112]. Moreover, this method allows controlling of the crystal growth without the need to use additional surfactants or ligands. The authors have shown that such nanoparticles are then easily surface functionalized. Polyethylene glycol phosphonate moieties (PO-PEG) are used as surface ligands. The phosphonate group presents high affinity for the metallic surface [113] whereas the PEG chain improves the biodistribution of the PLNPs *in vivo* (Figure 28D) [114].

A third method was reported the same year by Han and co-workers to prepare water-soluble  $\text{ZnGa}_2\text{O}_4\text{Cr}_{0.004}$  PLNPs, with sub-10 nm size and intense PL properties, directly synthesized in aqueous solution by a hydrothermal method [115]. The authors

attempted to prepare such PLNPs by using a hydrothermal process at higher temperature (220°C) for 10 hours with a Zn:Ga:Cr molar ratio of 1:2:0.004. Under these conditions, they found that ZGC nanocrystals are obtained with an average size of ~18 nm. They then systemically varied precursor composition, from 0.7:2:0.004, 1:2:0.004 to 2:2:0.004, to adjust the size of the PLNPs. Their results showed that the molar ratio of Zn/Ga is critical to the size of the as-synthesized PLNPs. Under a Zn/Ga molar ratio of 2:2, ZGC PLNPs are generated with a narrow size distribution and an average size of  $8 \pm 4$  nm (denoted as ZGC-1; Figure 29A). This is likely a result of the well-established knowledge that excess  $Zn^{2+}$  can be readily dissolved during the synthesis by the formation of soluble ammonium complexes, and/or as a possible ZnO impurity which could later be removed by a washing procedure with hydrochloride solution. The authors discovered that ZGC-1 readily re-disperses in water to form a transparent colloidal

solution. Dynamic light scattering analysis was used to analyze the size of ZGC-1 in aqueous solution. They found a narrow mean hydrodynamic size distribution of 9 nm for the as synthesized ZGC-1 colloid. No significant change was observed even after storing for one month (Figure 29B). ZGC-1 was compared to ZGC-2 samples, synthesized by the classical high-temperature (750°C) annealing methods [79]. A comparison imaging experiment between ZGC-1 and ZGC-2 was performed *in vivo* by using a commercial white LED (5000 lm, CREE-T6) as a light source (Figure 29C). Simulated deep-tissue imaging was further performed with live mouse models covered by a pork slab ~1 cm thick (Figure 29C). The persistent luminescence of ZGC-2 could hardly be observed under our simulated deep-tissue environment (on the left in Figure 29C), whereas the small ZGC-1 still provides clear, quality images (right, Figure 29C).

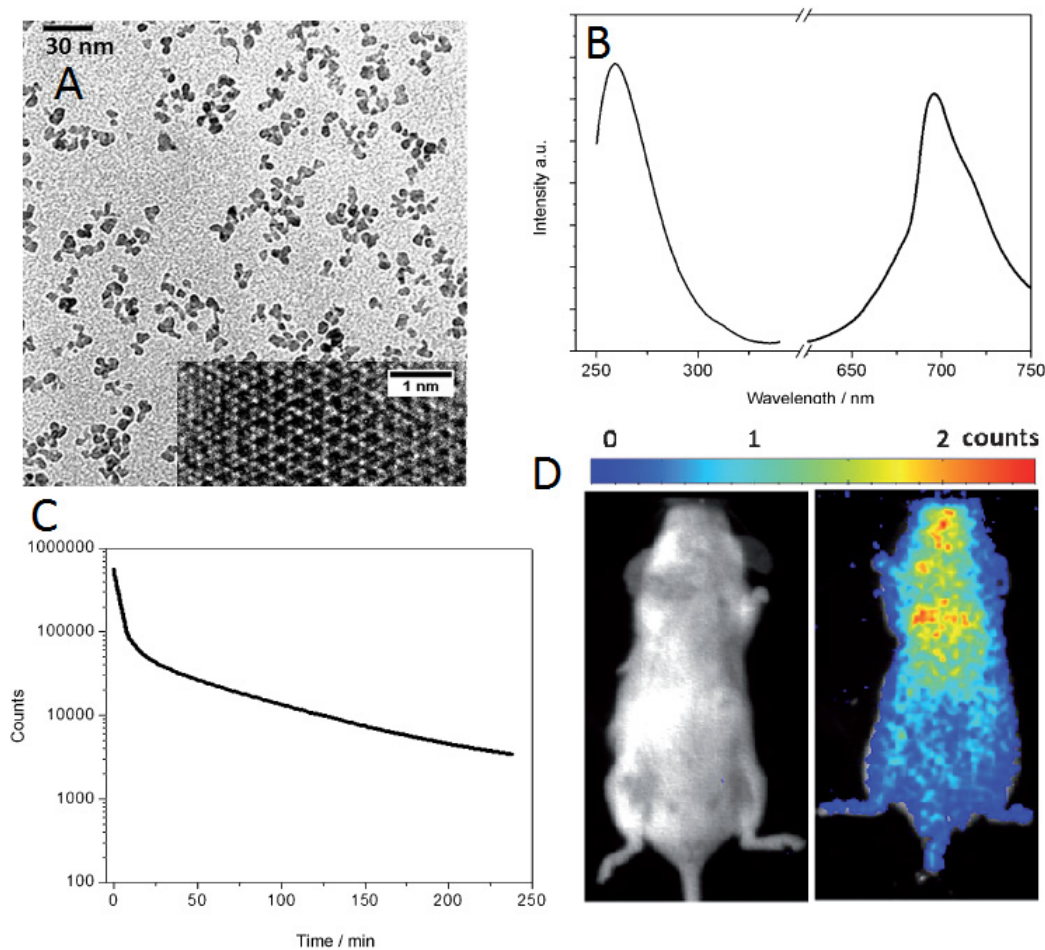


**Figure 28.** Small ZGO PLNPs for *in vivo* imaging. (A) TEM and HR-TEM (inset) of USPLNPs@PO-PEG. (B) Excitation (left, emission wavelength = 695 nm) and emission spectra (right, excitation wavelength = 254 nm) of USPLNPs in water. (C) NIR luminescence time decay after UV illumination of a suspension of PEGylated USPLNPs. (D) *In vivo* imaging in BALB/c mice injected with a suspension of PEGylated USPLNPs: a) visible preview; b) luminescence acquisition after UV excitation. Reproduced with permission from reference [109].

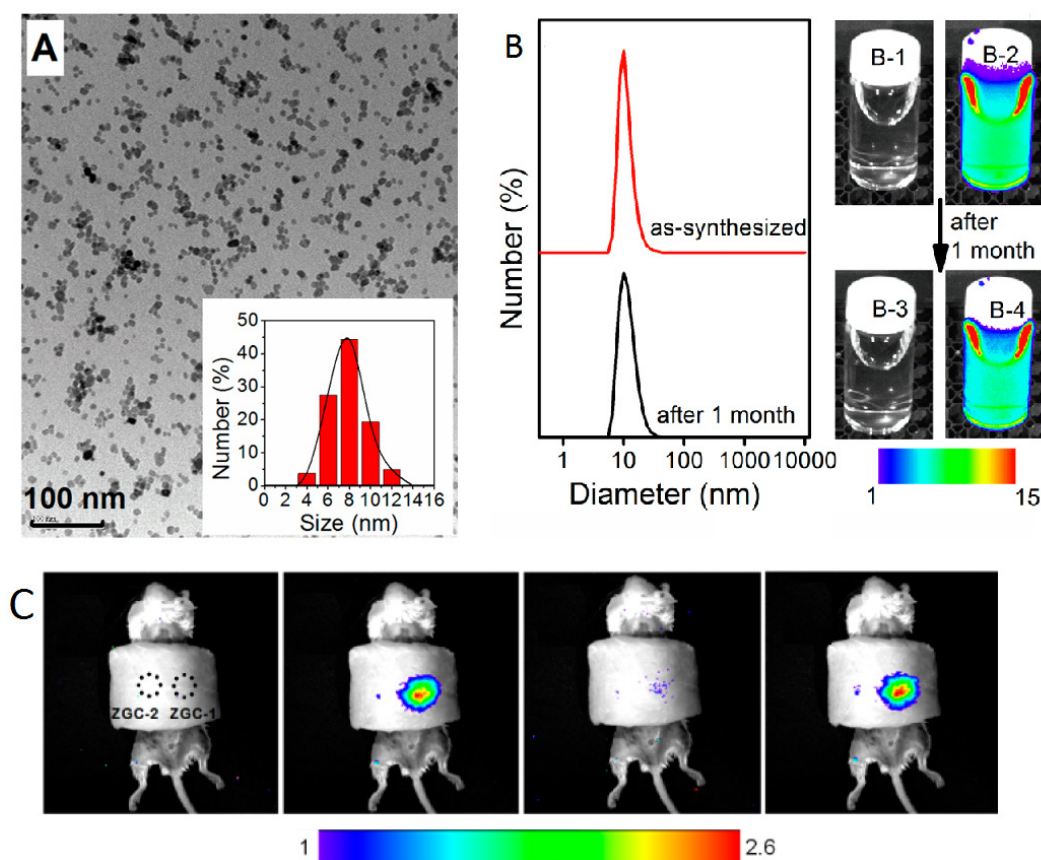


**Figure 29.** Small size ZGC-1 nanoparticles synthesized at 220°C for 10 hours using excess of Zn. (A) TEM image and size distribution. (B) Dynamic light scattering patterns of ZGC-1 in water before and after storage for 1 month. (B-1, B-3) bright field and (B-2, B-4) corresponding luminescence pictures of ZGC-1. (C) Deep tissue *in vivo* imaging before (left) and after (right) *in situ* excitations with a white LED (5000 lm) light for 30 s. Reproduced with permission from reference [115].

In 2016, Zhang and co-workers reported the development of a one-step synthetic method for preparing amino-functionalized ultrasmall PLNPs for bioimaging applications [116]. In their study, a one-step synthesis of amino-functionalized near infrared persistent luminescent  $\text{ZnGa}_2\text{O}_4:\text{Cr}^{3+}, \text{Eu}^{3+}$  nanoparticles (ZGO:Cr,Eu) was developed. This novel approach is based on a synthetic strategy where ethylenediamine (EDA) served as the reactant to fabricate the ZGO as well as the surfactant ligand to control the nanocrystal size and form surface amino groups under solvothermal conditions. In a typical procedure, metal acetylacetonates (Zn, Ga, Cr and Eu) were mixed with EDA according to the following chemical formula:  $\text{ZnGa}_2\text{O}_4:0.5\% \text{Cr}^{3+}, 0.1\% \text{Eu}^{3+}$ . The reaction mixture was transferred into an autoclave and heated at 200°C for 48 h. The resulting cloudy suspension was centrifuged, and the precipitate was thoroughly washed with ultrapure water and ethanol. The precipitate was dried in air at 50°C and further used for functionalizations. The amino-functionalized ZGO can be easily conjugated to carboxyl groups of biological target molecules. In addition, the ZGO exhibited bright NIR emission and a long afterglow time. More importantly, the ZGO achieved long

afterglow imaging using 650 nm and 808 nm NIR light *in situ* re-excitation, which is advantageous for long-term and high SNR *in vitro* and *in vivo* imaging. The process of synthesis, functionalization and imaging with these ZGO NPs is shown in Figure 30.

## Gallogermanates

### $\text{Zn}_3\text{Ga}_2\text{Ge}_2\text{O}_{10}:\text{Cr}^{3+}$ (ZGGO)

In 2012, Pan et al reported the optical characteristics of a bulk persistent luminescence material, consisting of a zinc gallogermanate matrix [117]. The authors have developed a series of  $\text{Cr}^{3+}$  doped zinc gallogermanate NIR persistent phosphors sintered at 1350°C that can be activated by solar radiation in various weather conditions and exhibiting an extremely long lasting NIR afterglow. These NIR phosphors may find many technologically important applications in security, solar energy utilization and also in medical diagnosis. For example, the phosphors could be used as tag, markers or signage in night vision surveillance, rescue or emergency (Figure 31).

In 2015, Zhang and co-workers reported bioimaging applications by functionalizing 50 nm

$Zn_3Ga_2Ge_2O_{10}:Cr^{3+}$  (ZGGO) nanoparticles with the antibody anti-EpCAM for labelling human breast cancer cells *in vitro* (Figure 32A) [118]. The antibody anti-EpCAM, whose corresponding antigen receptors are known to be overexpressed in both primary and metastatic breast cancer [119], were utilized as specific recognition agent to functionalize ZGGO surface. ZGGO-EpCAM can specifically recognize the long-term monitored breast cancer cells (MCF7) without persistent activation, which can obviously improve the SNR. With confocal microscopy, the authors demonstrated receptor-mediated recognition of ZGGO-Ep-CAM bioconjugates to breast cancer cells (Figure 32B-C).

### $Zn_{2.94}Ga_{1.96}Ge_2O_{10}:Cr^{3+}, Pr^{3+}$

In 2013 Yan and co-workers reported the synthesis, by a citrate sol-gel method, of functional long-persistent luminescent nanoparticles with a nominal composition of  $Zn_{2.94}Ga_{1.96}Ge_2O_{10}:Cr^{3+}, Pr^{3+}$  [120]. The persistent luminescence intensity and afterglow time of these PLNPs are significantly improved via codoping  $Pr^{3+}/Cr^{3+}$  and creating suitable Zn deficiency in zinc gallogermanate (ZGGO) host. The prepared PLNPs give distinguished advantages of bright NIR emission, long afterglow time (>15 days for the powder), excellent biocompatibility, and low toxicity, and are promising for long-term *in vivo* bioimaging applications (Figure 33).

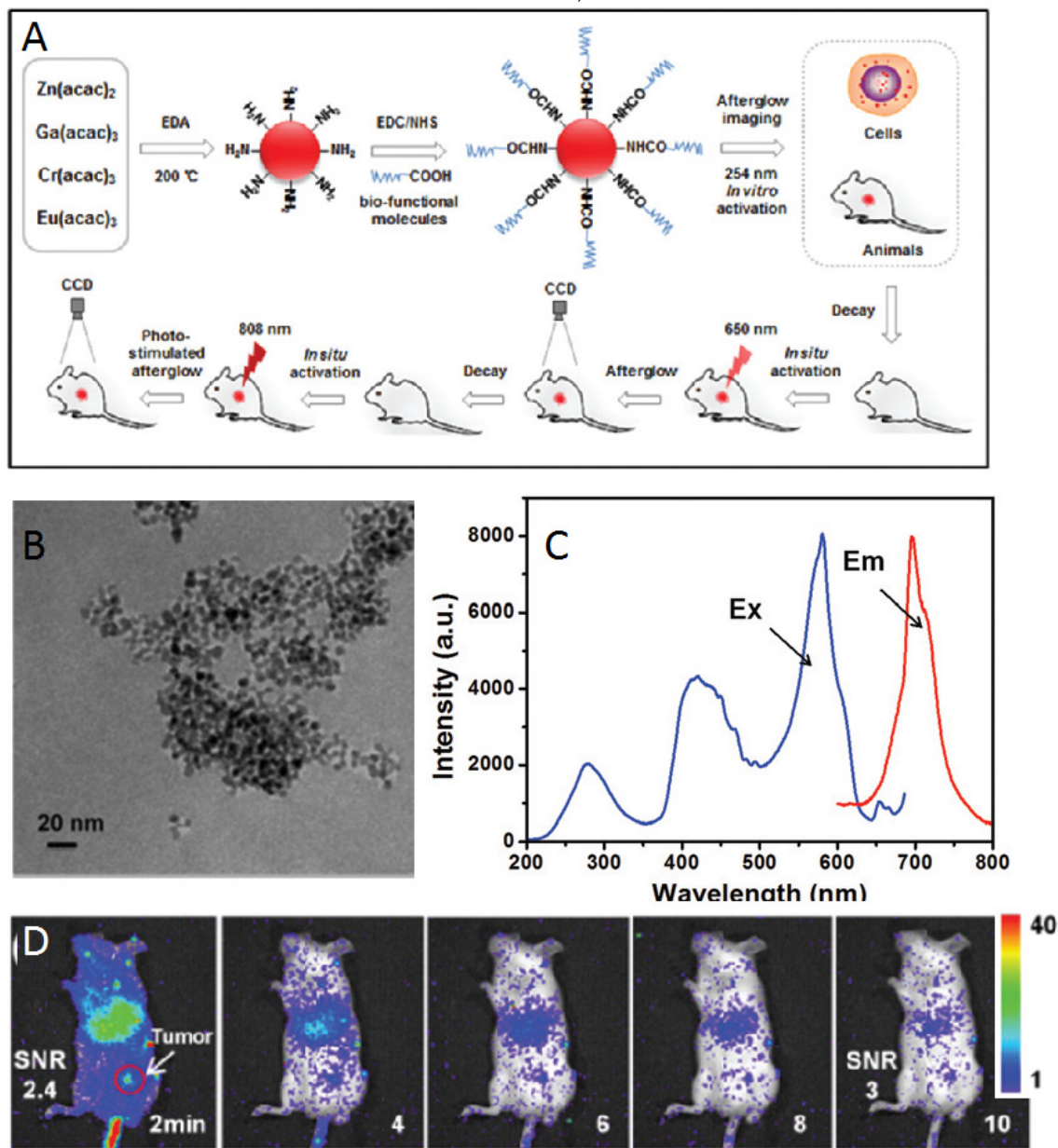


**Figure 30.** Up: Synthesis, functionalization and imaging of small ZGO:Cr,Eu NPs. Middle: TEM image of ZGO, excitation and emission spectra. Below: *In vivo* luminescent image of H22 tumor-bearing mice after intravenous injection of ZGO-FA, and luminescent images of re-excitation at 650 nm at the tumor site. Reproduced with permission from reference [116].

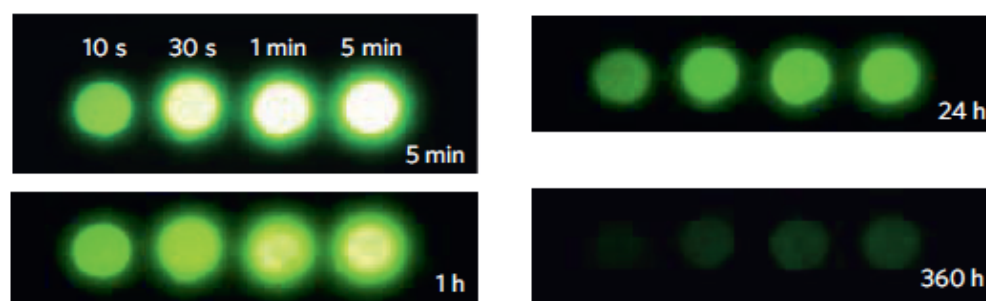


**Figure 31.** Persistent luminescence performances of  $\text{Zn}_3\text{Ga}_2\text{Ge}_2\text{O}_{10}:\text{Cr}^{3+}$  discs. NIR images of four phosphor discs taken at different afterglow times (5 min to 360 h) after irradiation by a 365 nm lamp for 10 s to 5 min. The discs were placed on a hot plate surface for imaging. Reproduced with permission from reference [117].

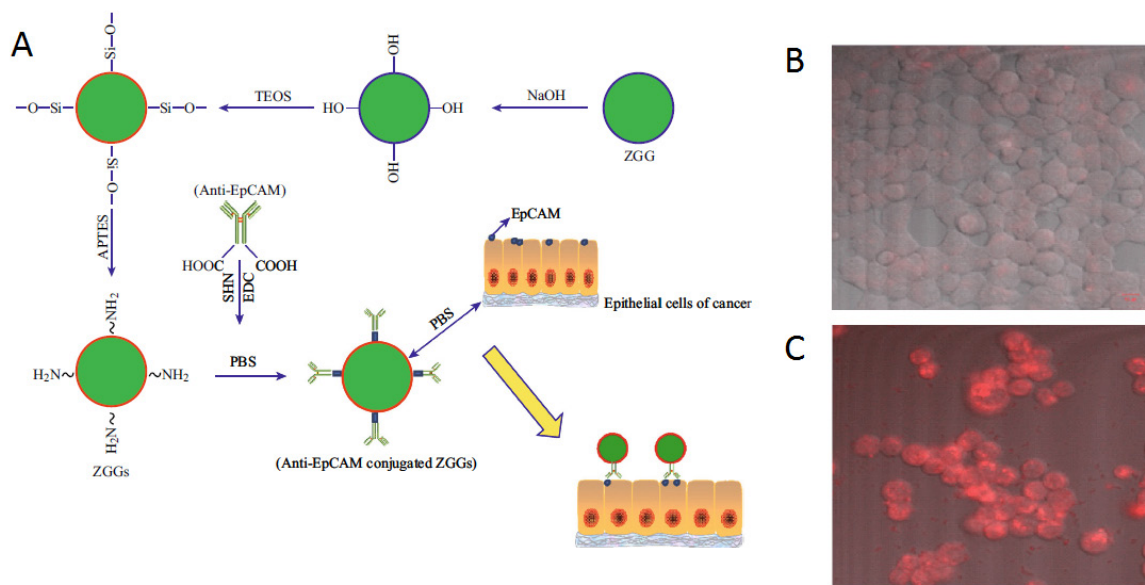


**Figure 32.** (A) Schematic illustration of the process and functionalization of  $\text{Zn}_3\text{Ga}_2\text{Ge}_2\text{O}_{10}:\text{Cr}^{3+}$  (ZGGO) with anti-EpCAM to target MCF7 cell lines. (B) Confocal microscopic images of a MCF7 cells treated with ZGGO- $\text{NH}_2$ . (C) MCF7 cells treated with ZGGO-EpCAM. Reproduced with permission from reference [118].

### $\text{Zn}_{1.1}\text{Ga}_{1.8}\text{Ge}_{0.1}\text{O}_4:\text{Cr}^{3+}, \text{Eu}^{3+}@\text{SiO}_2$

In 2015, as already presented before, Zhang and co-workers used the mesoporous silica nanospheres (MSNs) both as drug carriers and as a morphology controlling template to design porous PLNPs [121]. Furthermore, based on the previous section, the long afterglow performance of  $\text{Zn}_{1.1}\text{Ga}_{1.8}\text{Ge}_{0.1}\text{O}_4:\text{Cr}^{3+}$  was the best among those of all germanium substituted  $\text{ZnGa}_2\text{O}_4$  [117]. Thus, in their paper, the authors loaded  $\text{Zn}_{1.1}\text{Ga}_{1.8}\text{Ge}_{0.1}\text{O}_4:\text{Cr}^{3+}, \text{Eu}^{3+}$  into the pores of MSNs to prepare a novel trackable drug carrier ( $\text{Zn}_{1.1}\text{Ga}_{1.8}\text{Ge}_{0.1}\text{O}_4:\text{Cr}^{3+}, \text{Eu}^{3+}@\text{SiO}_2$ ) (PLNPs@MSNs). Due to the MSN templates, the obtained samples showed a porous structure, spherical morphology, narrow size distribution, large specific surface area and large pore capacity, indicating excellent drug carrier properties. Moreover, the authors reported that the PLNPs@MSNs demonstrated a brighter NIR emission (696 nm), and the long afterglow luminescence persisted for 15 days. In particular, the

PLNPs@MSNs could be excited by a red LED lamp *in vivo*, indicating the capacity for real-time tracking and imaging continuously *in vivo* for long periods of time. Furthermore, after surface modification with folic acid (FA), a tumor-targeting group, the PLNPs@MSNs exhibited tumor targeting ability with high sensitivity. All their results indicate that PLNPs@MSNs-FA can accurately diagnose tumors, be used for long term *in vivo* and *in situ* monitoring and release a drug *in situ* to cure tumors (Figure 34).

### Multimodal imaging agents

As discussed in section III.3, there are two main strategies to get bimodal (optical and MRI) imaging agents, either based on co-doping or on the use of surface chelating agents. In 2014, Yan and co-workers reported the surface functionalization of ZGGO with DTPA-Gd complexes to get bimodal imaging agents, able to be detected both by optical imaging (Figure 35, left) and as a positive  $T_1$  MRI contrast agent (Figure 35, right) [122].

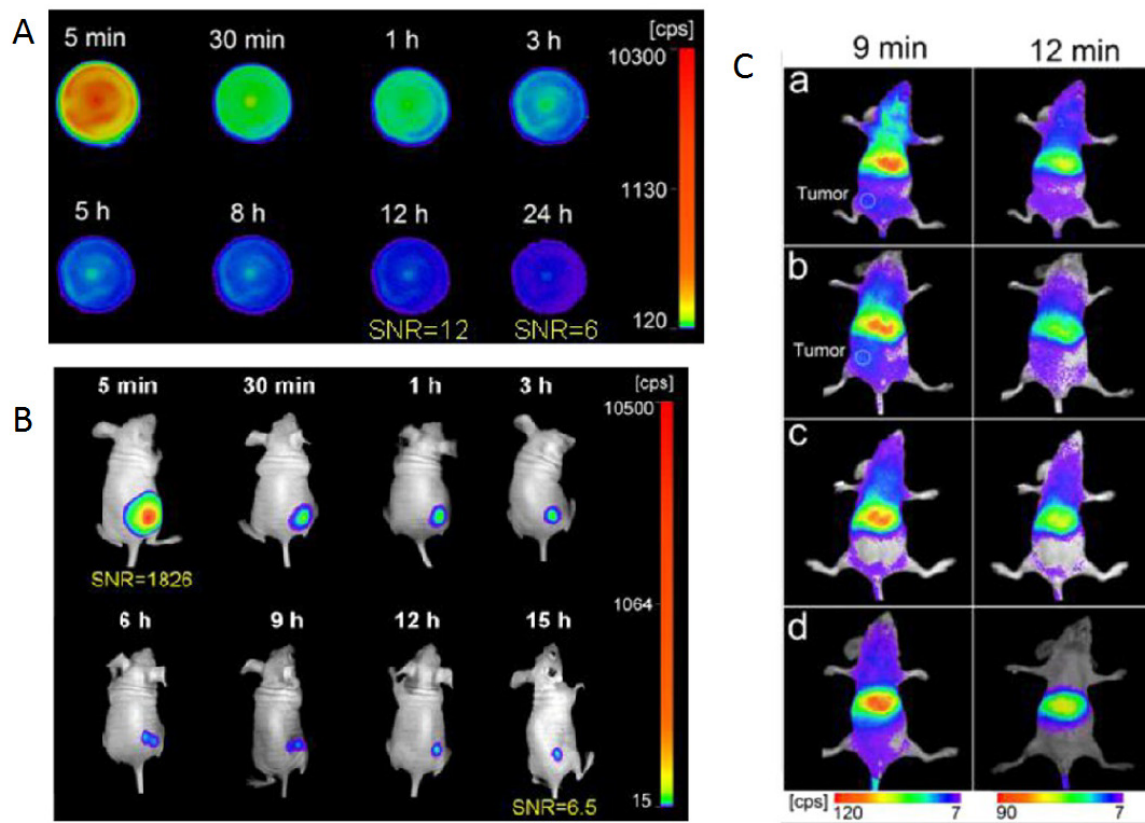


**Figure 33.**  $Zn_{2.94}Ga_{1.96}Ge_2O_{10}:Cr^{3+}, Pr^{3+}$  synthesis for long term *in vivo* imaging. (A) NIR afterglow decay images recorded by CCD camera at different times after stopping UV irradiation. (B) *In vivo* NIR luminescence images of a normal mouse after subcutaneous injection of PEG-PLNPs (0.4 mg, 10 min irradiation with a 254 nm UV lamp before injection). (C) *In vivo* NIR luminescence images of U87MG tumor-bearing mice (white circles locate the tumor site, a-b) and normal mice, (c,d) after intravenous injection of PEG-PLNPs (a, c) and RGD-PLNPs (b, d) (0.4 mg, 10 min irradiation with a 254 nm UV lamp before injection). Reproduced with permission from reference [120].

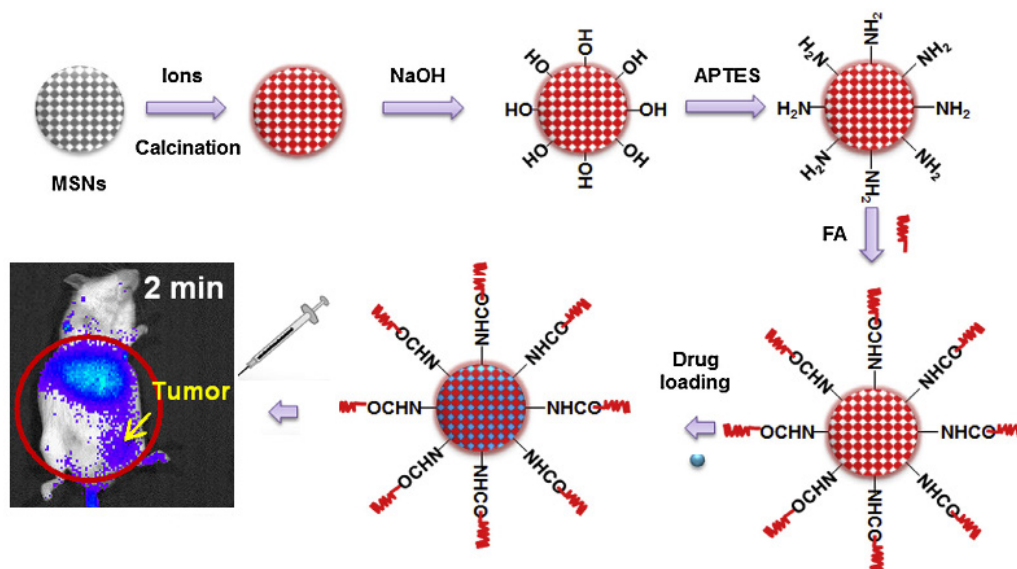


**Figure 34.** Schematic diagram for the synthesis, surface modification and application of NLPLNPs@MSNs for tumor imaging. Reproduced with permission from reference [121].

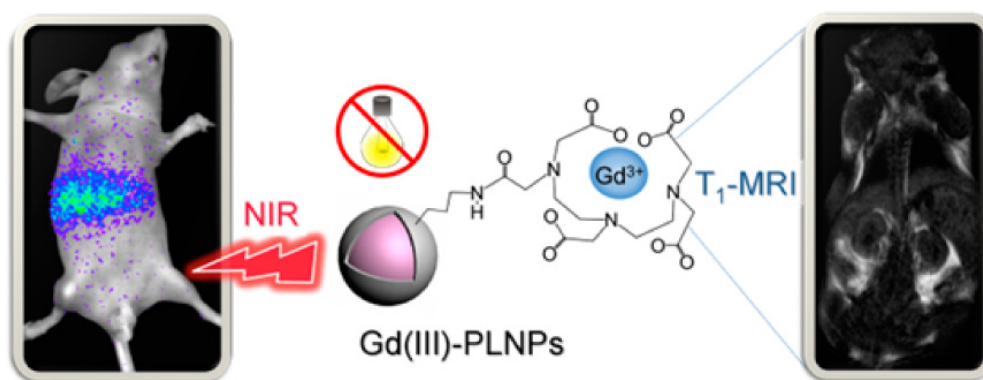


**Figure 35.** Bimodal imaging agent based on ZGGO nanoparticles coated with DTPA-Gd complexes for *in vivo* optical (left) and MRI (right). Reproduced with permission from reference [122].

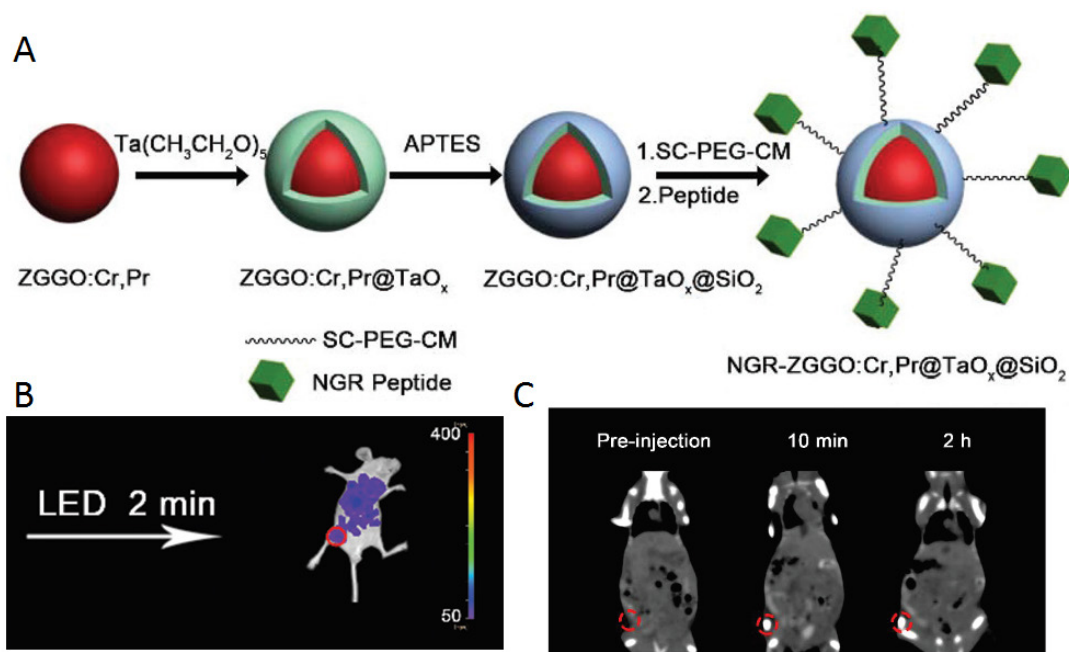


**Figure 36.** ZGGO:Cr,Pr@TaO<sub>x</sub>@SiO<sub>2</sub> nanoparticles for optical imaging and CT. (A) Schematic protocol for the preparation of core-shell structured ZGGO:Cr,Pr@TaO<sub>x</sub>@SiO<sub>2</sub>. (B) *In vivo* persistent luminescence imaging of HepG2 tumor bearing nude mice after tail vein injection with PEG-ZGGO:Cr,Pr@TaO<sub>x</sub>@SiO<sub>2</sub>. (C) *In vivo* CT imaging of HepG2 tumor-bearing mice with PEG-ZGGO:Cr,Pr@TaO<sub>x</sub>@SiO<sub>2</sub> via orthotopic injection: pre-injection, 10 min and 2 h post-injection. Reproduced with permission from reference [123].

### Zn<sub>2.94</sub>Ga<sub>1.96</sub>Ge<sub>2</sub>O<sub>10</sub>:Cr<sup>3+</sup>,Pr<sup>3+</sup>@TaO<sub>x</sub>@SiO<sub>2</sub>

As discussed above, the design and fabrication of multimodal imaging nanoparticles is of great importance in medical diagnosis. In 2015, Yan and co-workers reported the fabrication of core-shell structured Zn<sub>2.94</sub>Ga<sub>1.96</sub>Ge<sub>2</sub>O<sub>10</sub>:Cr<sup>3+</sup>,Pr<sup>3+</sup>@TaO<sub>x</sub>@SiO<sub>2</sub> nanoparticles for persistent luminescence and X-ray computed tomography (CT) imaging [123]. Persistent luminescent nanoparticles Zn<sub>2.94</sub>Ga<sub>1.96</sub>Ge<sub>2</sub>O<sub>10</sub>:Cr<sup>3+</sup>,Pr<sup>3+</sup> were used as the core to provide near-infrared luminescence, and a TaO<sub>x</sub> layer was grown on the core to serve as the contrast agent for CT (Figure 36A). CT serves as a medical imaging technique for a long time due to its advantages in illustrating biological structures, such as high spatial resolution and ease of

forming 3D visual image reconstruction for tissues of interest [124]. Considering the drawbacks of iodinated compounds, various kinds of nanoparticles with high atomic number metal elements as contrast agents have been developed for potential CT imaging. Recently, tantalum oxide (TaO<sub>x</sub>) nanoparticles have been demonstrated to be promising candidates as CT contrast agents [125]. However, CT has inherently low sensitivity due to its poor soft-tissue contrast. Thus, it is needed to introduce a complementary imaging modality for CT to gain accurate diagnosis. The integration of NIR-emitting PLNP and the CT contrast agent into one nanoplatform offers attractive synergistic advantages in biomedical application. Though recent work presents the MRI/persistent luminescent bi-modal imaging probe [126], no work

on CT/persistent luminescent bimodal imaging probe, had been reported before.

The TaOx and SiO<sub>2</sub> shells on ZGGO:Cr,Pr were prepared according to Oh et al. with modification [127]. ZGGO:Cr, Pr was redispersed in cyclohexane by sonication, then Igepal CO-520 was mixed with cyclohexane. After stirring for 2.5 h, NaOH was added and the mixture was stirred for another 1 hour. A syringe pump was used to control the addition of the cyclohexane solution of Ta(CH<sub>3</sub>CH<sub>2</sub>O)<sub>5</sub> within 30 min. To achieve high monodispersity, APTES was added into the mixture. The system was kept stirring for 24 h in the dark. Then, methanol was added to precipitate the nanoparticles which were collected by centrifugation. The as-prepared ZGGO:Cr,Pr@TaOx@SiO<sub>2</sub> nanoparticles were re-dispersed in ethanol by sonication and used for functionalization and *in vivo* applications (Figure 36B-C).

### Cell labelling

In 2016, Yan and co-workers reported the first fabrication of TAT penetrating peptide-functionalized NIR-emitting PLNPs with composition Zn<sub>1.1</sub>Ga<sub>1.8</sub>Ge<sub>0.1</sub>O<sub>4</sub>:Cr<sup>3+</sup>, Eu<sup>3+</sup> (LPLNP-TAT) for long-term tracking of stem cells [128]. The prepared LPLNP-TAT have been successfully used to label

stem cells and showed excellent biocompatibility, high signal-to-noise ratio (SNR). The authors demonstrated that labelling with LPLNP-TAT not only provides superior SNR for tracking adipose-derived mesenchymal stem cells (ASC) in skin-regeneration and tumor-homing models but also had no effect on either proliferation or multilineage differentiation of ASC (Figure 37B). The super-long persistent luminescence and red-light renewability makes functional PLNP very promising for long-term *in vivo* stem cell tracking and provided insights to explore the contribution and migration of ASC. Zn<sub>1.1</sub>Ga<sub>1.8</sub>Ge<sub>0.1</sub>O<sub>4</sub>:Cr<sup>3+</sup>, Eu<sup>3+</sup> have been synthesized via a hydrothermal process in combination with sintering in air, functionalized with TAT peptide for *in vivo* imaging (Figure 37A).

### Bioimaging with PLNPs made from other matrixes

As presented just before, most research developed using PLNPs for bioimaging are made using silicates, gallium oxide or gallogermanates matrixes. However, there are other possibilities as detailed below.

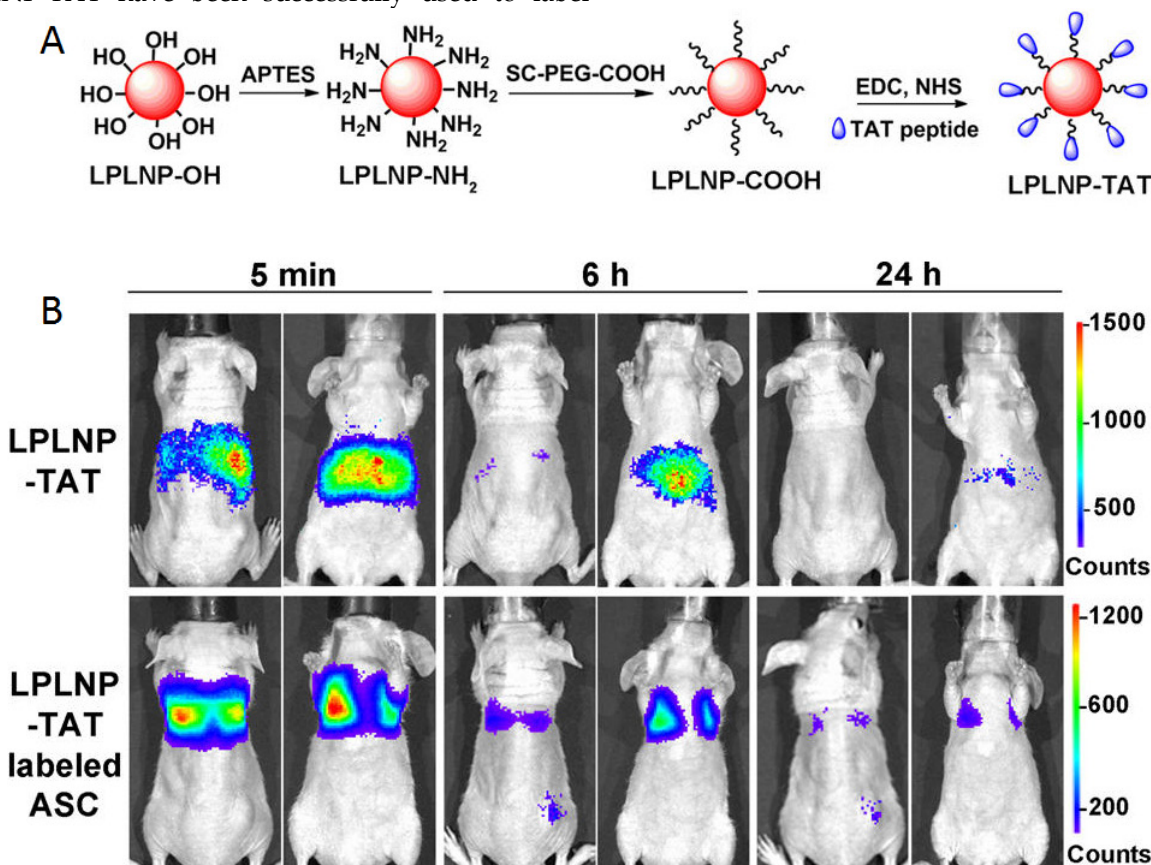


**Figure 37.** Zn<sub>1.1</sub>Ga<sub>1.8</sub>Ge<sub>0.1</sub>O<sub>4</sub>:Cr<sup>3+</sup>, Eu<sup>3+</sup> TAT PLNPs for *in vivo* imaging and cell tracking. (A) Schematic representation of LPLNP surface modification. (B) *In vivo* biodistribution of LPLNP-TAT and LPLNP-TAT-labeled ASC after intravenous injection. Reproduced with permission from reference [128].

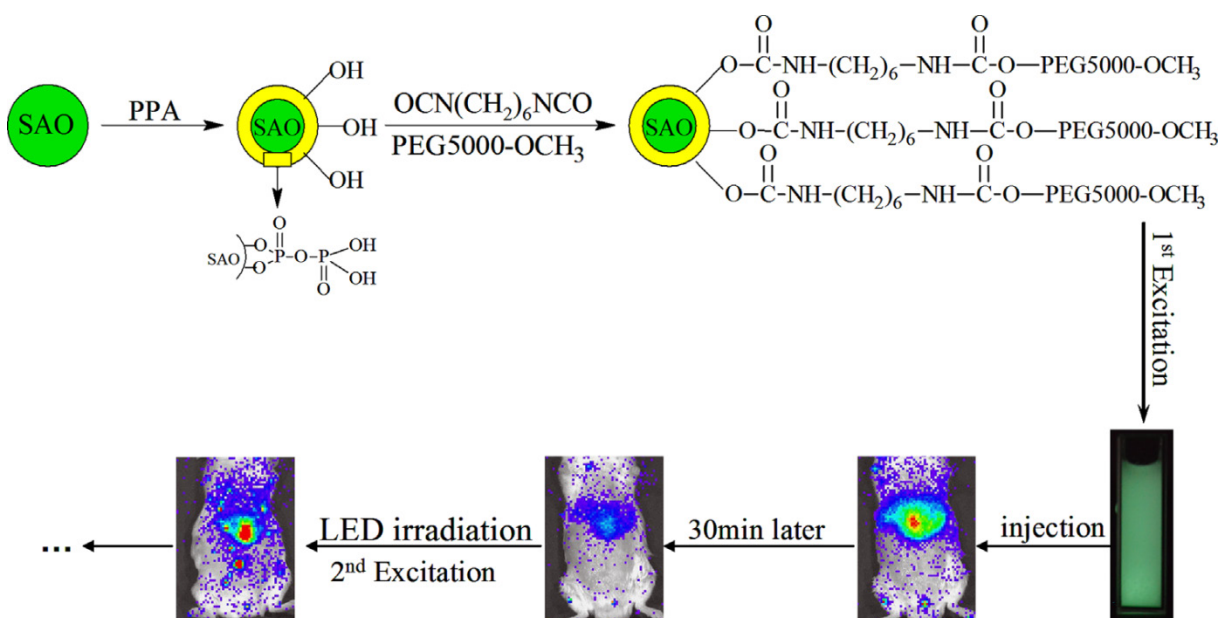


**Figure 38.** Principle of  $\text{SrAl}_2\text{O}_4:\text{Eu}^{2+},\text{Dy}^{3+}$  (SAO) coating with PPA and PEG and application for long-term *in vivo* imaging. Reproduced with permission from reference [129].

### $\text{SrAl}_2\text{O}_4:\text{Eu}^{2+}, \text{Dy}^{3+}$

In order to recharge the PLNPs *in vivo*, in 2014, Zhang and co-workers have chosen  $\text{SrAl}_2\text{O}_4:\text{Eu}^{2+}, \text{Dy}^{3+}$  (SAO) nanoparticles, which is a well-known representative persistent phosphor [129]. However, the obvious drawback of SAO nanoparticles is their poor water-resistance, which limits their application in the biological field [130]. The authors used pyrophosphoric acid (PPA) to modify the surface of SAO and avoid hydrolysis [131]. The modified SAO were further grafted with PEG-5000- $\text{OCH}_3$ , resulting in increased water-dispersibility and biocompatibility. These modified nanoparticles have been successfully applied for small animals imaging. After dispersion in 0.9% NaCl and irradiation with 365 nm UV light for 10 min, the afterglow signal can be observed in real time for more than 30 min in mouse after intravenous injection. In order to monitor for a super-long time, the mouse could be re-illuminated for 10 min with a white-light LED lamp and then the imaging signals were recovered and also persisted for 30 min again. The super-long time *in vivo* imaging was achieved by employing these repeatedly excited luminescent nanoprobes (Figure 38).

In 2014, Willson and co-workers used the same matrix for the development of new *in vitro* diagnostic tests [132]. The demand for reliable diagnostic tests for pathogens and disease biomarkers in low-resource and point-of-care (POC) settings has led to significant research in developing new assay technologies and improved photoluminescent reporters [133]. One of the most promising assay formats for POC diagnostics is the immuno-chromatographic lateral flow assay

(LFA), which is widely known from its use in home pregnancy tests. In 2014, Wilson and co-workers demonstrated the use of strontium aluminate PLNPs as reporters in LFAs with biotinylated hen egg lysozyme (bHEL) as a model analyte [132]. As discussed in the previous example, strontium aluminate hydrolyzes in water to form non luminescent aluminum hydroxide precipitate and soluble strontium hydroxide [134]. Several approaches have been investigated to improve water stability of strontium aluminate including encapsulation with silica by sol-gel or precipitation techniques, direct reaction with phosphoric acid, and encapsulation with triethanolamine [135]. Due to the wide use of trialkoxysilanes in bioconjugate chemistry and their high compatibility with silica surfaces, the authors used a modified Stober process to form a silica shell around the phosphors. They then demonstrated that such persistent luminescence nanoparticles could be used in LFA for rapid detection with high sensitivity without continuous excitation. The long luminescence lifetime of SAO can potentially alleviate design constraints on point-of-care diagnostic devices by eliminating the need for optical filters required for fluorescence measurements and also offers the advantage of reducing background auto-fluorescence when the particles are used in a time-resolved manner (Figure 39). The authors believe that future work with strontium aluminate and other persistent luminescence materials could lead to a new class of reporters for diagnostics and environmental monitoring.

### CaTiO<sub>3</sub>:Pr<sup>3+</sup>

Zhang and co-workers previously developed a convenient template method to synthesize novel PLNPs with a mesoporous structure and long persistent luminescent properties, which was suitable for trackable drug carriers [61]. However, these mesoporous PLNPs only possess luminescent characteristics but no magnetic properties. The same group synthesized in 2015 a new core/shell structure drug carrier via a facile template method [136]. Silica-coated Gd<sub>2</sub>O<sub>3</sub> spheres as the core, ordered mesoporous silica as the shell and CaTiO<sub>3</sub>:Pr<sup>3+</sup> were deposited into the pores of mesoporous silica to form the structure of Gd<sub>2</sub>O<sub>3</sub>@mSiO<sub>2</sub>@CaTiO<sub>3</sub>:Pr<sup>3+</sup> (GdSCTP). The GdSCTP holds ordered mesoporous characteristics and spherical morphology with a narrow size distribution and possesses the dual function of magnetism and long persistent luminescence. Moreover, the authors choose IBU (ibuprofen) as a drug model and reported that drug release could be monitored by the change of luminescence intensity. The luminescence intensity increases along with increasing the cumulative released drug. The authors explained that it might be related to the quenching effect of Pr<sup>3+</sup> emission caused by the organic groups in IBU molecules [137]. The quenching effect is weakened with the increasing drug release amount, resulting in the enhancement of luminescence intensity. This correlation between the luminescence intensity and drug release extent can be used for monitoring the efficiency of drug release.

After modification, the GdSCTP obtains a good biocompatibility, low toxicity and *in vivo* imaging for over 20 min. This drug delivery system seems to be ideal for tracking the delivery of loaded drugs *in vivo* based on its magnetic and luminescent properties (Figure 40).

### Calcium phosphate

Biocompatible nanoparticles possessing persistent luminescence properties offer attractive possibilities for *in vivo* imaging applications. In 2016, Chanéac and co-workers reported the synthesis of highly biocompatible calcium phosphate nanoparticles (HAp/ $\beta$ -TCP) doped with Eu<sup>2+</sup>, Mn<sup>2+</sup> and Ln<sup>3+</sup> ions (Ln<sup>3+</sup> = Dy<sup>3+</sup>, Pr<sup>3+</sup>) synthesized by hydrothermal route and tailored to present red-near infrared persistent luminescence after UV excitation [138]. Nanosized biphasic HAp/ $\beta$ -TCP compounds with sphere and rod-shaped were obtained. Two emission bands in the red-near infrared range were observed and attributed to <sup>4</sup>T<sub>1</sub> → <sup>6</sup>A<sub>1</sub> transitions of Mn<sup>2+</sup> ions in HAp/ $\beta$ -TCP. An annealing treatment in reductive atmosphere post-synthesis was essential to reveal persistent luminescence properties.

Indeed, such thermal treatment allowed reducing Eu<sup>3+</sup> ions in Eu<sup>2+</sup> ions and generating required defects as oxygen vacancies in the crystal necessary for red emission in accordance with persistent luminescence mechanism. The authors have tested these nanoparticles for *in vivo* imaging on small animal as proof of concept of prospective highly biocompatible nanoproboscopes (Figure 41).

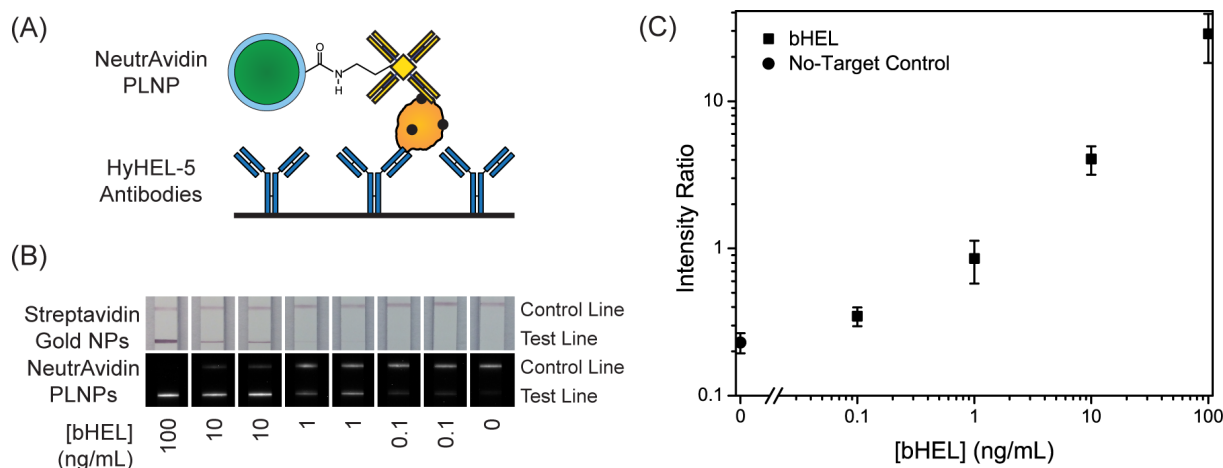


**Figure 39.** (A) Schematic of test line showing NeutrAvidin phosphor bound to bHEL captured by anti-HEL antibodies. (B) LFA strips showing bHEL serial dilutions with duplicates and detection with Streptavidin gold nanoparticles (top) and NeutrAvidin PLNPs (bottom). (C) Average intensity ratios ( $I_{\text{test line}}/I_{\text{control line}}$ ) and  $\pm$  standard deviations at different bHEL concentrations from LFA experiments with NeutrAvidin PLNPs. Reproduced with permission from reference [132].

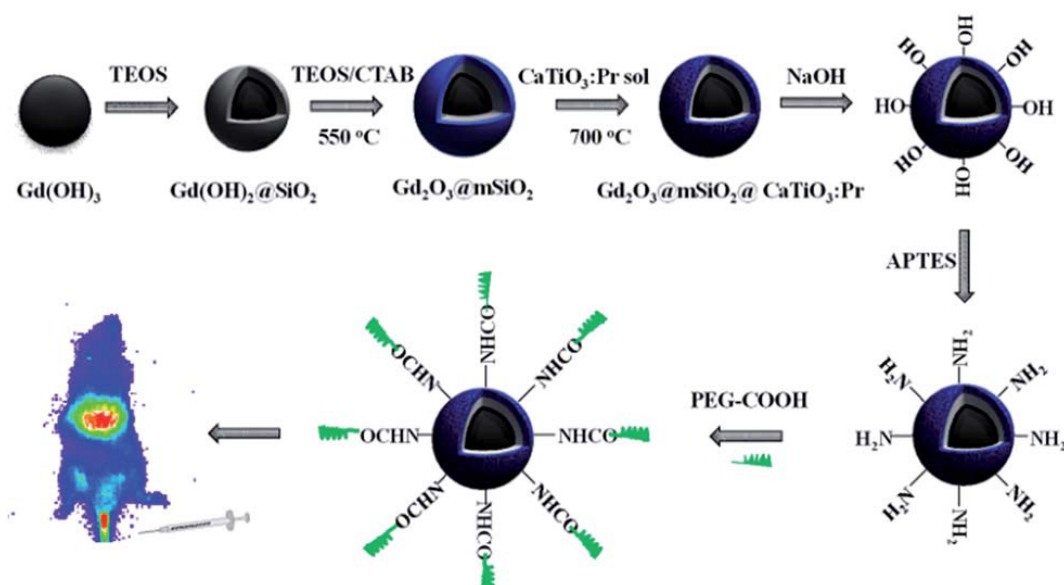


**Figure 40.** Schematic synthesis, surface modification of Gd<sub>2</sub>O<sub>3</sub>@mSiO<sub>2</sub>@CaTiO<sub>3</sub>:Pr<sup>3+</sup> (GdSCTP) PLNPs for *in vivo* imaging. Reproduced with permission from reference [136].

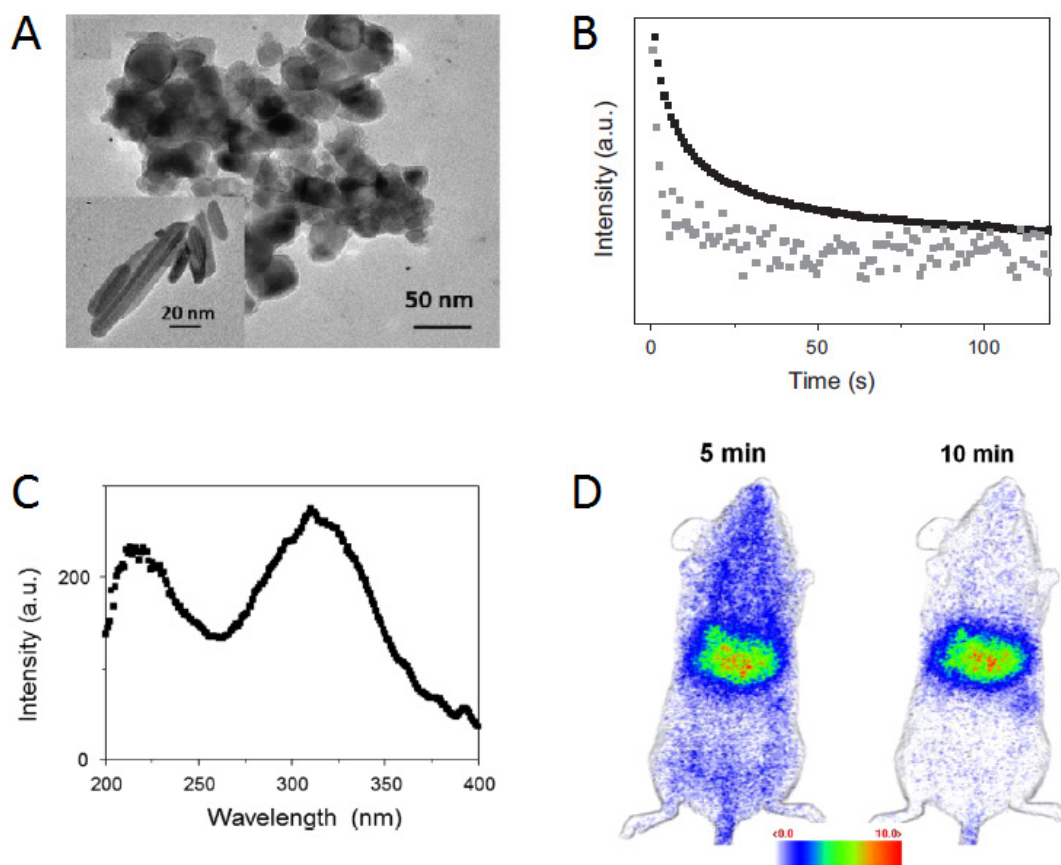


**Figure 41.** (HAp/β-TCP) doped with Eu<sup>2+</sup>, Mn<sup>2+</sup> and Ln<sup>3+</sup> ions (Ln<sup>3+</sup> = Dy<sup>3+</sup>, Pr<sup>3+</sup>) and proof of concept for *in vivo* imaging application. (A) TEM images of HAp/β-TCP nanoparticles synthesized by hydrothermal route, annealed under air and then under reductive atmosphere at 1000 °C: (a) spherical nanoparticles, (inset) nanorods. (B) Luminescence decay curves of HAp/β-TCP:Eu<sup>2+</sup>/Eu<sup>3+</sup> (1%), Mn<sup>2+</sup> (5%), Dy<sup>3+</sup> (2%) (in black) and of HAp/β-TCP:Eu<sup>2+</sup>/Eu<sup>3+</sup> (1%), Mn<sup>2+</sup> (5%), Pr<sup>3+</sup> (2%) (in grey), excitation wavelength 365 nm, excitation time 120 s. (C) Persistent luminescence spectra of HAp/β-TCP:Eu<sup>2+</sup>/Eu<sup>3+</sup> (1%), Mn<sup>2+</sup> (5%), Dy<sup>3+</sup> (2%) (in black) and of HAp/β-TCP:Eu<sup>2+</sup>/Eu<sup>3+</sup> (1%), Mn<sup>2+</sup> (5%), Pr<sup>3+</sup> (in grey), excitation wavelength 365 nm, excitation time 120 s. (D) Images of a Balb/c mouse obtained at 5 and 10 min after the injection of 0.8 mg nanoparticles of HAp/β-TCP doped Eu<sup>2+</sup>/Eu<sup>3+</sup>, Mn<sup>2+</sup> and Dy<sup>3+</sup> dispersed in 200 ml of 5% glucose. Reproduced with permission from reference [138].

**Sr<sub>2</sub>SnO<sub>4</sub>:Nd<sup>3+</sup>**

All PLNPs syntheses since a decade emit light below 800 nm. However, the demand for inorganic phosphors exhibiting longer NIR wavelengths is growing for high resolution *in vivo* imaging. Recently, the NIR persistent luminescence ranging from 800 to 1300 nm has been found in phosphors. Upon examining a number of Nd<sup>3+</sup> doped phosphors, Fujihala and co-workers discovered a new NIR persistent luminescent material Sr<sub>2</sub>SnO<sub>4</sub>:Nd<sup>3+</sup> [139]. The NIR persistent luminescence observed in Sr<sub>2</sub>SnO<sub>4</sub>:Nd<sup>3+</sup> ranged from 850 to 1400 nm with a major peak at around 1079 nm, which was ascribed to the electron transition of Nd<sup>3+</sup> ions. Furthermore, the authors successfully enhanced the intensity of NIR persistent luminescence by increasing the firing temperature; the intensity of Sr<sub>2</sub>SnO<sub>4</sub>:Nd<sup>3+</sup> fired at

1773K was three orders of magnitude higher than that of Sr<sub>2</sub>SnO<sub>4</sub>:Nd<sup>3+</sup> fired at 1473K at a decay time of 10 s after the removal of the excitation light. Sm<sup>3+</sup> doped Sr<sub>2</sub>SnO<sub>4</sub> phosphor has already been reported as a persistent luminescent material in the visible range [140]. However, previous to that work, there was no article reporting Nd<sup>3+</sup> doped Sr<sub>2</sub>SnO<sub>4</sub> phosphor and its NIR persistent luminescence properties. The authors have shown in Figure 42 that the NIR persistent luminescence from the 1773K sample could penetrate through the finger, where it is partially absorbed by hemoglobin in the veins, resulting in the visualization of the finger vein pattern. Therefore, Sr<sub>2</sub>SnO<sub>4</sub>:Nd<sup>3+</sup> could be a promising candidate as a luminescent probe for *in vivo* optical imaging (Figure 42).

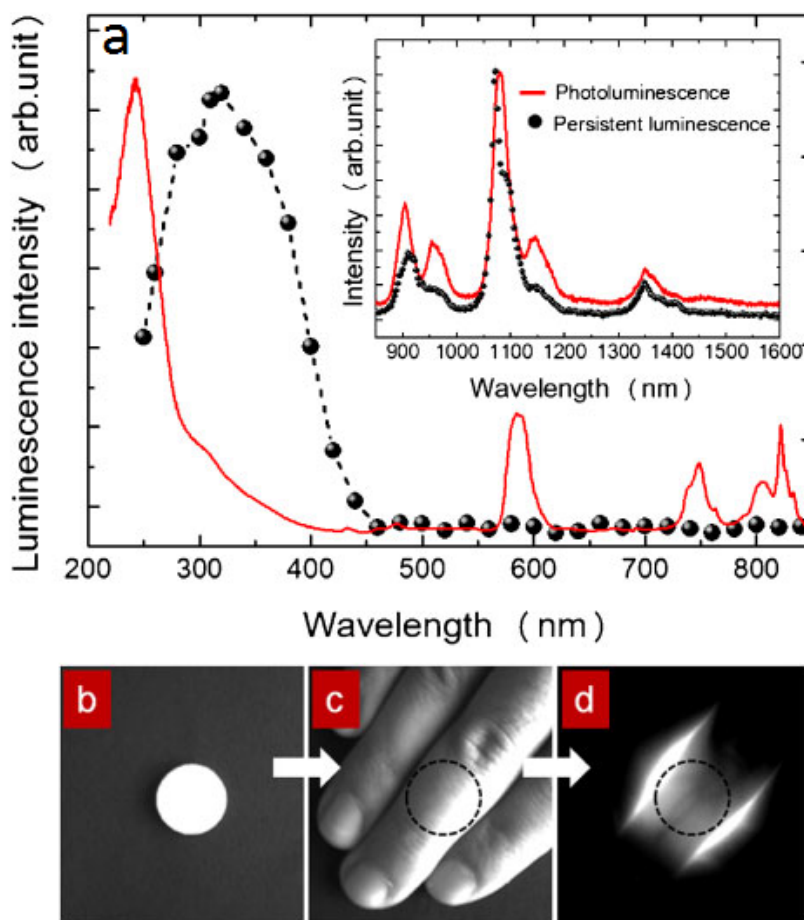


**Figure 42.** (a) Excitation wavelength dependence of the persistent luminescent intensity at 10s after the removal of the excitation ultraviolet light (= 365 nm, 7.43W/m<sup>2</sup>) from Sr<sub>2</sub>SnO<sub>4</sub>:Nd<sup>3+</sup> ceramic disk fired at 1773 K, which is monitored at 900 nm (solid circles), and PL excitation spectrum for Sr<sub>2</sub>SnO<sub>4</sub>:Nd<sup>3+</sup> (solid lines). The inset shows the PL emission spectrum (solid lines) and the persistent luminescence spectrum (solid circles) obtained at a decay time of 10 s after the removal of the excitation ultraviolet light (= 365 nm; 7.43W/m<sup>2</sup>). (b) Bright field image of the persistent luminescence from a Sr<sub>2</sub>SnO<sub>4</sub>:Nd<sup>3+</sup> ceramic disk fired at 1773 K. (c) The bright field image of the persistent luminescence from the Sr<sub>2</sub>SnO<sub>4</sub>:Nd<sup>3+</sup> ceramic disk was covered by a hand. The position of the ceramic disk is indicated by a broken line. (d) Dark field image of the persistent luminescence from Sr<sub>2</sub>SnO<sub>4</sub>:Nd<sup>3+</sup>. Reproduced with permission from reference [139].

## Conclusion and Perspectives

As shown in this review, a huge interest has been paid to persistent luminescence nanoprobe for bioimaging applications, since they have the advantages of high sensitivity, deep penetration, high signal to noise ratio (SNR) and no interference from tissue autofluorescence [83, 141, 142, 143, 144]. As readers may have noticed in this review, thanks to adequate chemistry, it is possible to prepare persistent luminescence nanoparticles with optimized properties.

Although imaging using such nanoprobe is successful in small animal models, further investigations are required to study unfavourable biodistribution and nonspecific accumulation of these probes. A major challenge will be to encapsulate or biofunctionalize these nanoprobe so that they can escape the RES. Innovations in the preparation of nanoprobe for imaging of deep tissues with high quantum yield and deep tissue penetration are also needed. Toxicological characterizations of the persistent luminescent nanomaterials have also been initiated, whatever the matrix and the dopants. To date the majority of the data has been mainly obtained from *in vitro* studies on several cell line cultures [83, 97, 101, 104, 105, 107, 115, 121, 122, 126], and a lesser number of *in vivo* toxicity studies on mice [83, 115, 122]. The data published in the literature do not suggest significant toxic effects.

Further investigations regarding nanomaterials with other matrixes could lead to the design of improved nanoprobe. Among the different possibilities, we can cite preliminary works on perovskites reported by Tanabe and co-workers [145] and works concerning PLNPs emitting in the second transparency window reported by Ueda and co-workers [146] and Pan and co-workers [147]. A limit with current probes is their long term chemical stability *in vivo*. In the future, researches using biodegradable materials could be envisioned such as recently reported by Capobianco and co-workers [148]. Another promising application of such nanoprobe is their use as theranostic agents. In 2006, Chen and co-workers reported the use of persistent luminescence nanoparticles attached to photosensitizers such as porphyrins for photodynamic therapy PDT [149]. The luminescence emitted from the nanoparticles activate the photosensitizers and as a consequence, singlet oxygen is produced to enhance the killing of cells by ionizing radiation. Finally, X-ray luminescence combining X-ray excitation and visible or near-infrared emission is a hot topic for preclinical imaging to improve image resolution [150,151].

There is a huge potential of discovering novel agents with advanced and more efficient properties by combining multidisciplinary areas such as chemistry, material science and bioengineering for preclinical researches [152, 153].

## Acknowledgments

This work was supported by the grants from Region Ile de France (In Actio project no. I07-876/R), European Community (Network of Excellence CLINIGENE LSHB-CT-2006-018933), CNRS (défi G3N and PhD grant), ANR Natlurim (ANR-08-NANO-025) and ANR PEPSI (ANR-14-CE08-0016-01), PRES Sorbonne Paris Cité (Odiceo project) and Biospace Lab. The authors acknowledge all their collaborators: Q. le Masne de Chermont, N. Wattier, M. Bessodes, A. Varenne, F. d'Orlyé, S. Gutiérrez-Granados, M. Martínez-Alfaro, R. Lai-Kuen, G. Byk, M. Kaikkonen, S. Yla-Herttuala, D. Gourier, A. Bessière, A. Lecointre, C. Chanéac, C. Rosticher, M. Pellerin, F. Apparailly, C.-H. Cottard, C. Boisson-Vidal, F. Gazeau, D. Alloeyau, O. Clément, S. Maitrejean and L. Laumonier.

## Competing Interests

The authors have declared that no competing interest exists.

## References

- Cai W, Chen X. Nanoplatforms for targeted molecular imaging in living subjects. *Small*. 2007; 3: 1840-1854.
- Lee DE, Koo H, Sun IC et al. Multifunctional nanoparticles for multimodal imaging and theragnosis. *Chem. Soc. Rev.* 2012; 7: 2656-2672.
- Xie J, Liu G, Eden HS et al. Surface-engineered magnetic nanoparticle platforms for cancer imaging and therapy. *Acc. Chem. Res.* 2011; 44: 883-892.
- Weissleder R, Pittet MJ. Imaging in the area of molecular oncology. *Nature*. 2008; 452: 580-589.
- Kobayashi H, Ogawa M, Alford R et al. New strategies for fluorescent probe design in medical diagnostic imaging. *Chem. Rev.* 2010; 110: 2620-2640.
- Duan H, Nie S. Cell-penetrating quantum dots based on multivalent and endosome-disrupting surface coating. *J. Am. Chem. Soc.* 2007; 129: 3333-3338.
- Chen GY, Ohulchanskyy TY, Kumar R et al. Ultrasmall monodisperse NaYF<sub>4</sub>:Yb<sup>3+</sup>/Tm<sup>3+</sup> nanocrystals with enhanced near-infrared to near-infrared upconversion photoluminescence. *ACS Nano*. 2010; 4: 3163-3168.
- Le Masne de Chermont Q, Chanéac C, Seguin J et al. Nanoprobes with near-infrared persistent luminescence for *in vivo* imaging. *Proc. Nat. Acad. Sci.* 2007; 104: 9266-9277.
- Hölsä J. Persistent Luminescence Beats the Afterglow: 400 Years of Persistent Luminescence. *The Electrochemical Society Interface*. 2009; 42-45
- Aitasala T, Deren P, Hölsä J et al. Persistent luminescence phenomena in materials doped with rare earth ions. *J. Solid State Chem.* 2003; 171: 114-122.
- Brito HF, Hölsä J, Laamanen T et al. Persistent luminescence mechanisms: human imagination at work. *Opt. Mater. Exp.* 2012; 2: 371-381.
- [Internet] <http://www.glo-techint.com/> and <http://www.studioroosegaard.net/>
- Yu F, Yang Y, Su X et al. Novel long persistent luminescence phosphors: Yb<sup>3+</sup> codoped MAI<sub>2</sub>O<sub>4</sub> (M=Ba,Sr). *Opt. Mater. Exp.* 2015; 5: 585-595.
- [Internet] <http://www.studioroosegaard.net/>
- Lin Y, Tang Z, Zhang Z et al. Influence of Codoping Different Rare-Earth Ions on the Luminescence of CaAl<sub>2</sub>O<sub>4</sub>-Based Phosphors. *J. Eur. Ceram. Soc.* 2003; 23: 175-178.
- Matsuzawa T, Aoki Y, Takeuchi T et al. A New Long Phosphorescent Phosphor with High-Brightness SrAl<sub>2</sub>O<sub>4</sub>: Eu<sup>2+</sup>, Dy<sup>3+</sup>. *J. Electrochem. Soc.* 1996; 143: 2670-2673.
- Murazaki Y, Arai K, Ichinomiya K. Luminescence properties of a new red long-lasting phosphor: Mg<sub>2</sub>SiO<sub>4</sub>:Dy<sup>3+</sup>, Mn<sup>2+</sup>. *Jpn Rare Earths*. 1999; 35: 41-45.
- Dorenbos P. Mechanism of Persistent Luminescence in Eu<sup>2+</sup> and Dy<sup>3+</sup> Codoped Aluminate and Silicate Compounds. *J. Electrochem. Soc.* 2005; 152: H107-H110.

19. Casillas-Trujillo L, Andersson DA, Dorado B et al. Intrinsic defects, nonstoichiometry, and aliovalent doping of  $A^{2+}B^{4+}O_3$  perovskite scintillators. *Phys. Stat. Solidi B*. 2014; 251: 2279-2286.
20. Holsa J, Aitasalo T, Jungner H et al. Role of defect states in persistent luminescence materials. *J. Alloys and Compounds*. 2004; 374: 56-59.
21. Bessiere A, Lecointre A, Benhamou RA et al. How to induce red persistent luminescence in biocompatible  $Ca_3(PO_4)_2$ . *J. Mater. Chem. C*. 2013; 1: 1252-1259.
22. Bos AJJ, Dorenbos P, Bessiere A et al. Lanthanide energy levels in  $YPO_4$ . *Radiat. Meas.* 2008; 43: 222-226.
23. Chuang YJ, Zhen Z, Zhang F et al. Photostimulable Near-Infrared Persistent Luminescent Nanoprobes for Ultrasensitive and Longitudinal Deep-Tissue Bio-Imaging. *Theranostics*. 2014; 4: 1112-1122.
24. Van den Eeckhout K, Bos AJJ, Poelman D et al. Revealing trap depth distributions in persistent phosphors. *Phys. Rev. B*. 2013; 87: 045126.
25. Botterman J, Van den Eeckhout K, De Baere I et al. Mechanoluminescence in  $BaSi_2O_7:Ni:Eu$ . *Acta Materialia*. 2012; 60: 5494-5500.
26. Van den Eeckhout K, Smet PF, Poelman D. Persistent Luminescence in  $Eu^{2+}$  Doped Compounds: A Review. *Materials*. 2010; 3: 2536-2566.
27. Van den Eeckhout K, Poelman D, Smet PF. Persistent Luminescence in Non  $Eu^{2+}$  Doped Compounds: A Review. *Materials*. 2013; 6: 2789-2818.
28. Singh SK. Red and near infrared persistent luminescence nano-probes for bioimaging and targeting applications. *RSC Advances*. 2014; 4: 58674-58698.
29. Qu B, Zhang B, Wang L, Zhou R, Zeng XC, Li L. Persistent Luminescence Hole-Type Materials by Design: Transition-Metal-Doped Carbon Allotrope and Carbides. *ACS Appl. Mater. Interfaces*. 2016; 8: 5439-5444.
30. Li Y, Gecevicius M, Qiu J. Long persistent phosphors from fundamentals to applications. *Chem. Soc. Rev.* 2016; 45: 2090-2136.
31. Zhuang Y, Katayama Y, Ueda J et al. A brief review on red to near-infrared persistent luminescence in transition metal activated phosphors. *Opt. Mater.* 2014; 36: 1907-1912.
32. Bunzli JCG, Eliseeva SV. Intriguing aspects of lanthanide luminescence. *Chem. Sci.* 2013; 4: 1939-1949.
33. Viana B, Sharma SK, Gourier D et al. Long term in vivo imaging with  $Cr^{3+}$  doped spinel nanoparticles exhibiting persistent luminescence. *J. Lumin.* 2016; 170: 879-887.
34. Jaque D, Richard C, Viana B et al. Inorganic nanoparticles for optical bioimaging. *Adv. Opt. Photon.* 2016; 8: 1-103.
35. Tang L, Yang X, Dobrucki LW et al. Aptamer-functionalized, ultra-small, monodisperse silica nanoconjugates for targeted dual-modal imaging of lymph nodes with metastatic tumors. *Angew. Chem. Int. Ed. Engl.* 2012; 51: 12721-12726.
36. Nel AE, Mädler L, Velegol D et al. Understanding biophysicochemical interactions at the nano-bio interface. *Nat. Mater.* 2009; 8: 543-557.
37. Smith AM, Mancini MC, Nie S. Bioimaging: Second window for *in vivo* imaging. *Nat. Nanotech.* 2009; 4: 710-711.
38. Biju V. Chemical modifications and bioconjugate reactions of nanomaterials for sensing, imaging, drug delivery and therapy. *Chem. Soc. Rev.* 2014; 43: 744-764.
39. Richard C, Maldiney T, le Masne de Chermont Q et al. Persistent luminescence nanoparticles for bioimaging. *Advances in Bio-Imaging: From Physics to Signal Understanding Issues*. 2012; 37-53.
40. Wang XJ, Jia D, Ye W.  $Mn^{2+}$  activated green, yellow, and red long persistent phosphors. *J. Lumin.* 2003; 102-103: 34-37.
41. le Masne de Chermont Q, Richard C, Seguin J et al. Silicates doped with luminescent ions: useful tools for optical imaging applications. *Proc. SPIE* 2009; 7189 (Colloidal Quantum Dots for Biomedical Applications IV), 71890B/1-71890B/9.
42. Maldiney T, Richard C, Seguin J et al. Effect of core diameter, surface coating, and PEG chain length on the biodistribution of persistent luminescence nanoparticles in mice. *ACS Nano*. 2011; 5: 854-862.
43. Maldiney T, Byk G, Wattier N et al. Synthesis and functionalization of persistent luminescence nanoparticles with small molecules and evaluation of their targeting ability. *Int. J. Pharm.* 2012; 423: 102-107.
44. Maldiney T, Kaikkonen MU, Seguin J et al. *In vitro* targeting of avidin-expressing glioma cells with biotinylated persistent luminescence nanoparticles. *Bioconj. Chem.* 2012; 23: 472-478.
45. Van den Eeckhout K, Smet PF, Poelman D. Persistent luminescence in rare-earth codoped  $CaSi_2N_8:Eu^{2+}$ . *J. Lumin.* 2009; 129: 1140-1143.
46. Van den Eeckhout K, Smet PF, Poelman D. Luminescent afterglow behavior in the  $M_2Si_2N_8:Eu$  family (M=Ca, Sr, Ba). *Materials*. 2011; 4: 980-990.
47. Smet PF, Van den Eeckhout K, Bos AJJ et al. Temperature and wavelength dependent trap filling in  $M_2Si_2N_8:Eu$  (M=Ca, Sr, Ba) persistent phosphors. *J. Lumin.* 2012; 132: 682-689.
48. Ledoux G, Amans D, Dujardin C et al. Facile and rapid synthesis of highly luminescent nanoparticles via pulsed laser ablation in liquid. *Nanotechnology*. 2009; 20: 445605.
49. Hahn A, Barcikowski S, Chichkov BN. Influence on Nanoparticle Production during Pulsed Laser Ablation. *J. Laser Micro/Nanoeng.* 2008; 3: 73-77.
50. Mafuné F, Kohno JY, Takeda Y et al. Formation and Size Control of Silver Nanoparticles by Laser Ablation in Aqueous Solution. *J. Phys. Chem. B*. 2000; 104: 9111-9117.
51. Usui H, Shimizu Y, Sasaki T et al. Photoluminescence of ZnO nanoparticles prepared by laser ablation in different surfactant solutions. *J. Phys. Chem. B*. 2005; 109: 120-124.
52. Amans D, Malaterre C, Diouf M et al. Synthesis of Oxide Nanoparticles by Pulsed Laser Ablation in Liquids Containing a Complexing Molecule: Impact on Size Distributions and Prepared Phases. *J. Phys. Chem. C*. 2011; 115: 5131-5139.
53. Yang L, May PW, Yin L et al. Direct growth of highly organized crystalline carbon nitride from liquid phase pulsed laser ablation. *Chem. Mater.* 2006; 18: 5058-5064.
54. Harame DL, Bousse LJ, Shott JD et al. Ion-sensing devices with silicon nitride and borosilicate glass insulators. *IEEE Trans. Electron. Dev.* 1987; 34: 1700-1707.
55. Maldiney T, Sraiki G, Viana B et al. *In vivo* optical imaging with rare earth doped  $Ca_2Si_2N_8$  persistent luminescence nanoparticles. *Opt. Mat. Exp.* 2012; 2: 261-268.
56. Lecointre A, Viana B, Le Masne Q et al. Red long-lasting luminescence in clinostatite. *J. Lumin.* 2009; 129: 1527-1530.
57. Lecointre A, Bessiere A, Viana B et al. Red persistent luminescence silicate nanoparticles. *Radiat. Meas.* 2010; 45: 497-499.
58. Maldiney T, Lecointre A, Viana B et al. Controlling electron trap depth to enhance optical properties of persistent luminescence nanoparticles for *in vivo* imaging. *J. Am. Chem. Soc.* 2011; 133: 11810-11815.
59. Maldiney T, Lecointre A, Viana B et al. Trap depth optimization to improve optical properties of diopside-based nanophosphors for medical imaging. *Proc. SPIE* 2012; 8263: 826318-826318-7.
60. Viana B, Maldiney T, Blahuta S et al. Control of the point defects in oxide materials to enhance functionalities in imaging. *Proc. SPIE*. 2013; 8626 (Oxide-Based Materials and Devices IV), 86260R/1-86260R/6.
61. Maldiney T, Viana B, Bessiere A et al. *In vivo* imaging with persistent luminescence silicate-based nanoparticles. *Opt. Mater.* 2013; 35: 1852-1858.
62. Qin L, Zhu Q, Li G et al. Controlled fabrication of flower-like  $ZnO-Fe_2O_3$  nanostructured films with excellent lithium storage properties through a partly sacrificed template method. *J. Mater. Chem.* 2012; 22: 7544-7550.
63. Tacchini I, Terrado E, Anson A et al. Anatase nanotubes synthesized by a template method and their application as a green photocatalyst. *J. Mater. Sci.* 2011; 46: 2097-2104.
64. Li ZP, Shi JP, Zhang HW et al. Highly controllable synthesis of near-infrared persistent luminescence  $SiO_2/CaMgSi_2O_6$  composite nanospheres for imaging *in vivo*. *Opt. Exp.* 2014; 22: 10509-10518.
65. Li ZJ, Zhang HW, Sun M et al. A facile and effective method to prepare long-persistent phosphorescent nanospheres and its potential application for *in vivo* imaging. *J. Mater. Chem.* 2012; 22: 24713-24720.
66. Wu BY, Wang HF, Chen JT et al. Fluorescence Resonance Energy Transfer Inhibition Assay for  $\alpha$ -Fetoprotein Excreted during Cancer Cell Growth Using Functionalized Persistent Luminescence Nanoparticles. *J. Am. Chem. Soc.* 2011; 133: 686-688.
67. Qin LX, Tang ZY. Randomized controlled trial of screening for hepatocellular carcinoma. *J. Cancer Res. Clin. Oncol.* 2004; 130: 417-422.
68. Wu BY, Yan XP. Bioconjugated persistent luminescence nanoparticles for Förster resonance energy transfer immunoassay of prostate specific antigen in serum and cell extracts without in situ excitation. *Chem. Commun.* 2015; 51: 3903-3906.
69. Pisanic TR, Zhang Y, Wang TH. Quantum dots in diagnostics and detection: principles and paradigms. *Analyst*. 2014; 139: 2968-2981.
70. Song SP, Qin Y, He Y et al. Functional nanoprobes for ultrasensitive detection of biomolecules. *Chem. Soc. Rev.* 2010; 39: 4234-4244.
71. Li N, Diao W, Han et al.  $MnO_2$ -Modified Persistent Luminescence Nanoparticles for Detection and Imaging of Glutathione in Living Cells and *In Vivo*. *Chem. Eur. J.* 2014; 20: 16488-16491.
72. Hwang C, Sinskey AJ, Lodish HF et al. Oxidized redox state of glutathione in the endoplasmic reticulum. *Science*. 1992; 257: 1496-1502.
73. Dalton TP, Shertzer HG, Puga A. Regulation of gene expression by reactive oxygen. *Annu. Rev. Pharmacol. Toxicol.* 1999; 39: 67-101.
74. Matthews CK, van Holde KE, Ahern KG. *Biochemistry*, Addison-Wesley Longman, San Francisco, 2000.
75. Li N, Li Y, Han Y et al. A Highly Selective and Instantaneous Nanoprobe for Detection and Imaging of Ascorbic Acid in Living Cells and *In Vivo*. *Anal. Chem.* 2014; 86: 3924-3930.
76. Chen Q, Espey MG, Sun AY et al. Pharmacologic doses of ascorbate act as a prooxidant and decrease growth of aggressive tumor xenografts in mice. *Proc. Natl. Acad. Sci. U.S.A.* 2008; 105: 11105-11109.
77. Zhang L, Lei J, Liu J et al. Persistent luminescence nanoprobe for biosensing and lifetime imaging of cell apoptosis via time-resolved fluorescence resonance energy transfer. *Biomaterials* 2015; 67: 323-334.
78. Jain RK, Stylianopoulos T. Delivering nanomedicine to solid tumours. *Nat. Rev. Clin. Oncol.* 2010; 7: 653-664.
79. Danhier F, Feron O, Pr at V. To exploit the tumour microenvironment: Passive and active tumour targeting of nanocarriers for anti-cancer drug delivery. *J. Control. Rel.* 2010; 148: 135-146.
80. Al-Jamal WT, Al-Jamal KT, Tianet B et al. Tumour Targeting of Functionalized Quantum Dot-Liposome Hybrids by Intravenous Administration. *Mol. Pharm.* 2009; 6: 520-530.
81. Park JH, Gu L, von Maltzahn G et al. Biodegradable luminescent porous silicon nanoparticles for *in vivo* applications. *Nat. Mater.* 2009; 8: 1-6.
82. Bessiere A, Jacquart S, Priolkar K et al.  $ZnGa_2O_4:Cr^{3+}$ : a new red long-lasting phosphor with high brightness. *Opt. Exp.* 2011; 9: 10131-10137.

83. Maldiney T, Bessière A, Seguin J et al. The *in vivo* activation of persistent nanophosphors for optical imaging of vascularization, tumours and grafted cells. *Nat. Mater.* 2014; 13: 418-426.
84. Bessière A, Sharma SK, Basavaraju N et al. Storage of Visible Light for Long-Lasting Phosphorescence in Chromium-Doped Zinc Gallate. *Chem. Mater.* 2014; 26: 1365-1373.
85. Li SD, Huang L. Pharmacokinetics and Biodistribution of Nanoparticles. *Mol. Pharmaceutics*, 2008; 5: 496-504.
86. Maldiney T, Rémond M, Bessodes M et al. Controlling aminosilane layer thickness to extend the plasma half-life of stealth persistent luminescence nanoparticles *in vivo*. *J. Mater. Chem. B*. 2015; 3: 4009-4016.
87. Sharma SK, Bessiere A, Gourier D et al. Optical properties and storage capabilities of  $AB_2O_4:Cr^{3+}$  (A=Zn, Mg, B=Ga, Al). *Proc. SPIE*. 2014; 8987: (Oxide-Based Materials and Devices V, 89870J/1-89870J/7).
88. Sharma SK, Bessiere A, Gourier D et al. Persistent luminescence of  $ZnGa_2O_4:Cr$ , an outstanding biomarker for *in vivo* imaging. *Proc. SPIE*. 2014; 8987: (Optical Components and Materials XI, 898215/1-898215/6).
89. Sharma SK, Gourier D, Viana B et al. Persistent luminescence of  $AB_2O_4:Cr^{3+}$  (A = Zn, Mg, B = Ga, Al) spinels: New biomarkers for *in vivo* imaging. *Opt. Mater.* 2014; 36: 1901-1906.
90. Viana B, Sharma SK, Gourier D et al. Long term *in vivo* imaging with  $Cr^{3+}$  doped spinel nanoparticles exhibiting persistent luminescence. *J. Lumin.* 2016; 170: 879-887.
91. Ramirez-Garcia G, d'Orlye F, Gutierrez-Granados S et al. Functionalization and characterization of persistent luminescence nanoparticles by dynamic light scattering, laser Doppler and capillary electrophoresis. *Coll. Surf. B: Biointerfaces* 2015; 136: 272-281.
92. Liu F, Yan W, Chuang YJ et al. Photostimulated near-infrared persistent luminescence as a new optical read-out from  $Cr^{3+}$  doped  $LiGa_3O_8$ . *Sci. Rep.* 2013; 3: 1554-1563.
93. Canton I, Battaglia G. Endocytosis at the nanoscale. *Chem. Soc. Rev.* 2012; 41: 2718-2739.
94. Cheng ZL, Zaki AA, Hui JZ et al. Multifunctional nanoparticles: cost versus benefit of adding targeting and imaging capabilities. *Science* 2012; 338: 903-910.
95. Cai W, Chen X. Multimodality molecular imaging of tumor angiogenesis. *J. Nucl. Med.* 2008; 49: S113-128.
96. Hood JD, Cheresah DA. Role of integrins in cell invasion and migration. *Nat. Rev. Cancer* 2002; 2: 91-100.
97. Chuang YJ, Zhen Z, Zhang F et al. Photostimulable Near-Infrared Persistent Luminescent Nanoprobes for Ultrasensitive and Longitudinal Deep-Tissue Bio-Imaging. *Theranostics* 2014; 4: 1112-1122.
98. Lee DE, Koo H, Sun IC et al. Multifunctional nanoparticles for multimodal imaging and theragnosis. *Chem. Soc. Rev.* 2012; 41: 2656-2672.
99. Harivardhan RL, Arias JL, Nicolas J et al. Magnetic Nanoparticles: Design and Characterization, Toxicity and Biocompatibility, Pharmaceutical and Biomedical Applications. *Chem. Rev.* 2012; 112: 5818-5878.
100. Maldiney T, Doan BT, Alloyeau D et al. Gadolinium-Doped Persistent Nanophosphors as Versatile Tool for Multimodal *In Vivo* Imaging. *Adv. Funct. Mater.* 2015; 25: 331-338.
101. Wang XS, Li WS, Situ JQ et al. Multi-functional mesoporous  $@-Ga_2O_3:Cr^{3+}$  nanorod with long lasting near infrared luminescence for *in vivo* imaging and drug delivery. *RSC* 2015; 12886-12889.
102. Clabau F, Rocquefelte X, Jobic S et al. Mechanism of Phosphorescence Appropriate for the Long-Lasting Phosphors  $Eu^{2+}$ -Doped  $SrAl_2O_4$  with Codopants  $Dy^{3+}$  and  $B^{3+}$ . *Chem. Mater.* 2005; 17: 3904-3912.
103. Li Z, Zhang Y, Wu X et al. *In Vivo* Repeatedly Charging Near-Infrared-Emitting Mesoporous  $SiO_2/ZnGa_2O_4:Cr^{3+}$  Persistent Luminescence Nanocomposites. *Adv. Sci.* 2015; DOI: 10.1002/adv.201500001.
104. Maldiney T, Ballet B, Bessodes M et al. Mesoporous persistent nanophosphors for *in vivo* optical bioimaging and drug delivery. *Nanoscale*, 2014; 6: 13970-13976.
105. Dai WB, Lei YF, Ye S et al. Mesoporous nanoparticles  $Gd_2O_3@mSiO_2/ZnGa_2O_4:Cr^{3+}, Bi^{3+}$  as multifunctional probes for bioimaging. *J. Mater. Chem. B*, 2016; 4: 1842-1852.
106. Bridot JL, Faure AC, Laurent S et al. Hybrid Gadolinium Oxide Nanoparticles: Multimodal Contrast Agents for *in Vivo* Imaging. *J. Am. Chem. Soc.* 2007; 129: 5076-5084.
107. Teston E, Lalatonne Y, Elgrabli D et al. Design, Properties, and *In Vivo* Behavior of Superparamagnetic Persistent Luminescence Nanohybrids. *Small* 2015; 11: 2696-2704.
108. Srivastava BB, Kuang A, Mao Y. Persistent luminescent sub-10 nm Cr doped  $ZnGa_2O_4$  nanoparticles by a biphasic synthesis route. *Chem. Commun.* 2015; 51: 7372-7375.
109. Teston E, Richard S, Maldiney T et al. Non-Aqueous Sol-Gel Synthesis of Ultra Small Persistent Luminescence Nanoparticles for Near-Infrared *In Vivo* Imaging. *Chem. Eur. J.* 2015; 21: 7350-7354.
110. Yu SH, Conte DE, Baek S et al. Structure-Properties Relationship in Iron Oxide-Reduced Graphene Oxide Nanostructures for Li-Ion Batteries. *Adv. Funct. Mater.* 2013; 23: 4293-4305.
111. Bilecka I, Djerdj I, Niederberger M. One-minute synthesis of crystalline binary and ternary metal oxide nanoparticles. *Chem. Commun.* 2008; 7: 886-888.
112. Boyle TJ, Yang P, Hattar K et al. Synthesis and Characterization of Solvothermal Processed Calcium Tungstate Nanomaterials from Alkoxide Precursors. *Chem. Mater.* 2014; 26: 965-975.
113. Demay-Drouhard P, Nehlig E, Hardouin J et al. Nanoparticles under the Light: Click Functionalization by Photochemical Thiol-yne Reaction, Towards Double Click Functionalization. *Chem. Eur. J.* 2013; 19: 8388-8392.
114. Kunjachan S, Pola R, Gremse F et al. Passive versus active tumor targeting using RGD- and NGR-modified polymeric nanomedicines. *Nano Lett.* 2014; 14: 972-981.
115. Li Z, Zhang Y, Wu X et al. Direct Aqueous-Phase Synthesis of Sub-10 nm "Luminous Pearls" with Enhanced *In Vivo* Renewable Near-Infrared Persistent Luminescence. *J. Am. Chem. Soc.* 2015; 137: 5304-5307.
116. Shi J, Sun X, Zhu J et al. One-step synthesis of amino-functionalized ultrasmall near infrared-emitting persistent luminescent nanoparticles for *in vitro* and *in vivo* bioimaging. *Nanoscale*, 2016; 8: 9798-9804.
117. Pan Z, Lu YY, Liu F. Sunlight-activated long-persistent luminescence in the near-infrared from  $Cr^{3+}$  doped zinc gallogermanates. *Nat. Mater.* 2012; 11: 58-63.
118. Li J, Shi J, Shen J et al. Specific Recognition of Breast Cancer Cells *In Vitro* Using Near Infrared-Emitting Long-Persistence Luminescent  $Zn_9Ga_2Ge_2O_{10}:Cr^{3+}$  Nanoprobes. *Nano Micro Lett.* 2015; 7: 138-145.
119. Melancon MP, Zhou M, Zhang R. Selective uptake and imaging of aptamer- and antibody-conjugated hollow nanospheres targeted to epidermal growth factor receptors overexpressed in head and neck cancer. *ACS Nano* 2014; 8: 4530-4538.
120. Abdukayum A, Chen JT, Zhao Q et al. Functional Near Infrared-Emitting  $Cr^{3+}/Pr^{3+}$  Co-Doped Zinc Gallogermanate Persistent Luminescent Nanoparticles with Superlong Afterglow for *In Vivo* Targeted Bioimaging. *J. Am. Chem. Soc.* 2013; 135: 14125-14133.
121. Shi J, Sun X, Li J et al. Multifunctional near infrared-emitting long-persistence luminescent nanoprobes for drug delivery and targeted tumor imaging. *Biomaterials* 2015; 37: 260-270.
122. Abdukayum A, Yang CX, Zhao Q et al. Gadolinium Complexes Functionalized Persistent Luminescent Nanoparticles as a Multimodal Probe for Near-Infrared Luminescence and Magnetic Resonance Imaging *in Vivo*. *Anal. Chem.* 2014; 86: 4096-4101.
123. Lu YC, Yang CX, Yan XP. Radiopaque tantalum oxide coated persistent luminescent nanoparticles as multimodal probes for *in vivo* near-infrared luminescence and computed tomography bioimaging. *Nanoscale*, 2015; 7: 17929-17937.
124. Lusic H, Grinstaff MW. X-ray-Computed Tomography Contrast Agents. *Chem. Rev.* 2012; 113: 1641-1666.
125. Lee N, Cho HR, Oh MH, et al. Multifunctional  $Fe_2O_3/TaOx$  Core/Shell Nanoparticles for Simultaneous Magnetic Resonance Imaging and X-ray Computed Tomography. *J. Am. Chem. Soc.* 2012; 134: 10309-10312.
126. Shi J, Fu H, Sun X et al. Magnetic, long persistent luminescent and mesoporous nanoparticles as trackable transport drug carriers. *J. Mater. Chem. B*, 2015; 3: 635-641.
127. Oh MH, Lee N, Kim H et al. Large-Scale Synthesis of Bioinert Tantalum Oxide Nanoparticles for X-ray Computed Tomography Imaging and Bimodal Image-Guided Sentinel Lymph Node Mapping. *J. Am. Chem. Soc.* 2011; 133: 5508-5515.
128. Wu SQ, Chi CW, Yang CX et al. Penetrating Peptide-Bioconjugated Persistent Nanophosphors for Long-Term Tracking of Adipose-Derived Stem Cells with Superior Signal-to-Noise Ratio. *Anal. Chem.* 2016; 88: 4114-4121.
129. Sun M, Li ZJ, Liu CL et al. Persistent luminescent nanoparticles for super-long time *in vivo* and *in situ* imaging with repeatable excitation. *J. Lumin.* 2014; 145: 838-842.
130. Luitel HN, Watari T, Torikai T et al. Highly water resistant surface coating by fluoride on long persistent  $Sr_4Al_3O_{25}:Eu^{2+}/Dy^{3+}$  phosphor. *Appl. Surf. Sci.* 2010; 256: 2347-2353.
131. Schneiders W, Reinstorf A, Pompe W et al. Effect of modification of hydroxyapatite/collagen composites with sodium citrate, phosphoserine, phosphoserine/RGD-peptide and calcium carbonate on bone remodelling. *Bone* 2007; 40: 1048-1059.
132. Paterson AS, Raja B, Garvey G et al. Persistent Luminescence Strontium Aluminate Nanoparticles as Reporters in Lateral Flow Assays. *Anal. Chem.* 2014; 86: 9481-9488.
133. Mudanyali O, Dimitrov S, Sikora U et al. Integrated rapid-diagnostic-test reader platform on a cellphone. *Lab on a Chip* 2012; 12: 2678-2686.
134. Lu X. Silica encapsulation study on  $SrAl_2O_4:Eu^{2+}, Dy^{3+}$  phosphors. *Mater. Chem. Phys.* 2005; 93: 526-530.
135. Ji PT, Chen XY, Wu Y. Encapsulating  $MAI_2O_4:Eu^{2+}, Dy^{3+}$  (M = Sr, Ca, Ba) phosphors with triethanolamine to enhance water resistance. *Appl. Surf. Sci.* 2011; 258: 1888-1893.
136. Shi J, Fu H, Sun X et al. Magnetic, long persistent luminescent and mesoporous nanoparticles as trackable transport drug carriers. *J. Mater. Chem. B*, 2015; 3: 635-641.
137. Doffek C, Alzakhem N, Bischof C et al. Understanding the Quenching Effects of Aromatic C-H and C-D Oscillators in Near-IR Lanthanoid Luminescence. *J. Am. Chem. Soc.*, 2012; 134: 16413-16423.
138. Rosticher C, Viana B, Maldiney T et al. Persistent luminescence of  $Eu, Mn, Dy$  doped calcium phosphates for *in vivo* optical imaging. *J. Lumin.* 2016; 170: 460-466.
139. Kamimura S, Xu CN, Yamada H et al. Long-persistent luminescence in the near-infrared from  $Nd^{3+}$  doped  $Sr_2SnO_4$  for *in vivo* optical imaging. *Jpn J. Appl. Phys.* 2014; 53: 092403.

140. Xu X, Wang Y, Gong Y et al. Effect of oxygen vacancies on the red phosphorescence of  $\text{Sr}_2\text{SnO}_4:\text{Sm}^{3+}$  phosphor. *Opt. Exp.* 2010; 18: 16989-16994.
141. Sharma SK, Gourier D, Teston E et al. Persistent luminescence induced by near infra-red photostimulation in chromium-doped zinc gallate for *in vivo* optical imaging. *Opt. Mater.* 2016; doi.org/10.1016/j.optmat.2016.06.053.
142. Lecuyer T, Teston E, Maldiney T et al. Physico-chemical characterizations of Cr doped persistent luminescence nanoparticles. *SPIE BIOS.* 2016; 97220X-97220X-8.
143. Sharma SK, Gourier D, Viana B et al. Persistent luminescence in nanophosphors for long term in-vivo bio-imaging. *SPIE BIOS* 2015; 93370I-93370I-6.
144. Sharma SK, Bessiere A, Gourier D et al. Optical properties and storage capabilities in  $\text{AB}_2\text{O}_4$ :  $\text{Cr}^{3+}$  (A= Zn, Mg, B= Ga, Al). *SPIE OPTO.* 2014; 89870J-89870J-7.
145. Xu J, Tanabe S, Sontakke AD et al. Near-infrared multi-wavelengths long persistent luminescence of  $\text{Nd}^{3+}$  ion through persistent energy transfer in  $\text{Ce}^{3+}$ ,  $\text{Cr}^{3+}$  co-doped  $\text{Y}_3\text{Al}_5\text{Ga}_3\text{O}_{12}$  for the first and second bio-imaging windows. *Appl. Phys. Lett.* 2015; 107: 081903.
146. Katayama Y, Kobayashi H, Tanabe S. Deep-red persistent luminescence in  $\text{Cr}^{3+}$  doped  $\text{LaAlO}_3$  perovskite phosphor for *in vivo* imaging. *Appl. Phys. Exp.* 2015; 8: 012102/1.
147. Liang Y, Liu F, Chen Y et al. New function of the  $\text{Yb}^{3+}$  ion as an efficient emitter of persistent luminescence in the short-wave infrared. *Light: Science & Applications*, doi: 10.1038/lsa.2016.124.
148. Rodriguez Burbano DC, Martin Rodriguez E, Dorenbos P et al. The near-IR photo-stimulated luminescence of  $\text{CaS}:\text{Eu}^{2+}/\text{Dy}^{3+}$  nanophosphors. *J. Mater. Chem. C.* 2014; 2: 228-231.
149. Chen W, Zhang J. Using nanoparticles to enable simultaneous radiation and photodynamic therapies for cancer treatment. *J. Nanosci. Nanotech.* 2006; 6: 1159-1166.
150. Carpentier CM, Sun C, Pratz G et al. Hybrid X-ray/optical luminescence imaging : characterization of experimental conditions. *Med. Phys.* 2010; 37: 4011-4018.
151. Cong W, Wang C, Wang G. Stored luminescence computed tomography. *Appl. Opt.* 2014; 53: 5672-5676.
152. Maldiney T, Scherman D, Richard C. Functional nanoparticles for bioanalysis, nanomedicine, and bioelectronic devices. *ACS symposium series* 2012; 2: 1113
153. Richard C, Doan BT, Mignet N. Increased sensitivity for medical imaging using non-ionizing nanomedicine as contrast agents. *Nanotheranostics for Personalized Medicine.* 2016; World Scientific.